INL/EXT-12-27057

HTR-PROTEUS Pebble Bed Experimental Program Core 4: Random Packing With a 1:1 Moderator-to-Fuel Pebble Ratio

John D. Bess
Leland M. Montierth
James W. Sterbentz
Luka Snoj
Igor Lengar
Oliver Köberl

March 2013

The INL is a U.S. Department of Energy National Laboratory
operated by Battelle Energy Alliance

INL/EXT-12-27057

HTR-PROTEUS Pebble Bed Experimental Program Core 4: Random Packing With a 1:1 Moderator-to-Fuel Pebble Ratio

John D. Bess
Leland M. Montierth
James W. Sterbentz
Luka Snoj[1]
Igor Lengar[1]
Oliver Köberl[2]

[1]Jožef Stefan Institute
[2]Paul Scherrer Institut

March 2013

Idaho National Laboratory
Idaho Falls, Idaho 83415

http://www.inl.gov

Prepared for the
U.S. Department of Energy
Office of Nuclear Energy
Under DOE Idaho Operations Office
Contract DE-AC07-05ID14517

NEA/NSC/DOC(2006)1

Gas Cooled (Thermal) Reactor – GCR

PROTEUS-GCR-EXP-002
CRIT

HTR-PROTEUS PEBBLE BED EXPERIMENTAL PROGRAM
CORE 4: RANDOM PACKING
WITH A 1:1 MODERATOR-TO-FUEL PEBBLE RATIO

Evaluators

John D. Bess
Leland M. Montierth
Idaho National Laboratory

Internal Reviewer
James W. Sterbentz

Independent Reviewers

Luka Snoj
Igor Lengar
Jožef Stefan Institute

Oliver Köberl
Paul Scherrer Institut

ACKNOWLEDGMENTS

The authors would like to express gratitude for the initial efforts performed by Barbara H. Dolphin, William K. Terry, and Charles A. Wemple at the Idaho National Laboratory as well as Luka Snoj and Igor Lengar at the Jožef Stefan Institute.

This project was supported by the U.S. Department of Energy, Assistant Secretary for Nuclear Energy, under DOE Idaho Operations Office Contract DE-AC07-05ID14517.

The authors would particularly like to acknowledge the indispensable work of Christine E. White in the preparation and deciphering of most of the drawings and graphics. IRPhEP working group provided much appreciated assistance, useful comments, and observations in the final preparation of this evaluation.

Gas Cooled (Thermal) Reactor – GCR

PROTEUS-GCR-EXP-002
CRIT

Status of Compilation / Evaluation / Peer Review

Section 1	Compiled	Independent Review	Working Group Review	Approved
1.0 DETAILED DESCRIPTION				
1.1 Description of the Critical and / or Subcritical Configuration	YES	YES	YES	YES
1.2 Description of Buckling and Extrapolation Length Measurements	NA	NA	NA	NA
1.3 Description of Spectral Characteristics Measurements	NA	NA	NA	NA
1.4 Description of Reactivity Effects Measurements	NA	NA	NA	NA
1.5 Description of Reactivity Coefficient Measurements	NA	NA	NA	NA
1.6 Description of Kinetics Measurements	NA	NA	NA	NA
1.7 Description of Reaction-Rate Distribution Measurements	NA	NA	NA	NA
1.8 Description of Power Distribution Measurements	NA	NA	NA	NA
1.9 Description of Isotopic Measurements	NA	NA	NA	NA
1.10 Description of Other Miscellaneous Types of Measurements	NA	NA	NA	NA
Section 2	**Evaluated**	**Independent Review**	**Working Group Review**	**Approved**
2.0 EVALUATION OF EXPERIMENTAL DATA				
2.1 Evaluation of Critical and / or Subcritical Configuration Data	YES	YES	YES	YES
2.2 Evaluation of Buckling and Extrapolation Length Data	NA	NA	NA	NA
2.3 Evaluation of Spectral Characteristics Data	NA	NA	NA	NA
2.4 Evaluation of Reactivity Effects Data	NA	NA	NA	NA
2.5 Evaluation of Reactivity Coefficient Data	NA	NA	NA	NA
2.6 Evaluation of Kinetics Measurements Data	NA	NA	NA	NA
2.7 Evaluation of Reaction Rate Distributions	NA	NA	NA	NA
2.8 Evaluation of Power Distribution Data	NA	NA	NA	NA
2.9 Evaluation of Isotopic Measurements	NA	NA	NA	NA
2.10 Evaluation of Other Miscellaneous Types of Measurements	NA	NA	NA	NA

Gas Cooled (Thermal) Reactor – GCR

PROTEUS-GCR-EXP-002
CRIT

Section 3	Compiled	Independent Review	Working Group Review	Approved
3.0 BENCHMARK SPECIFICATIONS				
3.1 Benchmark-Model Specifications for Critical and / or Subcritical Measurements	YES	YES	YES	YES
3.2 Benchmark-Model Specifications for Buckling and Extrapolation Length Measurements	NA	NA	NA	NA
3.3 Benchmark-Model Specifications for Spectral Characteristics Measurements	NA	NA	NA	NA
3.4 Benchmark-Model Specifications for Reactivity Effects Measurements	NA	NA	NA	NA
3.5 Benchmark-Model Specifications for Reactivity Coefficient Measurements	NA	NA	NA	NA
3.6 Benchmark-Model Specifications for Kinetics Measurements	NA	NA	NA	NA
3.7 Benchmark-Model Specifications for Reaction-Rate Distribution Measurements	NA	NA	NA	NA
3.8 Benchmark-Model Specifications for Power Distribution Measurements	NA	NA	NA	NA
3.9 Benchmark-Model Specifications for Isotopic Measurements	NA	NA	NA	NA
3.10 Benchmark-Model Specifications of Other Miscellaneous Types of Measurements	NA	NA	NA	NA
Section 4	**Compiled**	**Independent Review**	**Working Group Review**	**Approved**
4.0 RESULTS OF SAMPLE CALCULATIONS				
4.1 Results of Calculations of the Critical or Subcritical Configurations	YES	YES	YES	YES
4.2 Results of Buckling and Extrapolation Length Calculations	NA	NA	NA	NA
4.3 Results of Spectral Characteristics Calculations	NA	NA	NA	NA
4.4 Results of Reactivity Effect Calculations	NA	NA	NA	NA
4.5 Results of Reactivity Coefficient Calculations	NA	NA	NA	NA
4.6 Results of Kinetics Parameter Calculations	NA	NA	NA	NA
4.7 Results of Reaction-Rate Distribution Calculations	NA	NA	NA	NA
4.8 Results of Power Distribution Calculations	NA	NA	NA	NA
4.9 Results of Isotopic Calculations	NA	NA	NA	NA
4.10 Results of Calculations of Other Miscellaneous Types of Measurements	NA	NA	NA	NA
Section 5	**Compiled**	**Independent Review**	**Working Group Review**	**Approved**
5.0 REFERENCES	YES	YES	YES	YES
Appendix A: Computer Codes, Cross Sections, and Typical Input Listings	YES	YES	YES	YES

HTR-PROTEUS PEBBLE BED EXPERIMENTAL PROGRAM CORE 4 RANDOM PACKING WITH A 1:1 MODERATOR-TO-FUEL PEBBLE RATIO

IDENTIFICATION NUMBER: PROTEUS-GCR-EXP-002
CRIT

KEY WORDS: critical facility, graphite-moderated, graphite-reflected, intermediate enriched uranium dioxide, Paul Scherrer Institut, pebble bed arrangement, PROTEUS, TRISO, zero-power experiment

SUMMARY

1.0 DETAILED DESCRIPTION

PROTEUS is a zero-power research reactor based on a cylindrical graphite annulus with a central cylindrical cavity; it is a part of the Paul Scherrer Institute (formerly EIR) and is situated near Würenlingen in the canton of Aargau in northern Switzerland. The graphite annulus remains basically the same for all experimental programs, but the contents of the central cavity are changed according to the type of reactor being investigated. Through most of its service history, PROTEUS has represented light-water reactors, but from 1992 to 1996 PROTEUS was configured as a pebble-bed reactor (PBR) critical facility and designated as HTR-PROTEUS. The nomenclature was used to indicate that this series consisted of High Temperature Reactor experiments performed in the PROTEUS assembly. During this period, seventeen critical configurations were assembled and various reactor physics experiments were conducted. These experiments included measurements of criticality, differential and integral control rod and safety rod worths, kinetics, reaction rates, water ingress effects, and small sample reactivity effects (Ref. 3).

HTR-PROTEUS was constructed, and the experimental program was conducted, for the purpose of providing experimental benchmark data for assessment of reactor physics computer codes. Considerable effort was devoted to benchmark calculations as a part of the HTR-PROTEUS program. References 1 and 2 provide detailed data for use in constructing models for codes to be assessed. Reference 3 is a comprehensive summary of the HTR-PROTEUS experiments and the associated benchmark program. This document draws freely from these references.

Four benchmark reports were prepared to document evaluation of the experimental configurations according to core packing and the moderator-to-fuel pebble ratios:

- PROTEUS-GCR-EXP-001
  - Cores 1, 1A, 2, and 3
  - Hexagonal Close Packing
  - 1:2 Moderator-to-Fuel Pebble Ratio
- PROTEUS-GCR-EXP-002
  - Core 4
  - Random Packing
  - 1:1 Moderator-to-Fuel Pebble Ratio
- PROTEUS-GCR-EXP-003
  - Cores 5, 6, 7, and 8
  - Columnar Hexagonal Point-On-Point Packing
  - 1:2 Moderator-to-Fuel Pebble Ratio
- PROTEUS-GCR-EXP-004
  - Cores 9 and 10
  - Columnar Hexagonal Point-On-Point Packing
  - 1:1 Moderator-to-Fuel Pebble Ratio

In its deployment as a pebble bed reactor critical facility from 1992 to 1996, the reactor was designated as HTR-PROTEUS. This experimental program was performed as part of an International Atomic Energy Agency (IAEA) Coordinated Research Project (CRP) on the Validation of Safety Related Physics Calculations for Low Enriched HTGRs (High Temperature Gas-cooled Reactors). Additional historical data regarding this IAEA CRP and the PROTEUS facility are provided in Appendix D (Ref. 3). Figure 1.0-1 shows a generic HTR-PROTEUS configuration.

Within this project, critical experiments were conducted for graphite moderated LEU (low enriched uranium) systems to determine core reactivity, flux and power profiles, reaction-rate ratios, the worth of control rods (both in-core and reflector based), the worth of burnable poisons, kinetic parameters, and the effects of moisture ingress on these parameters. Fuel for the experiments was provided by the KFA Research Center in Jülich, Germany. Initial criticality was achieved on July 7, 1992. These experiments were conducted over a range of experimental parameters such as carbon-to-uranium ratio (C/U), core height-to-diameter ratio, and simulated moisture concentration (Ref. 3).

In any PBR, the fuel elements are spherical “pebbles” roughly the size of billiard balls, composed of a graphite matrix in which thousands of tiny (~1 mm diameter) coated fuel particles are embedded. These particles are known as tristructural-isotropic (TRISO) and are composed of a central UO_2 kernel surrounded by thin layers of graphite and silicon-carbide.

In the PROTEUS set of experiments, ten different core configurations were constructed and studied. Several cores had more than one reference state either to test reproducibility or further simplify or improve upon the core configuration from the previous reference state. This means that there are slight changes but the basic core configuration remains the same. Core 4 is the only configuration using randomly placed pebbles in the core barrel. All other configurations used hand-stacked pebbles in known packing configurations. The experimenters used the term “deterministic” to denote these regular core lattices. These lattices were either hexagonal close-packed (HCP) or columnar hexagonal point-on-point (CHPOP) configurations. The former arrangement can be visualized as oranges placed in a crate (Figure 1.0-2). In the latter configuration, the pebbles in successive layers form columns without any relative lateral displacement (Figure 1.0-3). The deterministic arrangements are considered much more useful for benchmarking reactor physics computer codes.

Theoretical pebble packing fractions for the HCP and CHPOP configurations are 0.7405 and 0.6046, respectively. A reference value for the random packing of pebbles in the HTR-PROTEUS assembly is

0.61.[a] The packing fraction of the CHPOP configuration is very close to that of a PBR, as a value of 0.61 is a good approximation for the inner part of a PBR, whereas the packing fraction decreases at the core/reflector interface.[b]

Table 1.0-1 provides a brief explanation of the cores and their reference states. Additional descriptions of each core and reference state will appear throughout the reports.

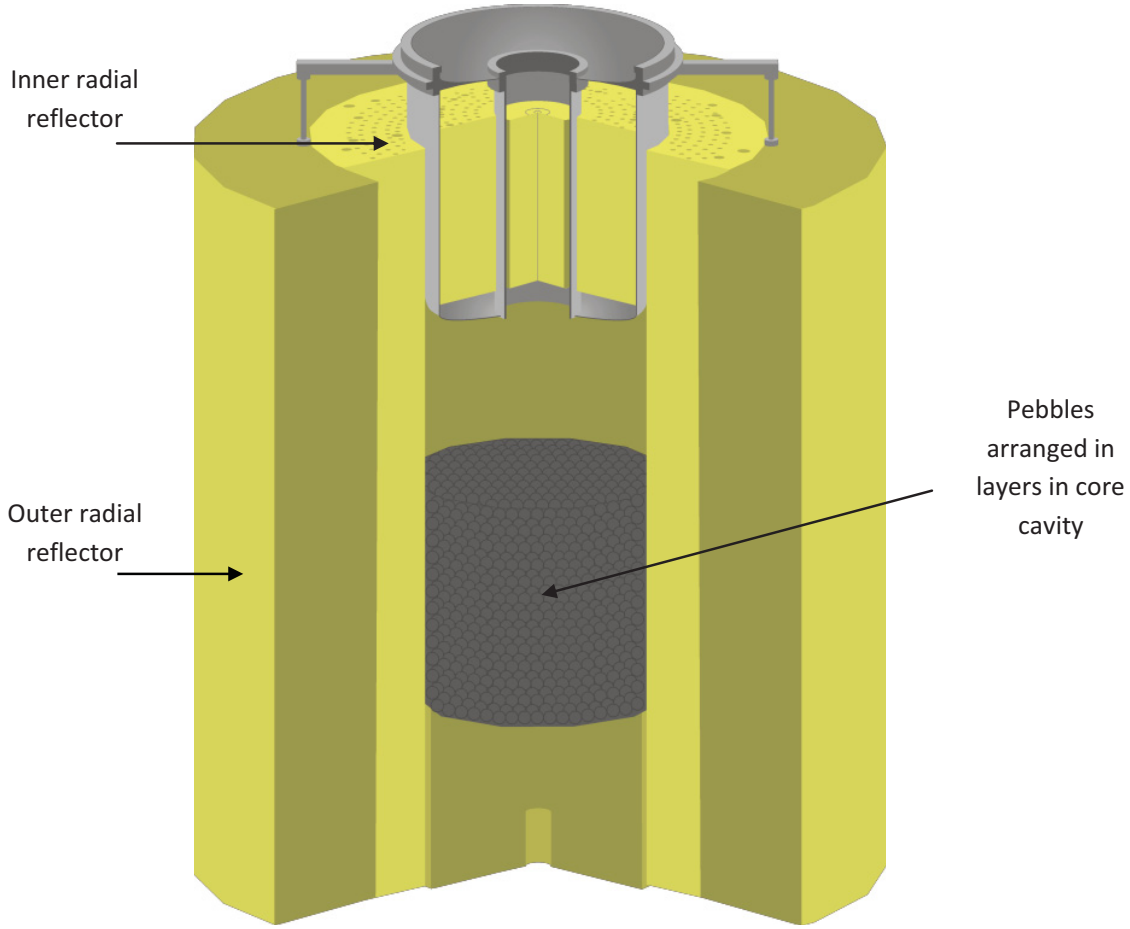

Figure 1.0-1. Generic HTR-PROTEUS Configuration (derived from Ref. 2).

[a] Difilippo, F. C., "Monte Carlo Calculations of Pebble Bed Benchmark Configurations of the PROTEUS Facility," Nucl. Sci. Eng., 143, 240-253 (2003).
[b] Personal communication with Oliver Köberl at PSI (September 2, 2011).

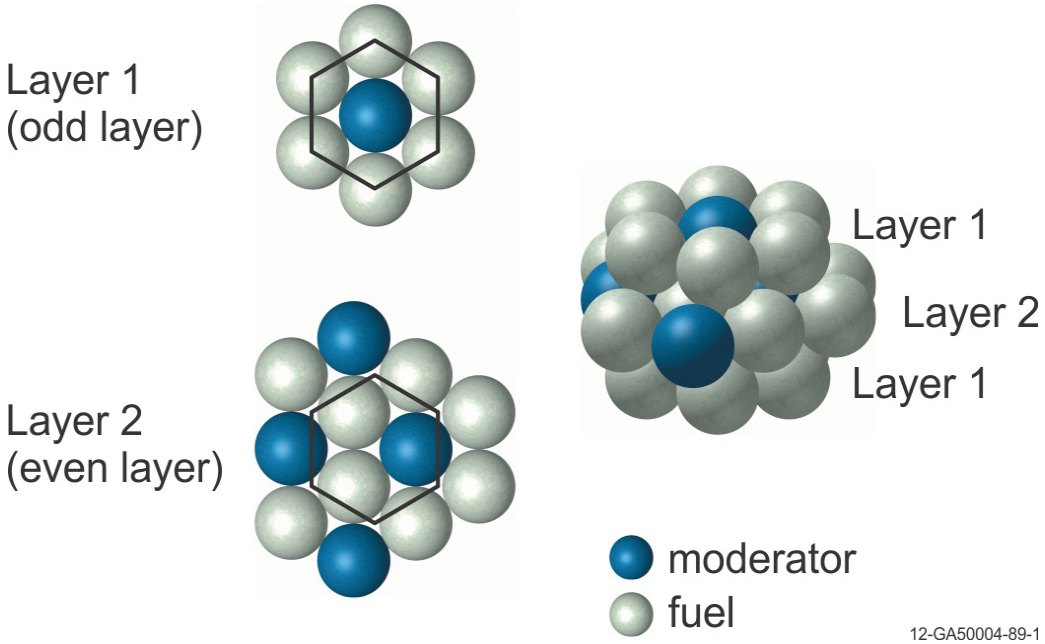

Figure 1.0-2. Subunit for Construction of the Hexagonal Close-Packed (HCP) Cell.

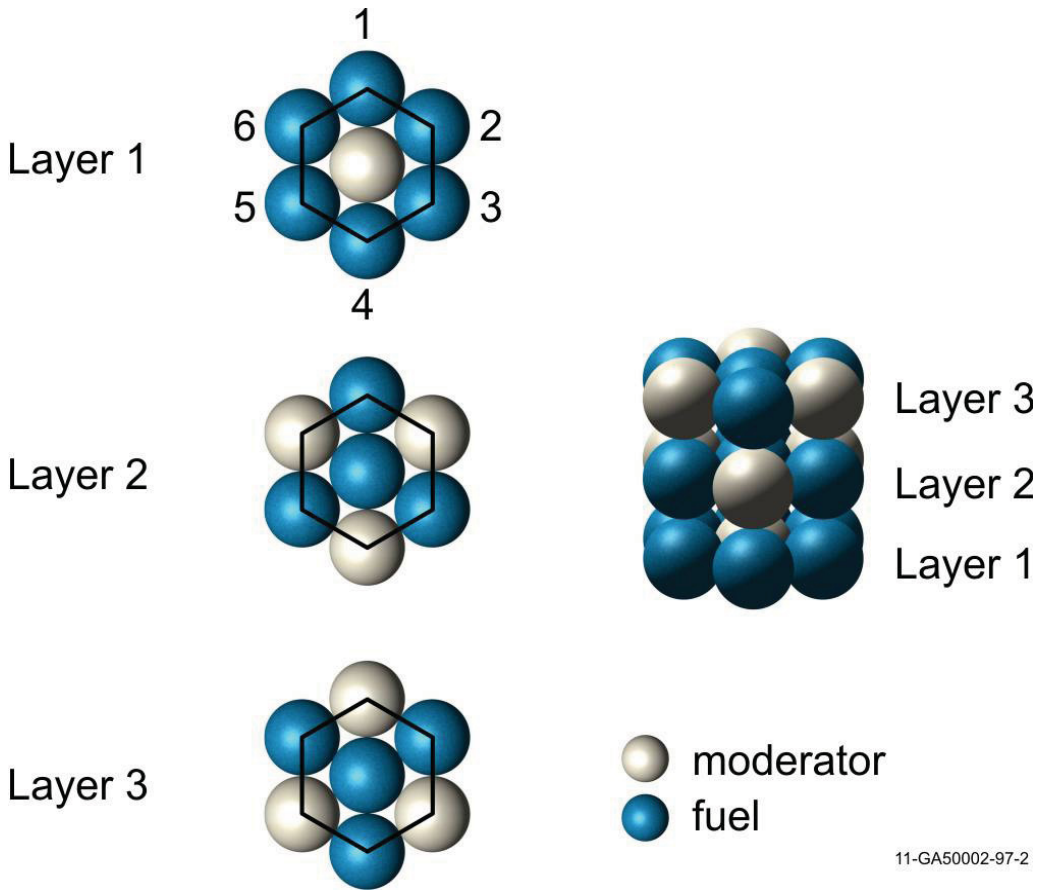

Figure 1.0-3. Subunit for Construction of the Columnar Hexagonal Point-On-Point (CHPOP) Cell.

Table 1.0-1. HTR-PROTEUS Core Configurations (Ref. 1 and 3).

Core	State	Notes
1	1	Only configuration that used ZEBRA control rods. Hexagonal close-packed pebbles.
1A	1 2	Equivalent to Core 1, ZEBRA control rods replaced with withdrawable control rods. Repeat of State #1 to check reproducibility with minor configuration changes.
2	1	Similar to Core 1A with decreased core height and increased upper graphite reflection. Used to investigate "cavity effect".
3	1	Similar to Core 1A with polyethylene rods added to simulate water ingress. Every available vertical channel between pebbles contained an 8.9-mm-diameter polyethylene rod.
4.1 4.2 4.3	1 1 1	Random pebble loading using separate fuel and moderator pebble delivery tubes. Random pebble loading using a single pebble delivery tube. Random pebble loading using a single pebble delivery tube (core reload for reproducibility).
5	1 2 3	Columnar hexagonal point-on-point packing implemented to improve homogeneity of core. Coolant channels in bottom reflector open. Equivalent to Core 5, State #1, with coolant channels in bottom reflector filled with graphite. Repeat of State #2 to check reproducibility and complete some additional reactor physics measurements.
6	1	Similar to Core 5 with hollow polyethylene rods added to simulate water ingress. Copper wire absorbers were placed within the polyethylene rods to compensate for the positive reactivity addition. Maximum polyethylene loading.
7	1	Similar to Core 5 with polyethylene rods added to simulate water ingress. Maximum polyethylene loading compensated by reduced core height.
8	1	Similar to Core 5 with short polyethylene rods added to simulate water ingress in lower core region. Every vertical channel contained a 15 cm long triangular polyethylene rod.
9	1 2	Columnar hexagonal point-on-point packing with increased moderator pebble content. Essentially Core 5 with an equal number of fuel and moderator pebbles. Repeat of State #1 with additional layer of moderator pebbles.
10	1	Similar to Core 9 with polyethylene rods added to simulate water ingress. Maximum polyethylene loading compensated by reduced core height.

1.1 Description of the Critical and / or Subcritical Configuration

1.1.1 Overview of Experiment

Only Core 4 is evaluated in this benchmark report due to the uniqueness in its construction. The other core configurations of the HTR-PROTEUS program are evaluated in their respective reports as outlined in Section 1.0.

Core 4 was evaluated and determined to be an acceptable benchmark experiment.

1.1.2 Geometry of the Experiment Configuration and Measurement Procedure

The PROTEUS assembly can basically be described as a graphite cylinder with an outer diameter of 3262 mm and a height of 3304 mm. It has a central cavity that sits 780 mm above the bottom of the radial and lower axial reflectors and consists of a 22-sided polygon with a flat-to-flat separation distance of 1250 mm. Random or deterministic lattices of pure graphite moderator pebbles and fuel (16.7 wt.% enriched in ^{235}U) pebbles were arranged within this cavity. Additional graphite filler pieces were utilized to provide support for the irregular outer surface of the deterministic pebble arrangements, providing a 12-sided core cavity region with a flat-to-flat separation distance of ~1205 mm. A removable, 1235-mm-high, upper axial reflector assembly consisted of an aluminum tank containing a 780-mm-high graphite reflector; normally an air gap was between the upper reflector and the topmost layer of the pebble bed. An aluminum safety ring is located 1764 mm above the floor of the cavity to prevent the upper reflector from falling onto the pebble bed. Reactor shutdown was achieved using four boron-steel rods placed at a radius of 680 mm; reactor control was typically performed using four fine control rods

placed at a radius of 900 mm. In Core 1, however, Cd Shutter, or ZEBRA type, rods were used in place of the fine control rods. Water ingress was simulated by using polyethylene rods introduced axially into vertical channels of the deterministic cores (Ref. 2). Schematic representations of the PROTEUS assembly are shown in Figures 1.1-1 and 1.1-2.

While there are many components of the PROTEUS that remain unchanged throughout the course of the HTR-PROTEUS experiments, many parameters did change between experiments, such as the use of graphite filler pieces, control rod types and locations, the presence of polyethylene rods to simulate water ingress, core pebble packing, and conditions at criticality. Section 1.1.2.1 provides information regarding general components common to all HTR-PROTEUS configurations. Section 1.1.2.2 provides information specific to the core configurations evaluated in this report.

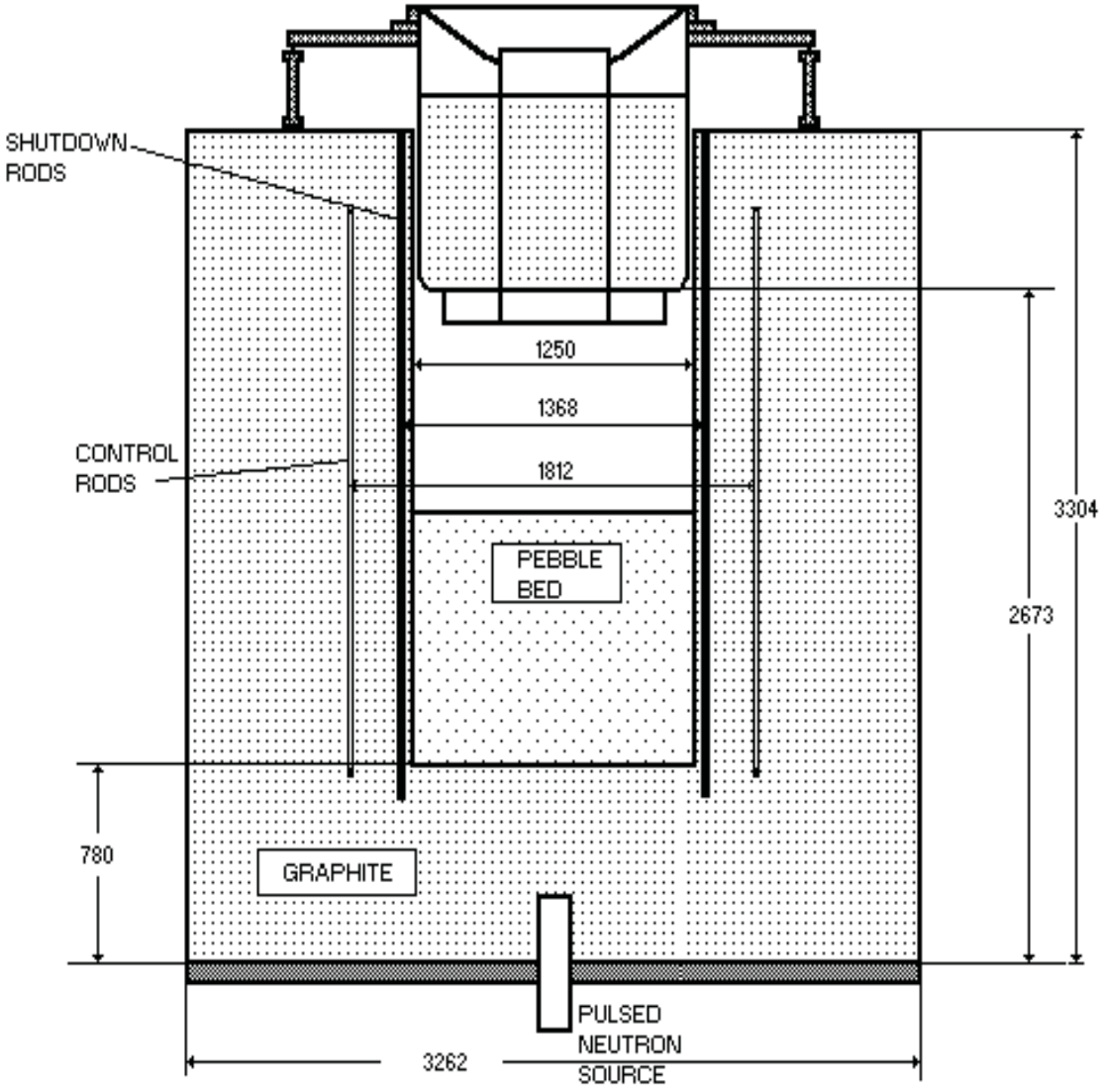

Figure 1.1-1. Schematic Side View of the HTR-PROTEUS Facility (dimensions in mm), (Ref. 2 and 3).

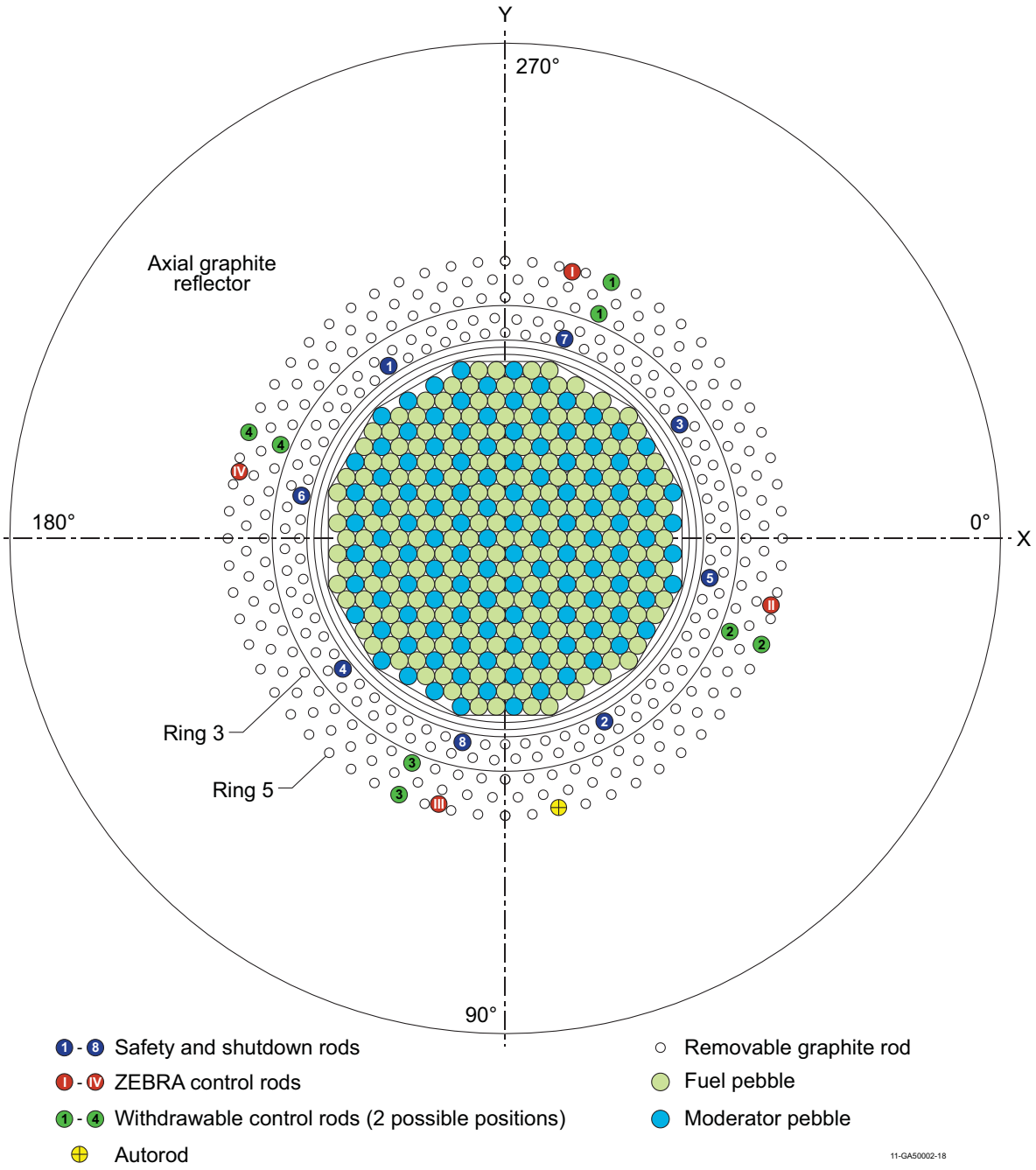

Figure 1.1-2a. HTR-PROTEUS Control Rod Positions and Bore Hole Locations (derived from Ref. 2). Figure is schematic and does not represent a random core pebble packing.

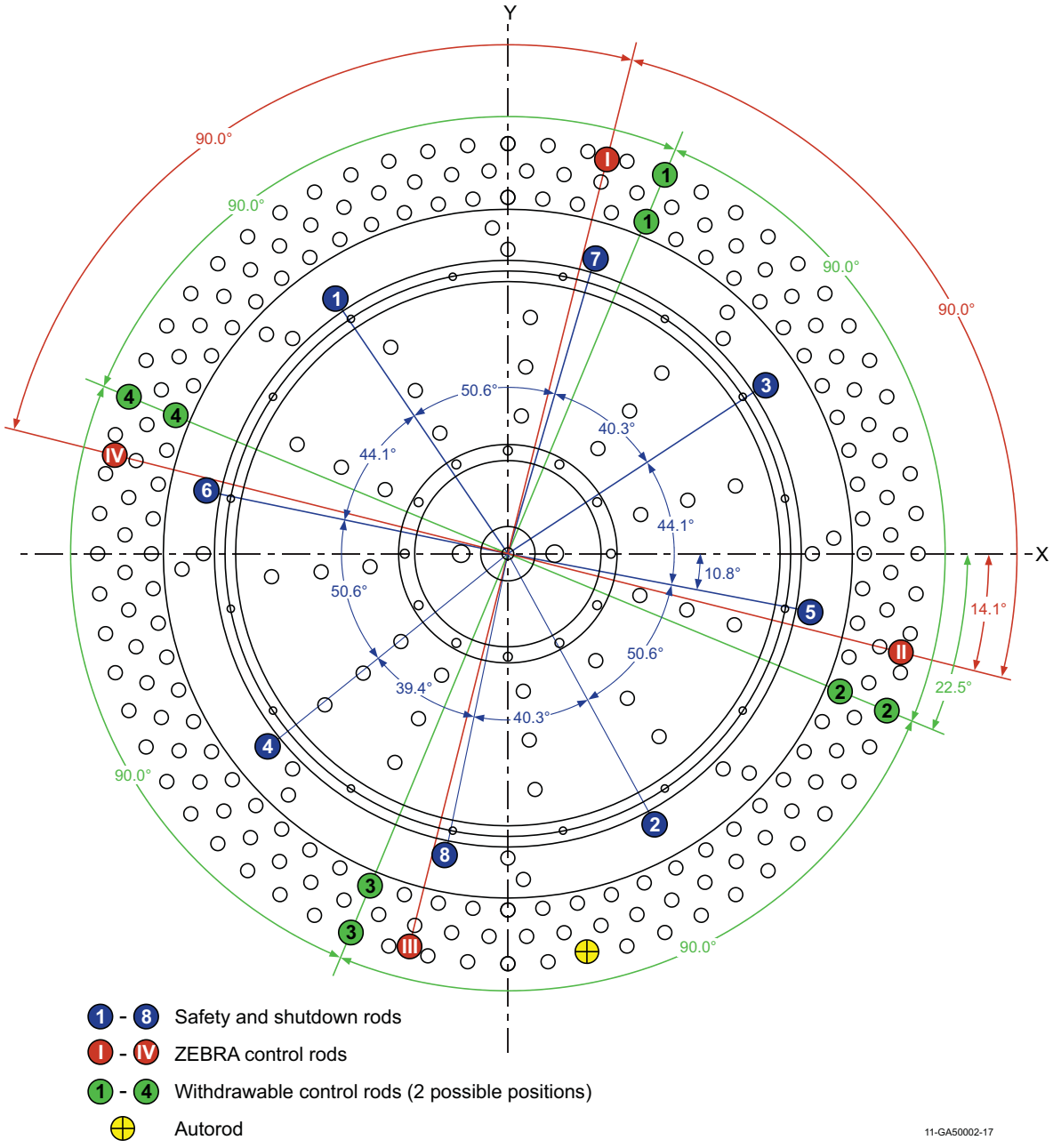

Figure 1.1-2b. HTR-PROTEUS Control Rod Positions and Bore Hole Locations (Ref. 2).

1.1.2.1 General HTR-PROTEUS Components

The following components are common to all HTR-PROTEUS core configurations.

Concrete

Concrete shielding surrounds the reactor system entirely (Ref. 2). The reactor is surrounded by 800 mm of concrete shielding. No significant room return effects from neutron streaming were measured.[a]

Steel Plate Pedestal

The PROTEUS assembly rests upon a stainless steel plate pedestal.[b]

Radial Reflector

The radial reflector was a 22-sided polygon with a height of 3304 mm and outer diameter of 3262 mm (see Figures 1.1-1 and 1.1-3). A central cavity sat with its base 780 mm above the reflector base and had a flat-to-flat separation distance of 1250 mm (Ref. 2 and 3). The central cavity contained fuel (16.7 wt.% enriched in ^{235}U) and moderator (pure graphite) pebbles either deterministically or randomly arranged in one of several different geometrical arrangements (Ref. 3).

The external boundary of the 22-sided polygon had sides located 1631.6 mm from the center, which would be an equivalent area cylinder of 1637.7 mm radius. The internal cavity was a 22-sided polygon with sides 626 mm from the center, which would be an equivalent area cylinder of 628.4 mm radius. In summary, the cavity had an average radial thickness ~1029 mm of graphite, and lower and upper axial thicknesses 780 mm of graphite.[b]

A cylindrical version of the radial reflector would have the following radius (the first value represents an equal perimeter, and the second value represents an equal area): external radius, 1643.6 and 1637.7 mm, respectively; internal radius for the 22-sided cavity, 630.6 and 628.4 mm, respectively.[c]

The radial reflector contains various minor penetrations serving as control rod and instrumentation channels. The reflector contained 308 C-Driver channels (see Figure 1.1-3), which were vertical channels of 27.43 mm diameter running the full height of the radial reflector and were left over from previous PROTEUS experiments. These channels were arranged in five concentric rings. Unless otherwise stated, these channels were filled with 26.5 mm diameter graphite rods (Ref. 2). These rods were relatively easy to remove and useful in estimating the effect of missing graphite (Ref. 3).

Attached to one side of the radial reflector was a reactor thermal column, which was a quasi-rectangular structure with a height and width of 1200 mm and a depth of ~500 mm. Its top surface was situated 1120 mm from the upper surface of the radial reflector (Ref. 2).

A safety ring was included in the design as an additional safety measure in the unlikely event that the upper axial reflector should fall into the cavity. It was comprised of a Peraluman ring 10 mm thick with inner and outer radii of 604 and 700 mm, respectively. It was situated 1764 mm above the floor of the cavity, as depicted in Figure 1.1-4 (Ref. 2).

---

[a] Williams, T., "HTR PROTEUS CORE 1: Reactivity Corrections for the Critical Balance," TM-41-93-20, Paul Scherrer Institut, Villigen, October 7, 1993.
[b] Difilippo, F. C., "Monte Carlo Calculations of Pebble Bed Benchmark Configurations of the PROTEUS Facility," *Nucl. Sci. Eng.*, **143**, 240-253 (2003).
[c] Difilippo, F. C., "Applications of Monte Carlo Simulations of Thermalization Processes to the Nondestructive Assay of Graphite," *Nucl. Sci. Eng.*, **133**, 163-177 (1999).

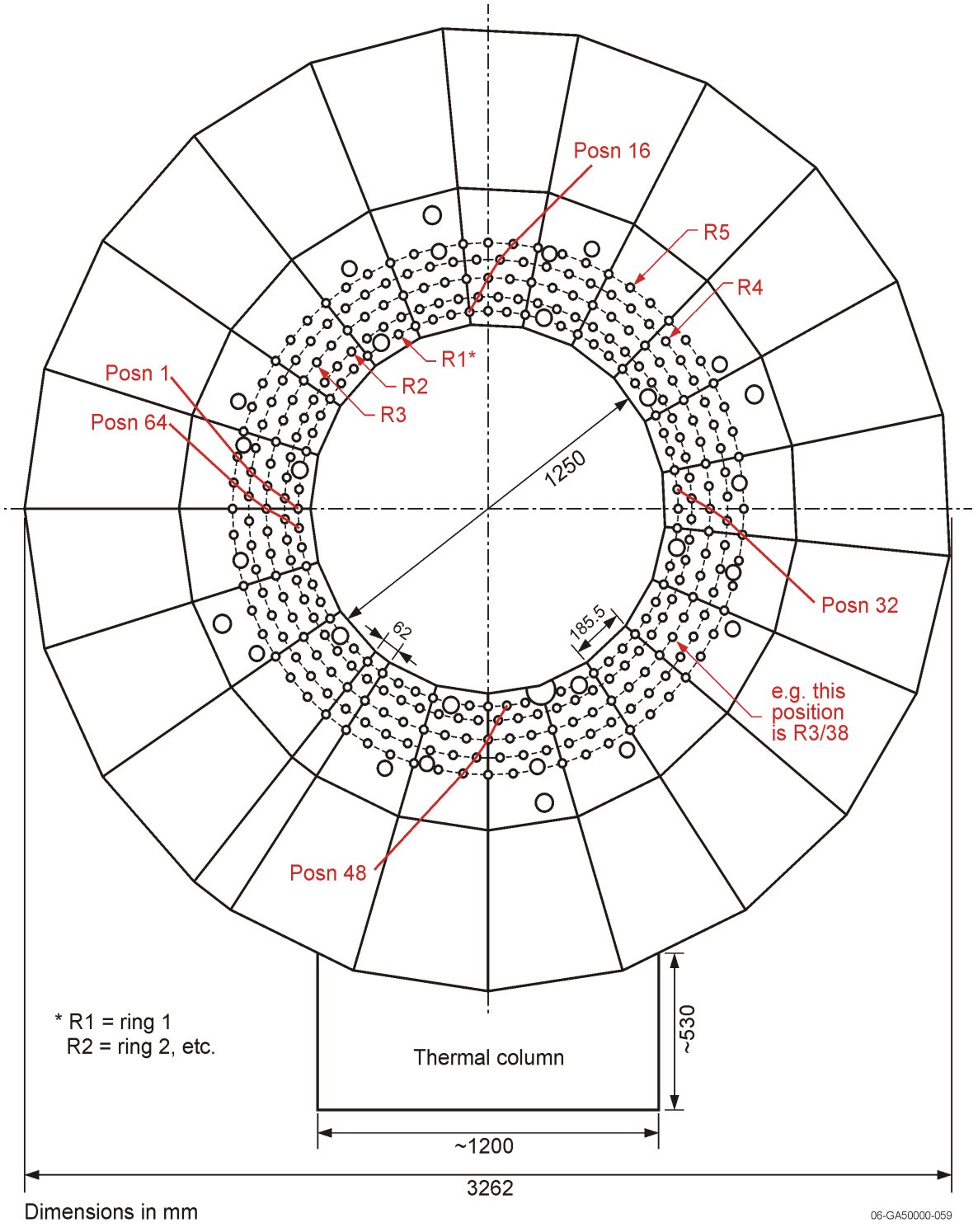

Figure 1.1-3. Cross Section View of the Radial Reflector (Ref. 2).

The radial reflector contained various minor penetrations for the introduction of instrumentation and sources. Explicit geometries and descriptions are unavailable. When not in use, the penetrations were filled with graphite plugs.

Upper Axial Reflector

Detailed drawings of the upper axial reflector and its aluminum housing are shown in Figures 1.1-4 through 1.1-6. The graphite has two components; the first component is a central cylinder of 394 mm diameter with a central, open, 27.43 mm diameter channel, surrounded by the second component, an annulus with an inner diameter of 418.6 mm and an outer diameter of 1234 mm. The annulus contains 33 coolant channels corresponding with those found in the lower axial reflector. All 34 channels are always open. The outer graphite annulus includes a separate outer shell consisting of 36 smaller, individual rectangular pieces that do not fit exactly flush with the bulk graphite. The upper axial reflector graphite had a height of 780 mm (Ref. 2).

The upper reflector tank is a complex structure that supports the upper axial graphite reflector in place above the cavity. It was comprised of two main parts, an inner and an outer tank. The inner tank, which contained the graphite cylinder, was removable, and it had to be removed before the outer tank could be removed. The outer tank contained the graphite annulus. The dimensions and layout of the upper reflector are shown in Figures 1.1-4 through 1.1-6. A steel lid and flanges, external to the core reflector, were used to hold the upper reflector above the core cavity (Ref. 2).

The upper axial reflector closed the cavity at a height of 1863 mm from the bottom of the cavity.[a]

[a] Difilippo, F. C., "Monte Carlo Calculations of Pebble Bed Benchmark Configurations of the PROTEUS Facility," *Nucl. Sci. Eng.*, **143**, 240-253 (2003).

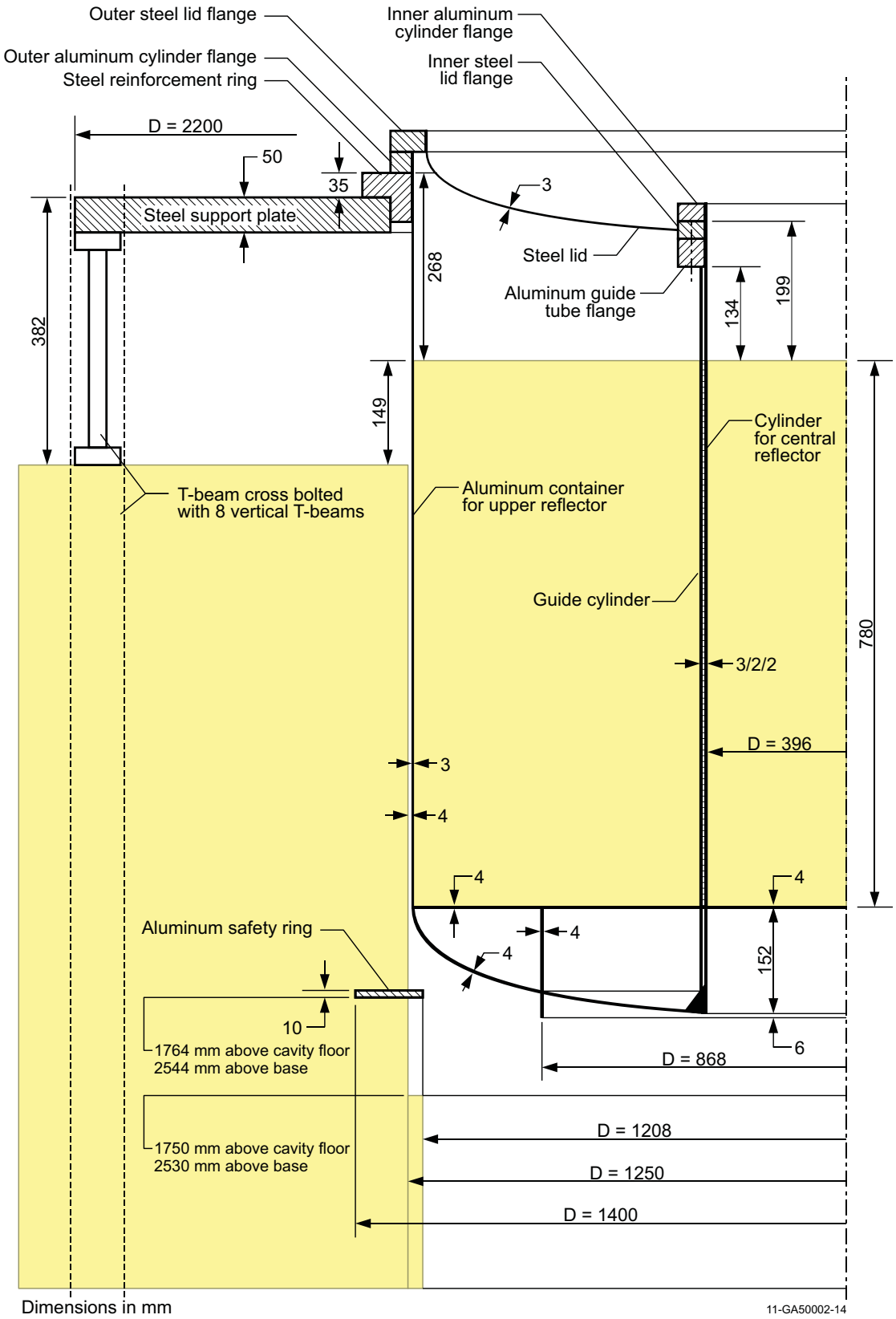

Figure 1.1-4. Placement of the Upper Axial Reflector (Ref. 2).

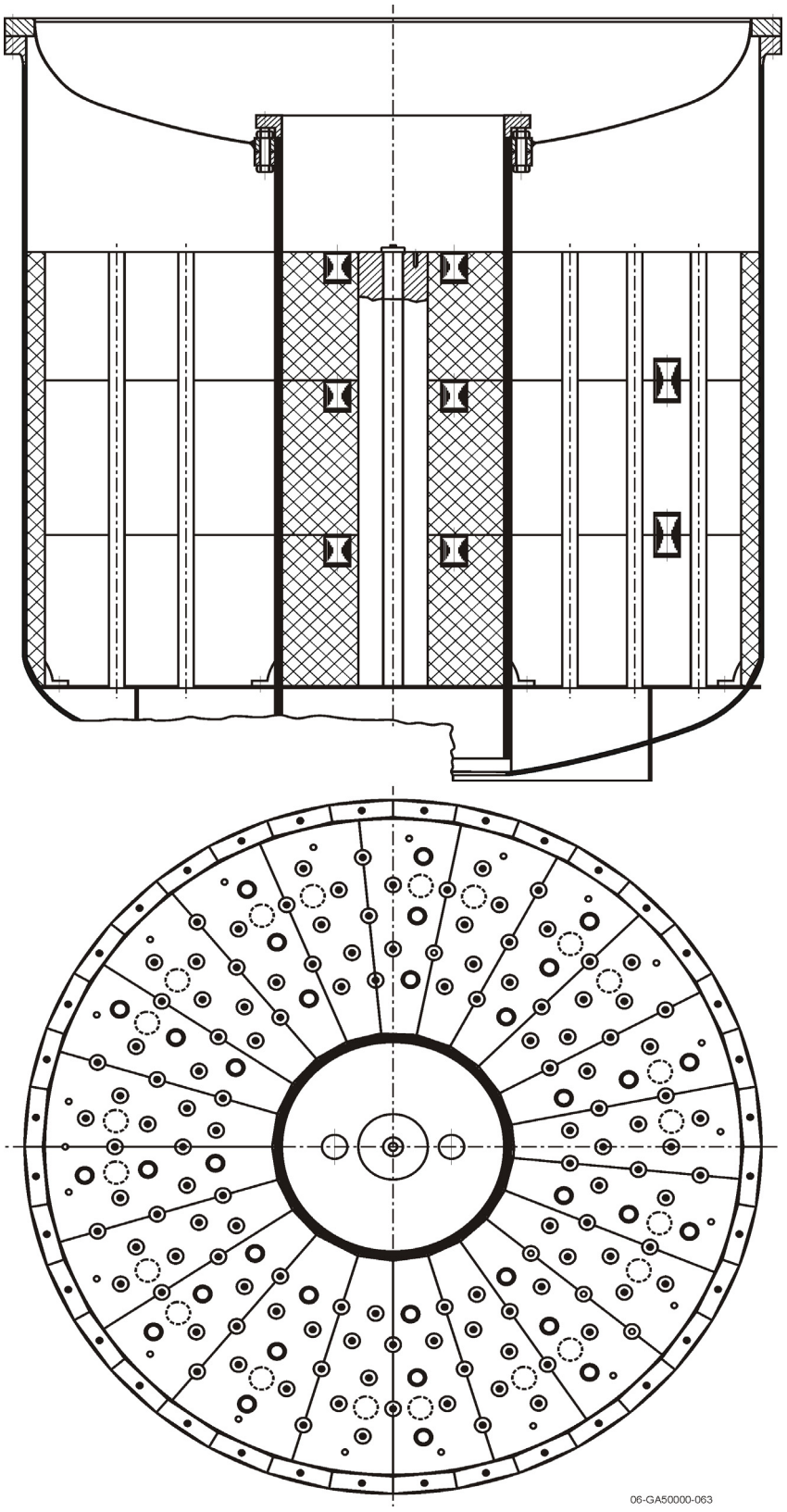

Figure 1.1-5. Non-dimensional Cross Sections of the Upper Axial Reflector (Ref. 2).

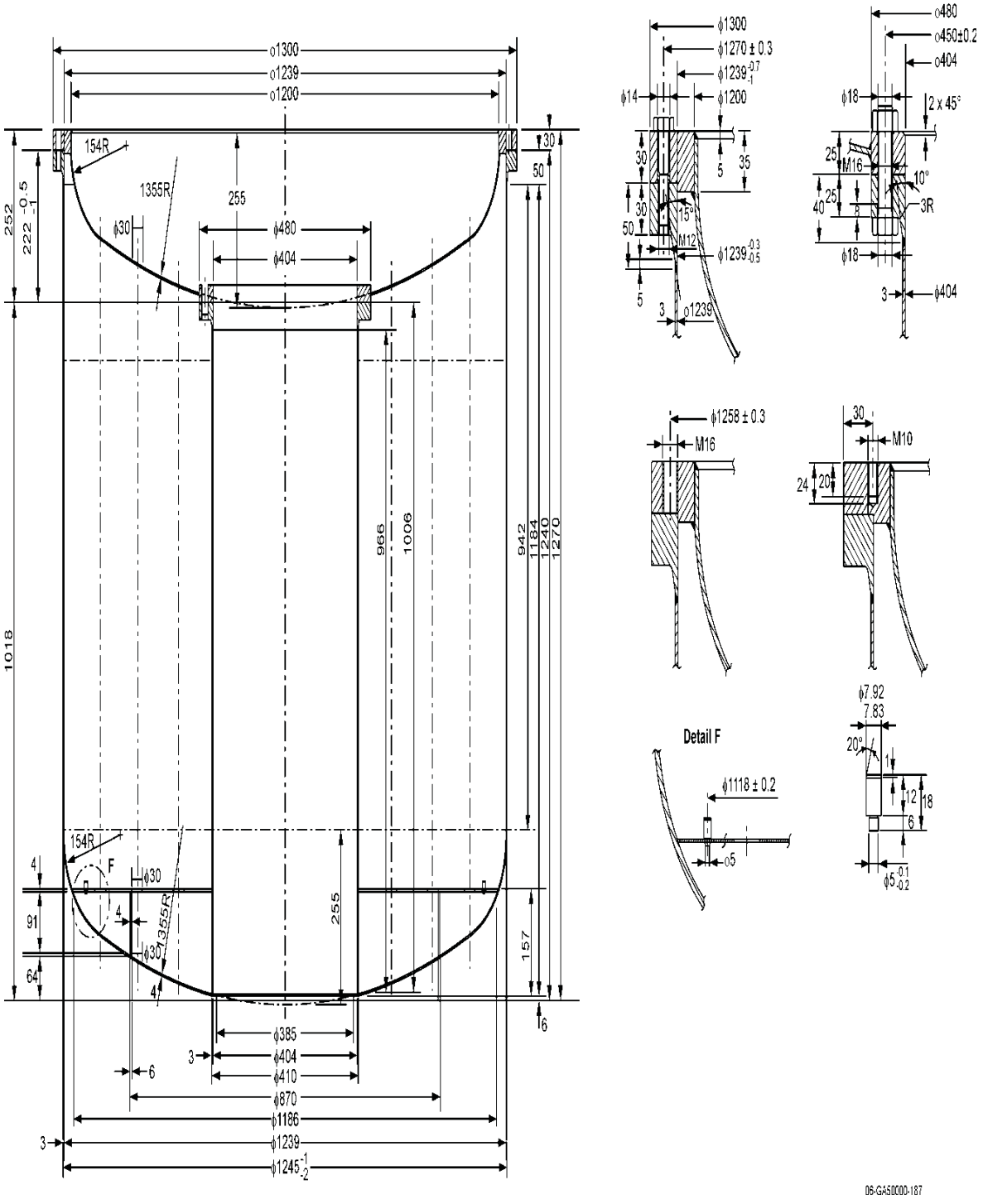

Figure 1.1-6. Details of the Main Aluminum Structure of the Upper Axial Reflector (Ref. 2). Units are in millimeters.

Lower Axial Reflector

The lower axial reflector is 780 mm thick and contains, for historical reasons, 160 symmetrically positioned 27.42 mm diameter channels. At least 127 of these channels were filled with 780 mm long, 26.5 mm diameter graphite rods. The dimensions of the lower axial reflector are shown in Figure 1.1-7; the positions of the 33 (typically open) coolant channels are also indicated. The open channels are arranged in three concentric rings of radii 300, 410, and 515 mm, with each ring containing eleven channels. The channels in each ring are positioned at azimuthal angles of 16.875, 50.625, 84.375, 118.125, 140.625, 174.375, 208.125, 241.875, 275.625, 309.375, and 343.125º, as measured in the clockwise direction from the +x-axis, as shown in Figure 1.1-2 (Ref. 2). In some of the core configurations all of the coolant channels in the lower axial reflector were filled with graphite plugs (Ref. 3). In all the deterministic cores, ~12 pebbles were directly over one of the 33 cooling channels in the lower axial reflector. To avoid pebble displacement in these cases, special aluminum plugs were developed to support the pebbles in Core 1. In later cores, simple graphite rods were used (Ref. 3).

A special, 121 mm diameter, channel was provided in the center of the lower axial reflector with approximately 500 mm of graphite separating it from the core. This channel could be used for measurements using the pulsed neutron source. The pulsed neutron source, when used for subcriticality measurements, was partially inserted into the lower axial reflector. When not in use, it was replaced with a plug of graphite of dimensions 250 mm in height and 120 mm in diameter (Ref. 2 and 3).

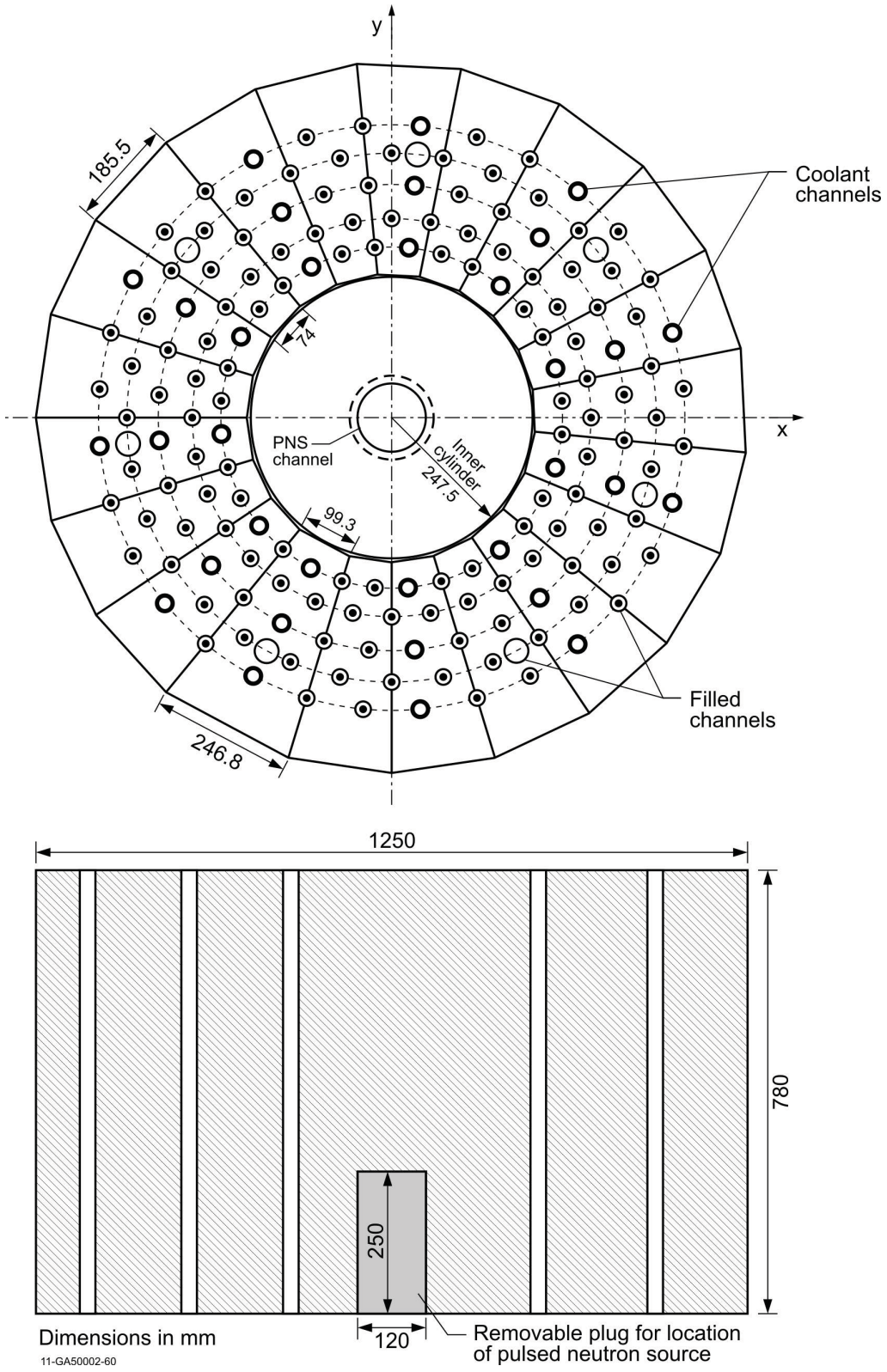

Figure 1.1-7. Details of the Lower Axial Reflector. Note the 33 coolant channels, the small air gap between outer and inner parts, and the position of the pulsed source channel (Ref. 2).

Safety/Shutdown Rods

There were eight, identical, borated-steel safety/shutdown rods located adjacent to the core in the radial reflector (see Figure 1.1-2). These rods were separated into two groups of four rods (rods 1-4 and rods 5-8). One of these groups was selected as the "safety rod" group and the other as the "shutdown rod" group. These rods were not used as control rods, such as the four ZEBRA type rods used in Core 1 or the withdrawable stainless steel control rods used in Cores 1A through 10 (Ref. 2 and 3).

Rods numbered 1 through 4 are the shutdown rods and rods numbered 5 through 8 are the safety rods.[a]

The safety/shutdown rods consisted of 35 mm diameter borated steel rod sections enclosed in 18/8 stainless steel tubes with an inside diameter of 36 mm and outside diameter of 40 mm. The rods were located in 45 mm inner diameter graphite guide tubes within the radial reflector. The centers of the guide tubes were 684 mm from the center of the core, or about 59 mm from the inner surface of the radial reflector (without filler pieces). The azimuthal positions of the eight rods are shown in Figure 1.1-2, in which the slight azimuthal asymmetry of the rod positions should be noted (Ref. 2 and 3).

A diagram of a safety/shutdown rod is shown in Figure 1.1-8; the borated steel portion of the rods was 2100 mm in length. The fully in and out positions of the rods are shown in Figure 1.1-9; the rods traveled a total distance of 2900 mm (2530 mm free fall plus 370 mm braking distance) from fully withdrawn to fully inserted positions. When fully inserted, the bottom of the borated steel region is located 350 mm below the bottom of the reactor cavity with the top of the borated steel region slightly above the top of the 1730 mm high cavity. When fully withdrawn, the bottom of the borated steel region is 26 mm below the top surface of the radial reflector (Ref. 2).

Each rod contains six, 35 mm diameter, 350 mm long, cylindrical pieces of borated steel. Aluminum and steel shock dampers were located under each of the safety/shutdown rods, as shown in Figure 1.1-9, to prevent damage in case one of the rod cables should fail. A gap of approximately 30 mm separated the bottom of the safety rod from the upper, aluminum part of the shock damper. The aluminum parts of the shock damper was comprised of a 280.5 mm long hollow tube with 29 mm inner diameter, 40 mm outer diameter, and capped at both ends with aluminum of 2 mm thickness. The steel parts of the shock dampers (end caps, springs, and damper chamber) were affixed to the underside of the lower support plate, which itself is ~75 mm thick; only a fraction of the total mass of these components resided within the graphite reflector (Ref. 2).

The safety rods were always maintained in withdrawn positions, i.e., out of the reflector. Criticality was achieved when the four shutdown rods were also fully withdrawn and only the four control rods and the autorod were partially inserted for fine control.[b,c]

[a] Köberl, O., and Seiler, R., "Detailed Analysis of Pebble-Bed HTR PROTEUS Experiments with the Monte Carlo Code TRIPOLI4," Proc. 2nd Int. Topical Mtg. on High Temperature Reactor Technology, Beijing, China, September 22-24, 2004.
[b] Chawla, R., Joneja, O. P., Rosselet, M., and Williams, T., "Definition and Analysis of an Experimental Benchmark on Shutdown Rod Worths in LEU-HTR Configurations," *Nucl. Technol.*, **139**, 50-60 (2002).
[c] Köberl, O., Seiler, R., and Chawla, R., "Experimental Determination of the Ratio of 238U Capture to 235U Fission in LEU-HTR Pebble-Bed Configurations," *Nucl. Sci. Eng.*, **146**, 1-12 (2004).

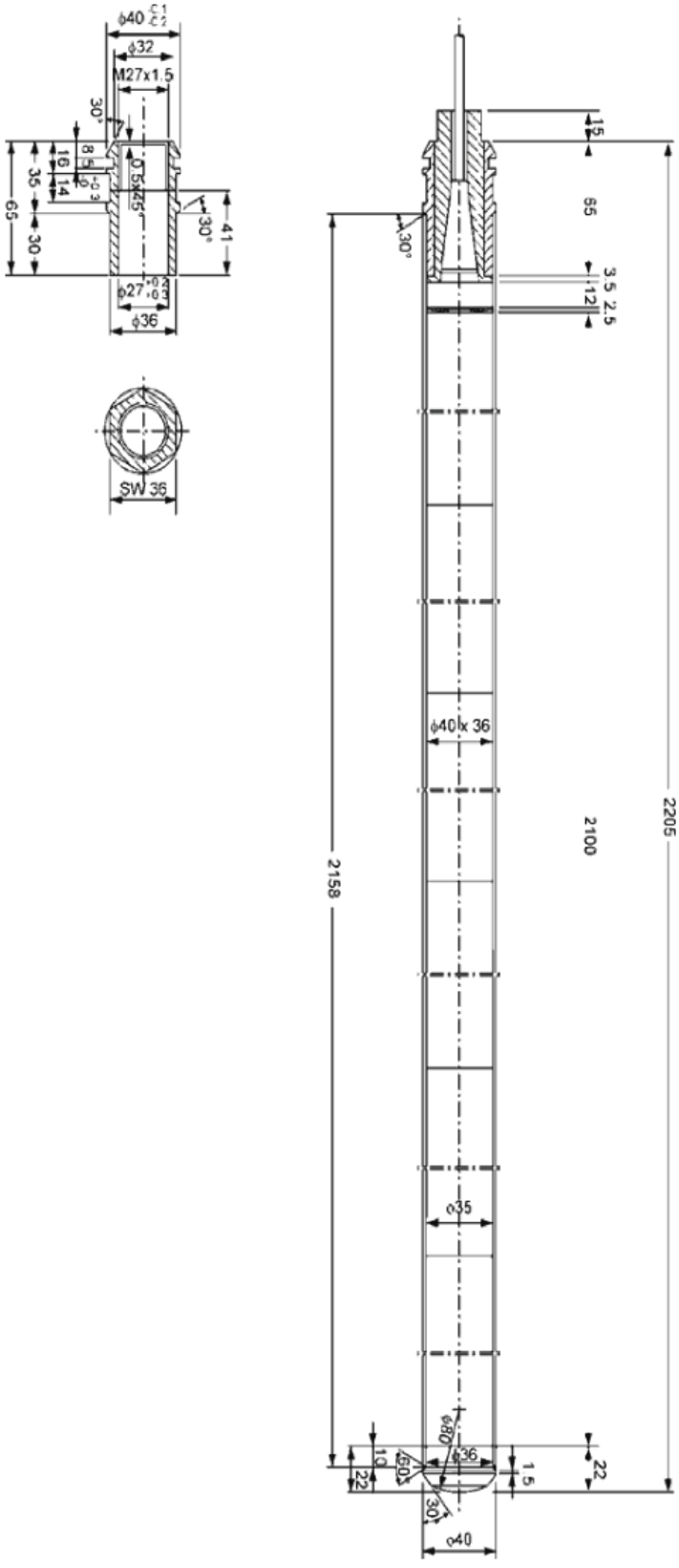

Figure 1.1-8. Details of Safety/shutdown Rods (Ref. 2). Units are in millimeters.

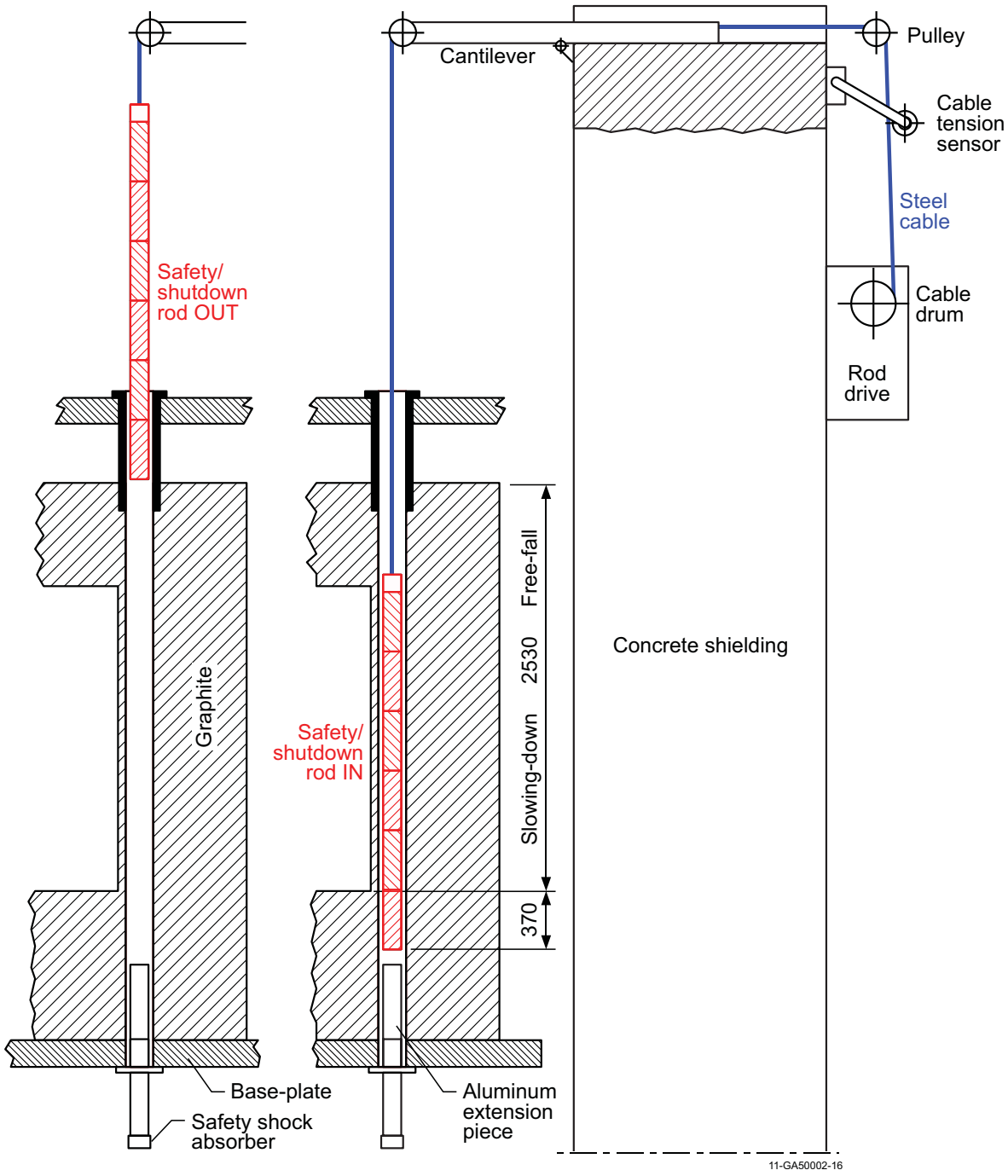

Figure 1.1-9. Safety/shutdown Rod Movement (Ref. 2). Units are in millimeters.

Automatic Control Rod (Autorod)

A single, fine control rod (Figure 1.1-10) was utilized to automatically maintain reactor criticality at a nominal required power. It responded to signals from a single ionization chamber (deviation channel) located in the radial reflector 810 mm above the cavity floor and ~500 mm from the outer radial boundary of the core. The rod itself is located in a vertical channel with an inside diameter of 55 mm situated 890 mm from the radial center of the system; it was located azimuthally ~80º from the x-direction in a clockwise direction (see Figure 1.1-2). The rod was comprised of a wedge shaped copper plate supported within an aluminum tube with an outer diameter of 44 mm. The copper plate was 3 mm thick, 2300 mm long, and 39 mm at its wide end with a reduction in width along its length of 17 mm per meter. The rod was fully inserted when the position display showed 0 mm and the pointed end of the copper plate was flush with the underside of the steel plate upon which the reactor stands. The complete withdrawal of the autorod was indicated by a display of 1000 mm when the pointed end of the copper plate was ~200 mm above the base of the core cavity and the blunt end was 79 mm below the top of the radial reflector graphite. Because the rod remains within the system even when fully "withdrawn" it has a significant rest worth that is larger than the total max-min worth of the rod.

The worth of the autorod exhibits a linear response over the range of 200 to 800 mm with a differential control rod worth of 6.3×10^{-3} ¢/mm (β_{eff} = 0.00723) and an uncertainty of around 5 %. The autorod response was intercalibrated with the ZEBRA (and later withdrawable) control rods.[a]

[a] Williams, T., "HTR PROTEUS CORE 1: Reactivity Corrections for the Critical Balance," TM-41-93-20, Paul Scherrer Institut, Villigen, October 7, 1993.

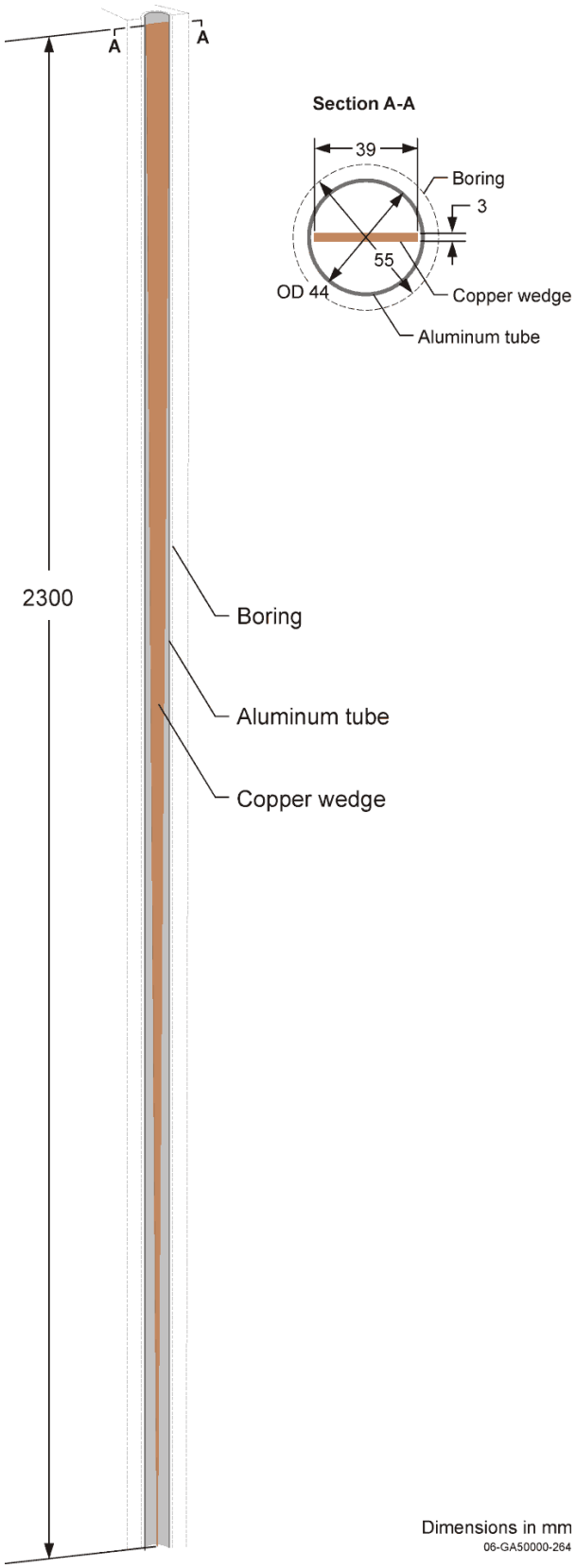

Figure 1.1-10. Automatic Control Rod (derived from Ref. 2).

Static Measurement Rods

Simulated control rods were manufactured for these experiments to investigate the spatial dependence of control rod worths in a particular configuration; this was necessary because the operational control rods were very restricted in their locational possibilities. These rods were designed to be inserted in either C-Driver channels in the radial reflector or into a specially designed graphite sleeve which replaced a column of pebbles in the columnar hexagonal cores. Because the core and radial reflectors were of significantly different heights, two pairs of rods were produced; apart from the axial dimensions, they were nominally identical (Ref. 2 and 3).

The rods consisted of cylindrical assemblies with an outer diameter of 26 mm and 2 mm thick Peraluman R-257 wall. The shorter pair of tubes contained eleven, 22 mm diameter, borated steel pieces of various lengths between 120 and 180 mm, totaling 1581 ± 1 mm in each assembly. The longer pair contained a total of 1711 ± 1 mm of borated steel pieces. The longer rods also contained a graphite filler piece, above the borated steel section, with a length of 1414 mm. Figure 1.1-11 and 1.1-12 show the long and short variations of the static measurement rods, respectively. The dimensions of both pairs of rods were arranged such that the borated steel regions were similarly located with respect to the axial position of the fuelled region. When the longer rods were resident in the radial reflector, the bottom of the hole in the upper hanger was flush with the upper surface of the upper steel support plate. When the shorter rod was inserted in the core region, it rested on the cavity floor. The graphite sleeve for the shorter rods (shown in Figure 1.1-13) had a length of 1730 mm, an inner diameter of 27 mm, and an outer diameter of 60 mm (Ref. 2).

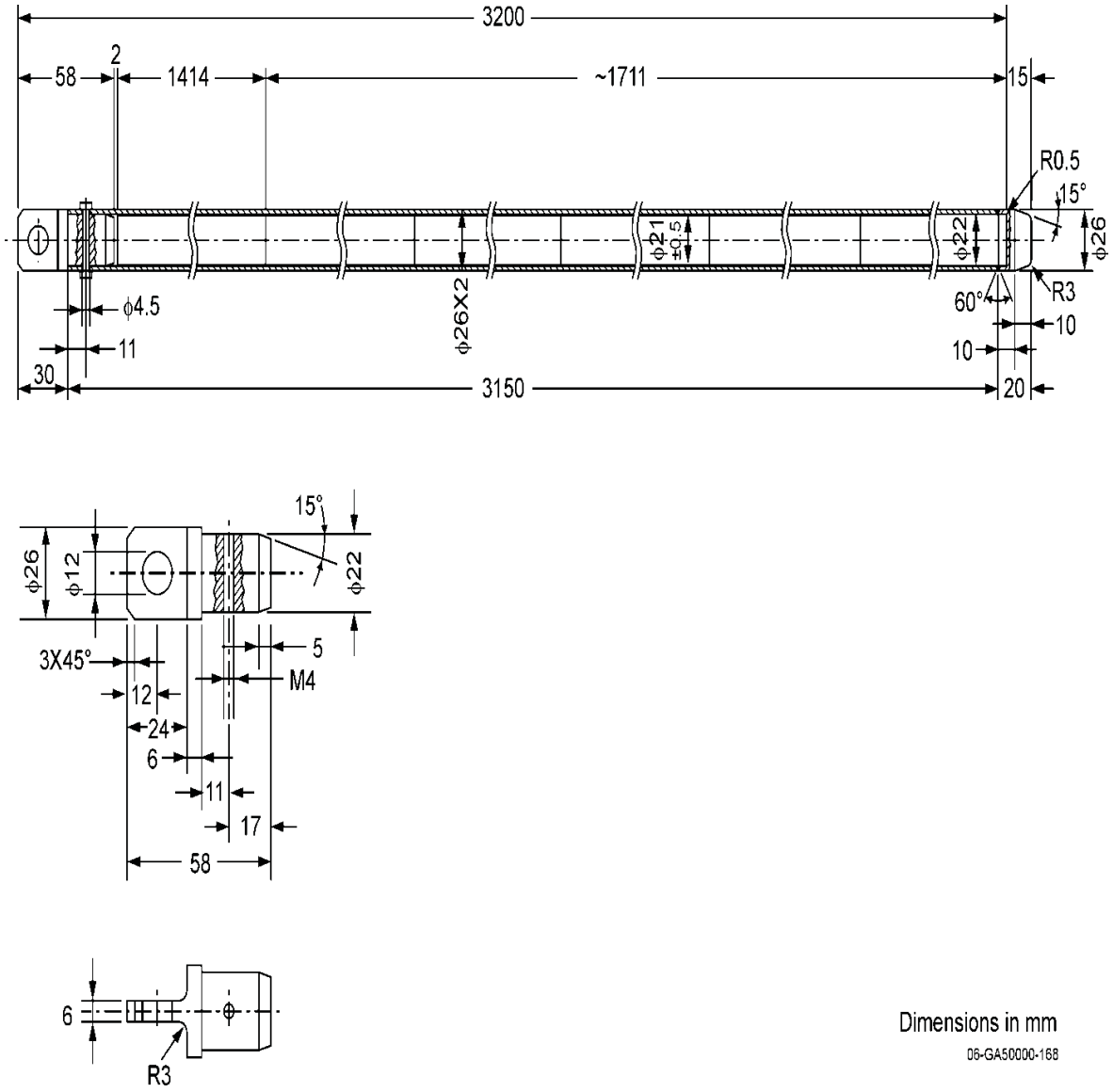

Figure 1.1-11. Details of the Long Static Measurement Rod (Ref. 2).

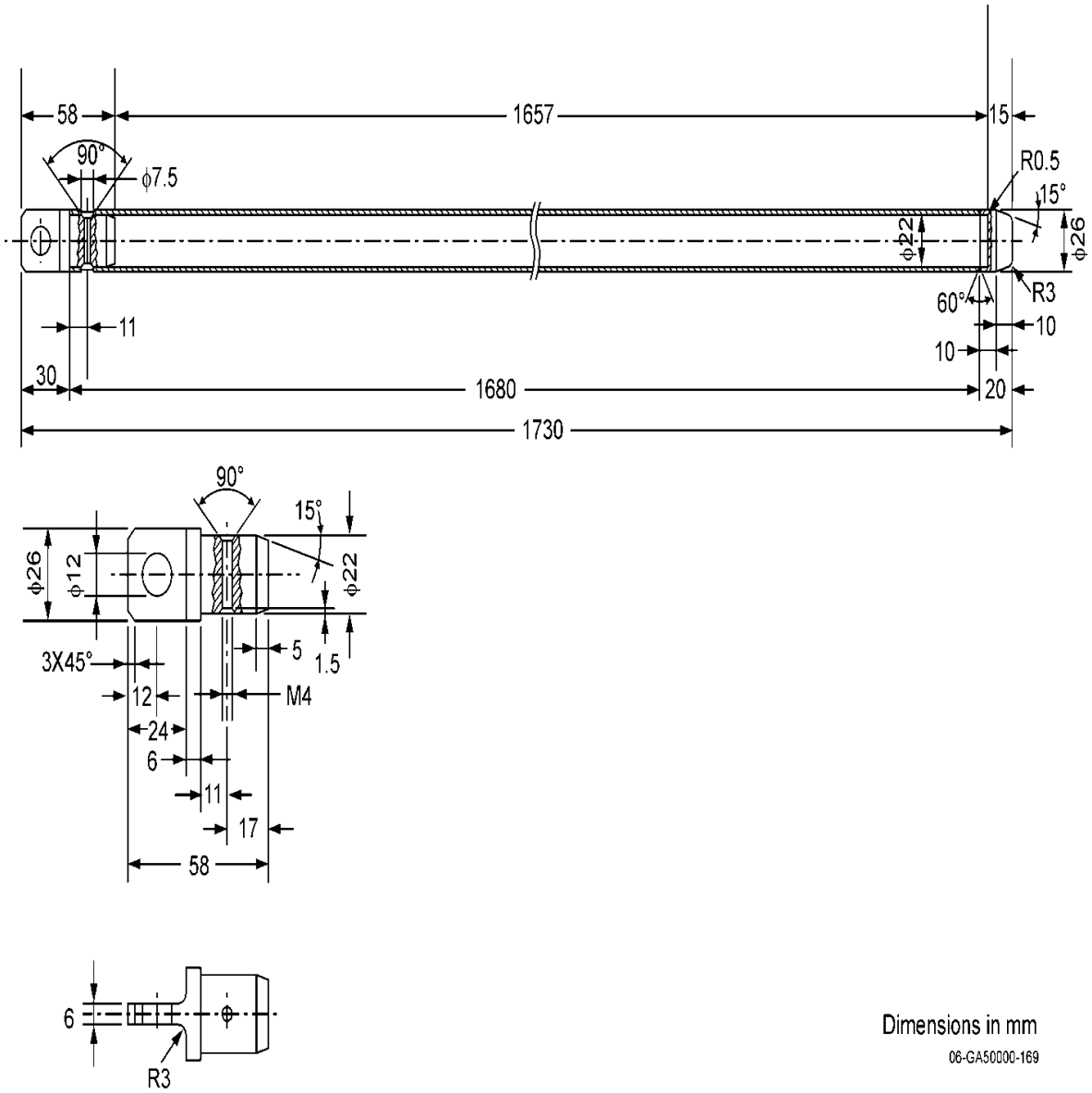

Figure 1.1-12. Details of the Short Static Measurement Rod (Ref. 2).

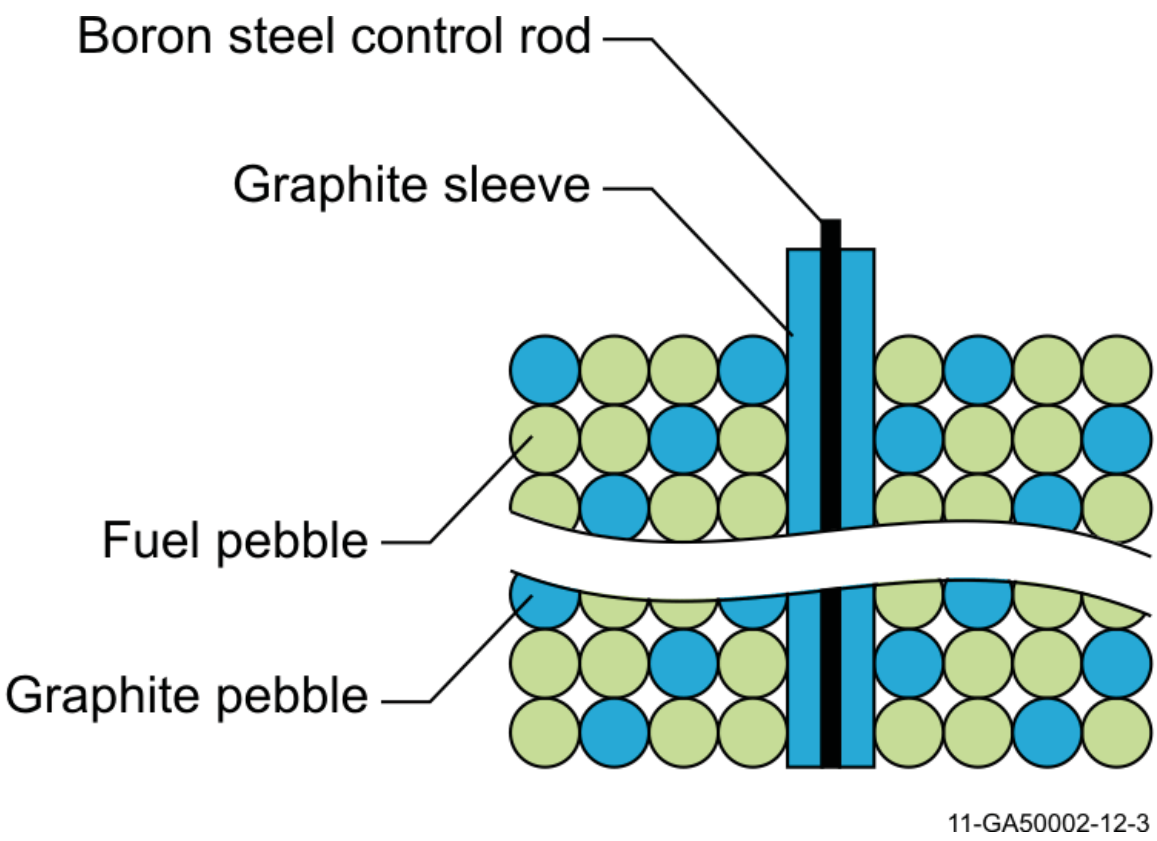

Figure 1.1-13. Graphite Sleeve for Short Static Measurement Rod (Ref. 2).
Figure is schematic and does not represent a random core pebble packing.

Fuel Pebbles

The fuel pebble physical properties are provided in Table 1.1-1. Unless otherwise noted, these properties were obtained from the original quality control records. The specified values are averages with their corresponding 1σ standard deviations. The diameter and mass of the fuel pebbles were measured at PSI on August 17, 1992, and again on October 30, 1995. The masses of the fuel pebbles did not change significantly over the >3 year time period. However, there was a slight reduction in the fuel pebble diameter, presumably due to slight indentations of the surface caused during the loading process, and is considered insignificant.[a] Measurements performed on August 17, 1992, are recommended by PSI for use in modeling these experiments (Ref. 2 and 3). The construction and dimensions of the fuel pebble are shown in Figure 1.1-14.

Fuel for the experiments was provided by the KFA Research Center in Jülich, Germany (Ref. 3).

Arbeitsgemeinschaft Versuchsreaktor (AVR)-type fuel pebbles were employed in the HTR-PROTEUS experiments. Fuel particles were distributed randomly throughout the graphite matrix of the fuel pebbles.[b]

Some 5460 LEU AVR fuel pebbles were transferred from the LEU HTR experimental program in the AVR test facility to the PROTEUS facility in March and April of 1992.[c]

There are 9394 fuel kernels in the fuel region of each fuel pebble.[d]

[a] The HTR-PROTEUS Core 5 had been loaded three times over the course of 1.5 years; the variation in the reactivity was insignificant, which is a strong indication that the change in mass was negligible.
[b] Chawla, R., Joneja, O. P., Rosselet, M., and Williams, T., "Definition and Analysis of an Experimental Benchmark on Shutdown Rod Worths in LEU-HTR Configurations," *Nucl. Technol.*, **139**, 50-60 (2002).
[c] Brogli, R., Mathews, D., and Seiler, R., "HTR Roteus Experiments," Proc. 2nd JAERI Symposium on HTGR Technologies, Oarai, Japan, October 21-23, 1992, p. 233-239, JAERI-M 92-215 (1993).
[d] Difilippo, F. C., "Monte Carlo Calculations of Pebble Bed Benchmark Configurations of the PROTEUS Facility," *Nucl. Sci. Eng.*, **143**, 240-253 (2003).

Table 1.1-1. Fuel Pebble Physical Specifications (Ref. 2 and 3).[a]

^{234}U mass per fuel pebble	0.008	±	0.001	gram
^{235}U mass per fuel pebble	1.000	±	0.010	gram
^{236}U mass per fuel pebble	0.005	±	0.001	gram
^{238}U mass per fuel pebble	4.953	±	0.050	gram
Total uranium mass per fuel pebble	5.966	±	0.060	gram
Carbon mass per fuel pebble	193.1	±	0.2	gram
Total mass per fuel pebble[b],[c]	202.22	±	0.18	gram
Fuel pebble inner (fueled) zone radius[d]	2.350[f]	±	0.025	cm
Fuel pebble outer radius	3.0006	±	0.002	cm
Radius of fuel particles (UO_2 substrates)[e]	0.02510[f]	±	0.0010[g]	cm
Thickness of particle buffer coatings (C)	0.00915	±	0.0025[h]	cm
Thickness of particle inner PyC coatings[e]	0.00399	±	0.0010[h]	cm
Thickness of particle SiC coatings	0.00353	±	0.0004[h]	cm
Thickness of particle outer PyC coatings[e]	0.00400	±	0.0008[h]	cm
Density of fuel particles (UO_2 substrates)	10.88	±	0.04	g/cm^3
Density of fuel particle buffer coatings (C)	1.10	+0	-0.11[i]	g/cm^3
Density of fuel particle inner PyC coatings	1.90	±	0.05	g/cm^3
Density of fuel particle SiC coatings	3.20	±	0.02	g/cm^3
Density of fuel particle outer PyC coatings	1.89	±	0.05	g/cm^3

(a) The fuel pebble masses and outer diameters were measured at PSI on August 17, 1992, and October 30, 1995. The second series of measurements indicated a significant reduction of the pebble diameter over the 3 years of operation; however, since the mass measurements indicated no such decrease it was assumed that the apparent diameter reduction was due to indentations in the pebbles caused during handling and not from a general loss of material.
(b) The total mass of oxygen and silicon in the fuel pebbles was not reported.
(c) There is a discrepancy of 0.86 g (0.43 %) in the total fuel pebble mass of 201.4 g computed from the individual components provided in the table as compared with the measured fuel mass of 202.22 ± 0.18 g on August 17, 1992.
(d) The 47 ± 0.5 mm diameter of the fuelled region obtained from neutron radiographs made by E. Lehmann at the PSI Saphir reactor corresponds with the 47 mm diameter fuelled region given by Gontard et al. (KFA Jülich report HBK-IB-10/86).
(e) There are slight differences in the reported radius/thickness between this table and Figure 1.1-14; the differences are within their reported 1σ uncertainties.
(f) The last significant digit on these two values, zero, is not reported in Reference 3 but is reported in Reference 2.
(g) The uncertainty in the UO_2 particle radius is a 90 % confidence value.
(h) The uncertainties in the particle coating thicknesses are 95 % (2σ) confidence values.
(i) The density of the fuel particle buffer coatings is stated to be ≤1.1 g/cm^3. The one-sided 10 % uncertainty (1σ) was assumed by the authors of the reference reports in the absence of measured data.

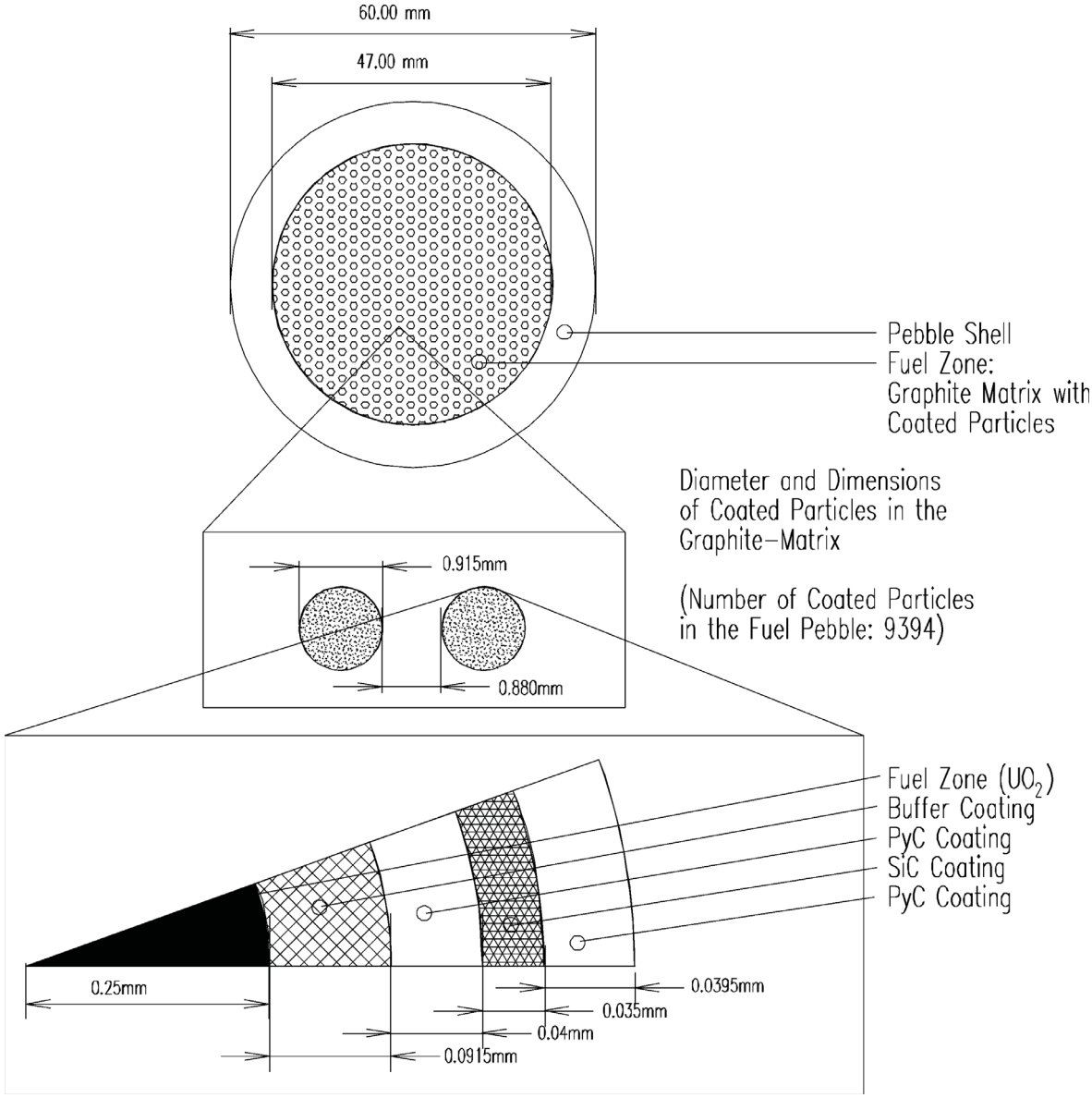

Figure 1.1-14. HTR-PROTEUS Fuel Pebble and Coated Fuel Particle (Ref. 2 and 3).

Moderator Pebbles

The physical properties of the moderator pebbles (Table 1.1-2) were obtained from measurements performed at PSI on August 17, 1992, May 3, 1995, and October 30, 1995. These values correspond well with those provided in relevant quality control records. The specified values are averages with a 1σ standard deviation. There were no significant changes noted in the properties of the moderator pebbles throughout the course of these experiments (Ref. 2).

Table 1.1-2. Moderator Pebble Physical Specifications (Ref. 2 and 3).

Moderator Pebble Mass	190.54	±	1.44	g
Moderator Pebble Outer Radius	2.9979	±	0.0015	cm

Start-Up Source

The reactor start-up sources were normally in their "in" position during reactor operation. At low fluxes their reactivity effect is positive by virtue of the apparent enhanced neutron multiplication; at normal operating fluxes of $>10^7$ n/cm^2/s, their effect was negative due to parasitic neutron absorption in the source and casing. The start-up sources pass through horizontal aluminum guide tubes situated in the radial reflector at about the level of the cavity floor (Ref. 3).

Detectors

There are a total of eight detection channels used for nuclear instrumentation: three safety channels, two impulse channels, one logarithmic channel, one linear channel, and one deviation channel. Apart from the two impulse channels, which were fission chambers, all the instrumentation consisted of large ionization chambers (220 mm × 90 mm Ø) situated in horizontal channels in the reflector at a radius of ~1000 mm (Ref. 3).

Temperature Sensors

There are typically four separate temperature sensors in the system: two in the core and two in the radial reflector (Ref. 3).

1.1.2.2 Components Unique to Core 4

The following components are unique to core configuration 4.

Graphite Fillers

Graphite filler pieces were utilized to support the outer surfaces of the various deterministic configurations and to modify the shape of the cavity floor to avoid ordering effects in random core configurations (Ref. 2). The graphite filler pieces used to modify the axial walls of the cavity were not used for Core 4.

The cavity floor fillers were comprised of 21wedge shaped pieces combined to form a quasi-conical bottom with a 10º slope from the cavity walls down to a point located at a radius of 250 mm from the center of the cavity. The central part of the cavity floor remained unchanged (Ref. 2). A depiction of the cavity floor fillers and their placement within the cavity is shown in Figure 1.1-15.

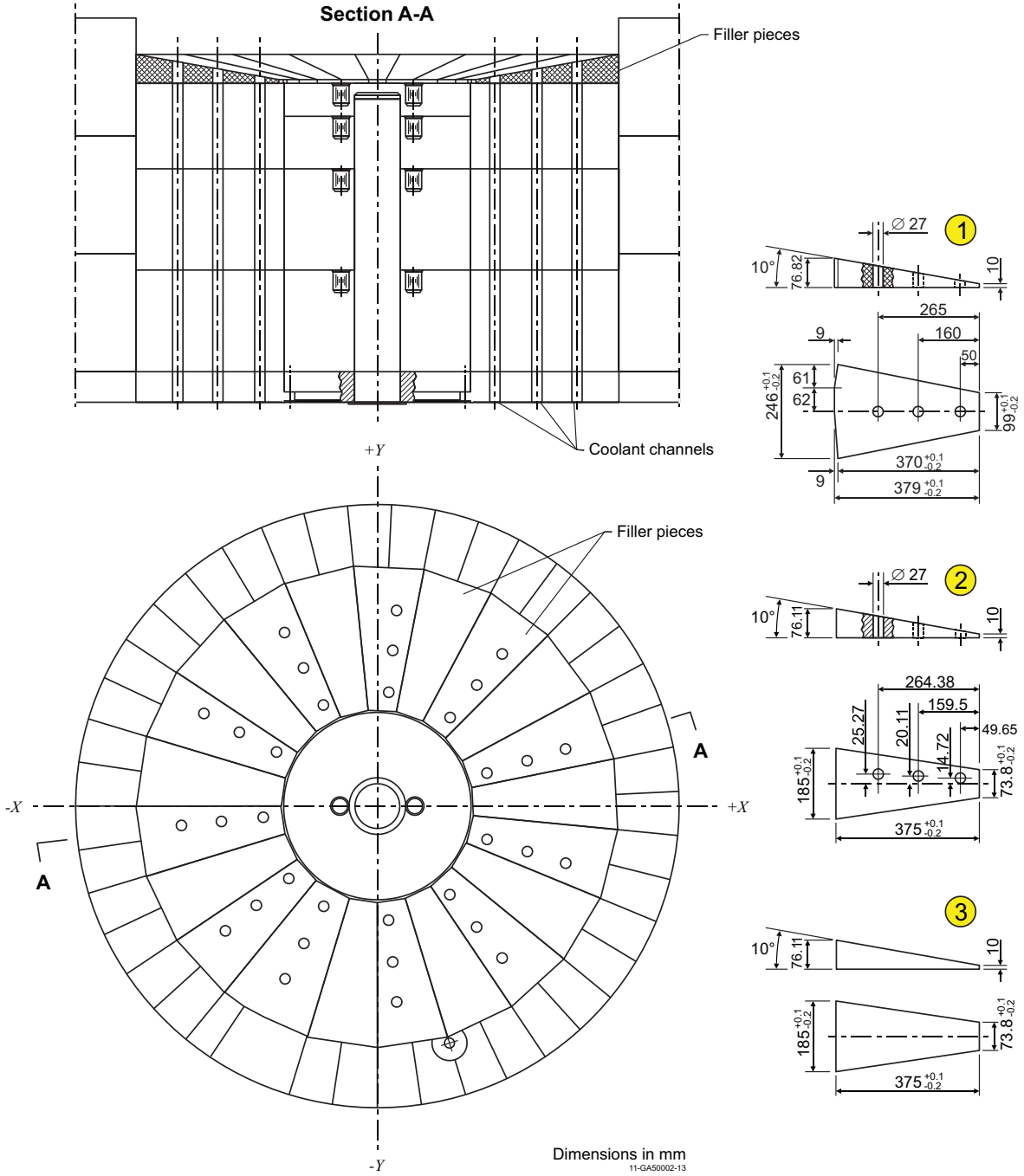

Figure 1.1-15. Positioning of the Cavity Floor Graphite Filler Pieces used in the Random Cores (Ref. 2).

ZEBRA Control Rods

The ZEBRA control rods were not used in the experiments with Core 4.

Withdrawable Stainless Steel Control Rods

The ZEBRA type control rods used in Core 1were replaced with four withdrawable stainless steel control rods for Cores 1A through 10. The stainless steel rods were placed in four C-Driver channels, instead of the channels used for the ZEBRA rods, but close to the original ZEBRA positions (see Figure 1.1-2). These rods were intended to increase operational flexibility and were designed to operate at two radii: 789 mm (ring 3) or 906 mm (ring 5). They were exclusively used in ring 5 throughout the measurements due to the thermal flux gradient in the radial reflector at these positions (Ref. 2 and 3).

Each rod was comprised of two concentric stainless steel tubes. The inner stainless steel (type St1.4301) tube had an inner diameter of 9.5 mm, outer diameter of 13.5 mm, and length of 2150 mm; this tube could contain various materials, such as B_4C pellets, to further adjust the rods' worth. The outer stainless steel (type St1.4541) rod had an inner diameter of 14 mm, outer diameter of 22 mm, and length of 2149 mm; this rod was added as a means of increasing rod mass to achieve a satisfactory cable tension. Stainless steel plugs were used to seal both ends of the tubes. The total rod length, including end-stops, was 2200 mm. Technical drawings of these rods are provided in Figure 1.1-16. The rods are fully inserted when the base of the cavity in the inner tube corresponded to the core cavity floor with the tips of the rods lying 25 mm below this; the indicated rod position on the control panel was 2500 mm. The rods are fully withdrawn when the control panel indicated ~6 mm and the rod tips were just 49 mm below the upper surface of the radial reflector. The total rod range was 2494 mm. The bottom of each control rod channel was filled with a 26.5 mm diameter, 730 mm long graphite plug, leaving an air gap of 25 mm below the rod tip (Ref. 2).

No inserts were placed within these stainless steel control rods (Ref. 2).

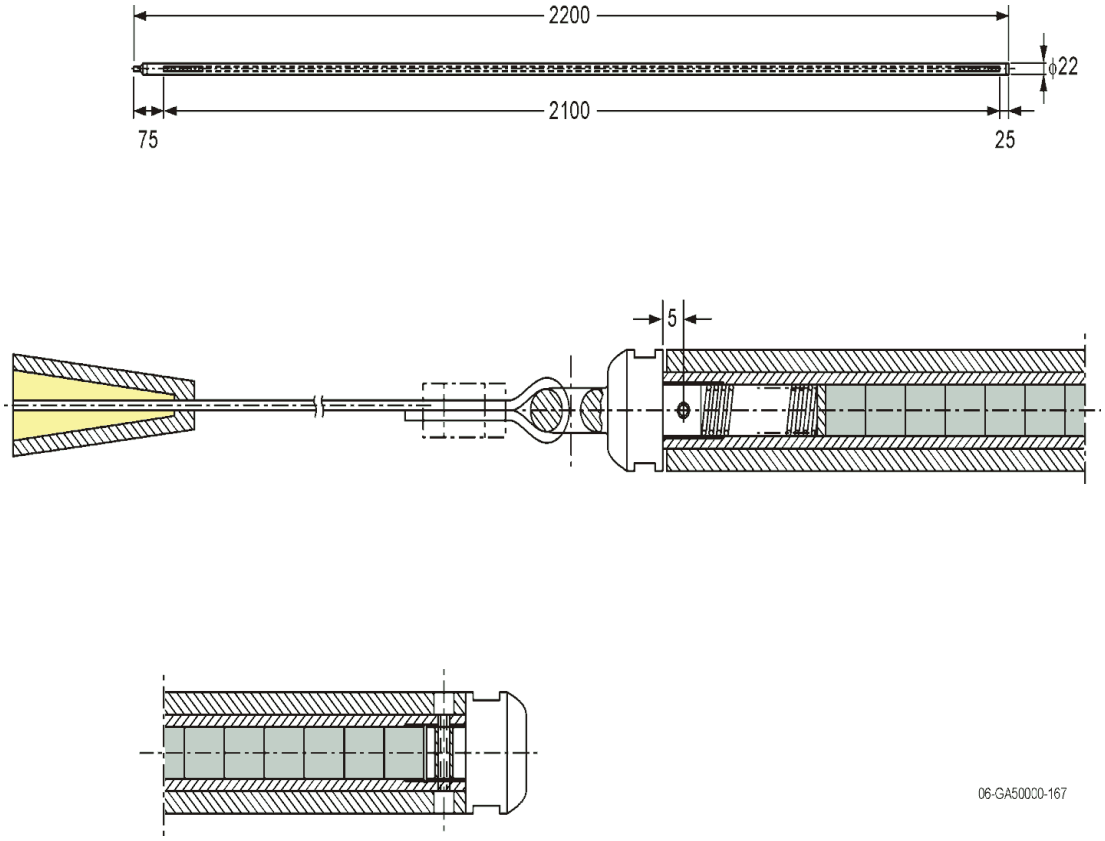

Figure 1.1-16. Details of the Withdrawable Stainless Steel Control Rods (Ref. 2).
Units are in millimeters.

Polyethylene Rods

Polyethylene rods were not used in the experiments with Core 4.

Copper Wire

Copper wire was not used in the experiments with Core 4.

Core Pebble Packing

Core 4 was randomly packed with pebbles.

The first random loading proceeded automatically, with pebbles falling under gravity, in the correct fuel-to-moderator pebble ratio, from individual delivery tubes (one for fuel and another for moderator pebbles) of the fueling machine. Although the positions of the delivery tubes were periodically changed, there were some doubts about the true randomness of the pebble distribution for Core 4.1 and it was not recommended by the experimenters for benchmarking purposes (Ref. 1).

A presumed better mixing of pebbles was obtained for the second randomly packed configuration of Core 4. A merging device was used such that both moderator and fuel pebbles were delivered through the same pipe, avoiding the possibility of systematic ordering effects. This method was also used for the third randomly packed configuration (Ref. 1).

Core Configurations

Tables 1.1-3 through 1.1-5 provide detailed summaries of the core description and critical balance information for Core 4. Core 4 consisted of three different random loadings; the core was unloaded completely prior to additional loadings (Ref. 1).

- Core 4 (reference state #1): Table 1.1-3
- Core 4 (reference state #1): Table 1.1-4
- Core 4 (reference state #1): Table 1.1-5

Where possible, experimental conditions had been measured directly (indicated by **M** in the tables) but in a few cases the values were estimated (**E**).

Excess reactivity worths for individual components in each core configuration are discussed in Section 1.1.5.

Table 1.1-3. Core 4.1 (Reference State #1) Critical Information (Ref. 1 and 3).

Core Description			
1st Criticality	March 31, 1994		
Unloaded	April 7, 1994		
Nominal Pebble Ratio	1:1 moderator:fuel		
Pebble Count	5020 moderator, 5020 fuel		
Pebble Packing	Random		
Polyethylene Loading	None		
Critical Balance			
Date	March 31, 1994		
Critical Loading	5020, 5020	**M**(a)	
Critical Height(b)	1.58 ± 0.01 m	**M**	Core surface "flattened" manually
Rod Positions (Control/Autorod)	1530/660 mm	**M**	0/1000 mm = fully out(c)
Nominal Flux	5×10^{7} n/cm^2/s	**M**	
Hall Temperature	20 ºC	**M**	
Core Temperatures (Center/Edge)	N/A	**M**	
Reflector Temperatures (R2,47/R2,15/R2,63)(d)	19.8/19.8/19.7 ºC	**M**	
Air Pressure	975 mbar	**M**	
Air Humidity	44 %	**M**	

(a) Directly measured experimental measurements are indicated with an **M**; sometimes a few values were estimated, and indicated with an **E**.

(b) The actual height of a random pebble bed is somewhat difficult to assess. Although the surface of the pebble bed was lightly flattened following each loading step, there was inevitably an uncertainty associated with the estimated position of the top of the system. In this case, a rigid rod was placed, as horizontally as possible on top of the pebbles and the distance between the safety ring and its under surface measured. This process was carried out at two orthogonal azimuthal angles and the results averaged. The result has been assigned a 1σ uncertainty of 1 cm but this is somewhat arbitrary.

(c) The withdrawable control rods and autorod are considered fully withdrawn when their positions indicate 0 and 1000 mm, respectively.

(d) The nomenclature for the channels in the radial reflector is described in Figure 1.1-3.

Table 1.1-4. Core 4.2 (Reference State #1) Critical Information (Ref. 1 and 3).[a]

Core Description			
1st Criticality	April 15, 1994		
Unloaded	May 30, 1994		
Nominal Pebble Ratio	1:1 moderator:fuel		
Pebble Count	4940 moderator, 4940 fuel		
Pebble Packing	Random		
Polyethylene Loading	None		
Critical Balance			
Date	April 15, 1994		
Critical Loading	4940, 4940[a]	**M**[b]	
Critical Height[c]	1.52 ± 0.1 m	**M**	Core surface "flattened" manually
Rod Positions (Control/Autorod)	1600/470 mm	**M**	0/1000 mm = fully out[d]
Nominal Flux	5×10^{7} n/cm^2/s	**M**	
Hall Temperature	19.2 ºC	**M**	
Core Temperatures (Center/Edge)	N/A	**M**	
Reflector Temperatures (R2,47/R2,15/R2,63)[e]	19.7/19.6/19.5 ºC	**M**	
Air Pressure	980 mbar	**E**	
Air Humidity	50 %	**E**	

(a) These values are erroneously listed as "1940, 1940" in Ref. 3.
(b) Directly measured experimental measurements are indicated with an **M**; sometimes a few values were estimated, and indicated with an **E**.
(c) The actual height of a random pebble bed is somewhat difficult to assess. Although the surface of the pebble bed was lightly flattened following each loading step, there was inevitably an uncertainty associated with the estimated position of the top of the system. In this case, a rigid rod was placed, as horizontally as possible on top of the pebbles and the distance between the safety ring and its under surface measured. This process was carried out at two orthogonal azimuthal angles and the results averaged. The result has been assigned a 1σ uncertainty of 1 cm but this is somewhat arbitrary.
(d) The withdrawable control rods and autorod are considered fully withdrawn when their positions indicate 0 and 1000 mm, respectively.
(e) The nomenclature for the channels in the radial reflector is described in Figure 1.1-3.

Table 1.1-5. Core 4.3 (Reference State #1) Critical Information (Ref. 1 and 3).[(a)]

Core Description			
1st Criticality	June 1, 1994		
Unloaded	June 22, 1994		
Nominal Pebble Ratio	1:1 moderator:fuel		
Pebble Count	4900 moderator, 4900 fuel		
Pebble Packing	Random		
Polyethylene Loading	None		
Critical Balance			
Date	June 1, 1994		
Critical Loading	4900, 4900	**M**[(a)]	
Critical Height[(b)]	1.50 ± 0.01 m	**M**	Core surface "flattened" manually
Rod Positions (Control/Autorod)	1620/500 mm	**M**	0/1000 mm = fully out[(c)]
Nominal Flux	5×10^{7} n/cm^2/s	**M**	
Hall Temperature	21 ºC	**M**	
Core Temperatures (Center/Edge)	N/A		
Reflector Temperatures (R2,47/R2,15/R2,63)[(d)]	21.3/21.2/21.2 ºC	**M**	
Air Pressure	980 mbar	**E**	
Air Humidity	50 %	**E**	

(a) Directly measured experimental measurements are indicated with an **M**; sometimes a few values were estimated, and indicated with an **E**.

(b) The actual height of a random pebble bed is somewhat difficult to assess. Although the surface of the pebble bed was lightly flattened following each loading step, there was inevitably an uncertainty associated with the estimated position of the top of the system. In this case, a rigid rod was placed, as horizontally as possible on top of the pebbles and the distance between the safety ring and its under surface measured. This process was carried out at two orthogonal azimuthal angles and the results averaged. The result has been assigned a 1σ uncertainty of 1 cm but this is somewhat arbitrary.

(c) The withdrawable control rods and autorod are considered fully withdrawn when their positions indicate 0 and 1000 mm, respectively.

(d) The nomenclature for the channels in the radial reflector is described in Figure 1.1-3.

1.1.2.3 Experimental Procedure

The approach to critical for each configuration was accompanied by the usual "inverse counts versus core loading" plot with an extrapolation to 1/counts = 0 being made after each pebble loading step to give the predicted critical loading. After the first two loading steps, which were administratively limited to 1/3 and 1/6 of the number of pebbles predicted for the critical loading respectively, the remaining steps were limited to one half of the predicted additional number of pebbles required to achieve criticality, or the worth of the control rod bank, whichever was the larger value. The count rates were measured using neutron detectors situated in the radial reflector. Because the loading of a pebble bed involves a continuous core height and thus core-detector geometry change, it was expected that the approach curves would show considerable spatial dependence. For this reason, early loadings were monitored with additional detectors. The approach curves showed considerable non-linearity for detectors close to the core, with a noticeable effect as the core upper surface reached the axial position of the detector. For this reason, all subsequent approaches were made with detectors situated further out in the radial reflector (Ref. 3).

Criticality is established and power is raised by means of control rod movements. Criticality is maintained via the autorod, which is a single, radial-reflector-based rod driven automatically by the signal from a "deviation channel", to maintain reactor power and thus criticality. Since the deviation channel was comprised of an ionization chamber situated in the radial reflector, the signal noise, and hence accuracy of the determination of a critical configuration, was determined by the flux level in the reactor. The autorod itself was typically worth a total of less than 0.1$ and the uncertainty in its position represented much less than ±5 % of this range, even at relatively low fluxes. An uncertainty of <±0.005$ was typically regarded as negligible (Ref. 3).

1.1.3 Material Data

While there are many components of the PROTEUS that remain unchanged throughout the course of the HTR-PROTEUS experiments, many parameters did change between experiments, such as the use of graphite filler pieces, control rod types and locations, the presence of polyethylene rods to simulate water ingress, core pebble packing, and conditions at criticality. Section 1.1.3.1 provides information regarding general components common to all HTR-PROTEUS configurations. Section 1.1.3.2 provides information specific to the core configurations evaluated in this report.

The PROTEUS was a zero-power critical facility. It was operated at low power and temperatures; therefore, burnup of the fuel, activation of the graphite, and heating effects were negligible.

1.1.3.1 General HTR-PROTEUS Components

The following components are common to all HTR-PROTEUS core configurations.

Concrete

Concrete shielding material properties were not provided in the references. It is indicated elsewhere that barium concrete walls surrounded the experimental facility.[a]

Steel Plate Pedestal

The stainless steel plate pedestal material properties were not available.

[a] Difilippo, F. C., "Monte Carlo Calculations of Pebble Bed Benchmark Configurations of the PROTEUS Facility," *Nucl. Sci. Eng.*, **143**, 240-253 (2003).

Radial Reflector

The HTR-PROTEUS reflectors consist of graphite of various ages from several different sources. The older graphite is mainly of type "Reactor Grade A" and made by British Achesons Electrodes Ltd., of Sheffield, England, in about 1968. Some less important sections, away from the core region, were made from a similar grade material from stock material at the facility. The new graphite was manufactured in Chedde, France, by the Sociéte des Electrodes et Réfractaires Savoie in several batches over the period 1991 to 1993. The location, densities, and nominal, "as delivered", impurity contents for the graphite are summarized in Table 1.1-6 (Ref. 2).

No attempt was made to describe the impurity content of individual reflector components. A recommended global value was measured and reported, an equivalent boron content of 4.09 ± 0.05 mbarn, which includes absorbed moisture and intergranular nitrogen from air (Ref. 3).[a]

Pulsed neutron measurements were performed in the empty PROTEUS graphite reflectors (lower axial and radial) to determine the effective impurity content. The corrected measurements provide a nominal ^{10}B absorption cross section in the cavity of 2.69 ± 0.16 mbarn, which is equivalent to a concentration of 0.2696 and 0.2591 ppm for the radial and axial graphite reflectors, respectively.[b]

[a] Williams, T., Mathews, D., and Yamane, T., "Measurement of the Absorption Properties of the HTR-PROTEUS Reflector Graphite by Means of a Pulsed-Neutron Technique," TM-41-93-34, Paul Scherrer Institut, Villigen, October 3, 1995.
[b] Difilippo, F. C., "Applications of Monte Carlo Simulations of Thermalization Processes to the Nondestructive Assay of Graphite," *Nucl. Sci. Eng.*, **133**, 163-177 (1999).

Table 1.1-6. Summary of Reactor Graphite in HTR-PROTEUS (Ref. 2 and 3).

Graphite Type	Occurrence	Density (g/cm^3)	Nominal σ_a (mbarn/atom)[(a)]
Old graphite remaining from previous experiments (~1968)	Majority of system	1.76 ± 0.01[(b)]	3.785 ± 0.3[(b)]
New graphite for HTR PROTEUS – Batch 1 (~1991) PSI Order Numbers 34618, 37129	1. Central part bottom axial reflector 2. Central part top axial reflector 3. Filler rods for ≈ 50 % "C-Driver" channels (inner channels) 4. Top 12 cm of radial reflector 5. Filler pieces to adjust cavity shape for required geometry	1.75 ± 0.007[(c)]	3.77 ± 0.09[(c)]
New graphite for HTR PROTEUS – Batch 2 (~1993) PSI Order Numbers 40442, 40901	1. Filler rods for ≈ 50 % "C-Driver" channels (outer channels) 2. Filler pieces for old ZEBRA rod channels 3. Alternative central part of bottom reflector with longitudinal channel to allow axial traverses	1.78[(d)]	4.08[(d)]
Moderator pebbles	Core	1.68 ± 0.03[(e)]	4.79[(e)]
Fuel pebbles	Core	1.73[(e)]	0.3829[(e)] ppm B

(a) σ_a is the neutron absorption cross section of the graphite.
(b) Reactor-based measurements reported in N.R.E. PROTEUS Construction Manual Section A.
(c) Reactor-based measurements SERS Test Certificates January 25, 1991, and October 10, 1991.
(d) Reactor-based measurements SERS Test Certificates January 7, 1993.
(e) Chemical analyses HOBEG GmbH Test Certificates for fuel and moderator pebbles.

The apparent density of seven samples from each of the four separate graphitizing heats (batches) of the Achesons graphite were measured (twenty-eight samples altogether). An average density of 1.763 ± 0.012 g/cm^3 was obtained (1σ standard deviation based on the twenty-eight reported results). Quality control documentation for the new graphite claimed densities between 1.75 and 1.78 g/cm^3, consistent with the older graphite value. The old graphite comprises the majority of the reflector system (Ref. 2).

Four samples of reflector graphite were heated to 500 ºC under vacuum for five hours at PSI on May 14, 1993. The results are shown in Table 1.1-7. Sample number three was from new graphite manufactured in 1990;[a] the other three samples were from the older 1968 graphite. The average weight loss of the older samples was 0.0241 wt.%, compared to a loss of 0.0156 wt.% for the newer graphite. The weight loss was assumed to be primarily due to the removal of absorbed moisture (Ref. 2).

[a] It is unclear how a piece of new graphite manufactured in 1990 was used in this analysis when the new graphite was delivered in batches over the course of 1991 to 1993.

Table 1.1-7. Reflector Graphite Weight Loss During Heating in a Vacuum (Ref. 2).

Sample Number (Graphite Type)	Diameter (cm)	Length (cm)	Original Mass (g)	Mass Loss	
				(g)	(wt.%)
1 (old)	4.4	6.0	150.742385	0.02033	0.0135
2 (old)	4.0	4.1	85.523130	0.02866	0.0335
3 (new)	2.65	6.0	57.980115	0.009055	0.0156
4 (old)	2.5	6.0	46.172465	0.01161	0.0251

The safety ring was comprised of Peraluman-300 (Table 1.1-8) and had a total mass of 10.42 kg (Ref. 2).

Table 1.1-8. Peraluman-300 (Ref. 2).

Element	Composition (wt.%)
B	<0.001
Mg	<3.1
Al	95.55
Si	0.4
Mn	<0.5
Fe	0.3
Cu	0.05
Zn	0.1
Ga	<0.01
Cd	<0.001

Upper Axial Reflector

The total mass of the graphite contained in the upper axial reflector was 1585.64 kg (Ref. 2).

The location of old and new graphite in the upper axial reflector is shown in Table 1.1-6.

The aluminum housing consisted of Peraluman-300, shown in Table 1.1-8. The total mass of Peraluman contained in this structure, below the upper surface of the graphite, was 71.48 kg (Ref. 2).

Lower Axial Reflector

The total mass of the graphite contained in the lower axial reflector was not reported.

The location of old and new graphite in the lower axial reflector is shown in Table 1.1-6.

Graphite Plugs

New graphite was used for the graphite plugs placed into holes in the reflectors (Table 1.1-6).

Safety/Shutdown Rods

The borated steel rod sections contain nominally 5 wt.% boron and are enclosed in 18/8 stainless steel tubes. The borated steel used in the HTR-PROTEUS experiments was similar to those used in previous

PROTEUS experiments but was manufactured in 1991 by Böhler AG, Edelstahlwerke, Düsseldorf, Germany for the HTR-PROTEUS experiments. The steel was chemically analyzed by the manufacturer and by PSI. The Böhler measurements, performed on June 14, 1991, indicated a boron content of 4.95 %; the PSI measurements, performed on January, 8, 1992, indicated a boron content of 4.70 %. Böhler indicated that their chemical analyses were performed prior to the final casting and machining steps and that some boron could have been lost during these steps. It was not originally reported whether these measurements were performed in at.% or wt.%; the measurements were believed to be in wt.% (Ref. 2).[a]

The borated steel density, 6.878 g/cc, was measured at PSI on December 15, 1993, and has the composition shown in Table 1.1-9. The 18/8 stainless steel cladding material (Table 1.1-10) had specified elemental compositions and density, 7.92 g/cc (Ref. 2).

The aluminum parts of the shock damper were pure aluminum alloy with a measured mass of 633.65 g (Ref. 2).

Table 1.1-9. Borated Steel (Ref. 2).(a)

Element	Composition (wt.%)
^{10}B	0.94
^{11}B	3.76
Si	1.02
Cr	40.4
Mn	1.30
Fe	41.8
Ni	9.83
Total	99.05

(a) Measurement performed on January 8, 1992, by R. Keil of PSI.

Table 1.1-10. 18/8 Stainless Steel (Ref. 2).

Element	Composition (wt.%)
Cr	18
Fe	74
Ni	8

Automatic Control Rod (Autorod)

The autorod is comprised of a copper plate within an aluminum tube. Detailed material properties were not available in the reference reports.

Static Measurement Rods

The static measurement rods were comprised of a Peraluman R-257 tube containing borated steel pieces. The Peraluman R-257 density was 2.65 g/cm^3 with the specified composition shown in Table 1.1-11. Peraluman R-257 has lower neutron absorption than Peraluman-300 due to the reduced manganese content. The borated steel had a nominal boron content of 5 wt.%. Some borated steel sections were

[a] A boron content of ~5 wt.% is equal to ~20 at.%; therefore, the assumption that the original measurements were reported in wt.% is correct.

analyzed separately at PSI on January 8, 1992 (see Table 1.1-9). The borated steel density was measured on December 17, 1993, using three as-built pieces; the density was 7.199 ± 0.029 g/cc. The long pair of rods also contained a graphite filler piece. The short pair of rods was placed within a graphite sleeve, which had a mass of 6.80 kg (Ref. 2).

Table 1.1-11. Peraluman R-257 (Ref. 2).

Element	Composition (wt.%)
B	<0.001
Mg	<2.8
Al	96.658
Si	0.2
Mn	<0.01
Fe	0.2
Cu	0.02
Zn	0.1
Ga	<0.01
Cd	<0.001

Fuel Pebbles

Fuel masses are shown in Table 1.1-1.

Impurities in the UO_2 used in the TRISO fuel particles are provided in Table 1.1-12. The specified values are averages taken from the fuel pebble quality control records. Impurity estimates for five elements contributing less than 1 % of the total boron equivalent were not given (Ref. 2).

The graphite impurities in the assembled fuel pebbles are provided in Table 1.1-13. The specified values are averages taken from the fuel pebble quality control records. Impurity estimates for five elements contributing less than 1 % of the total boron equivalent were not given (Ref. 2).

Table 1.1-12. UO_2 Impurities (Ref. 2).

Element	Concentration (ppm by wt.)
Ag	<0.2
B	0.085
Ca	51
Cd	<0.2
Cl	<3
Co	<1
Cr	23
Dy	<0.02
Eu	<0.02
Fe	28
Gd	<0.02
Li	<1
Mn	7.5
Mo	<3
Ni	2.5
S	<0.04
Ti	<10
V	<10

Table 1.1-13. Fuel Pebble Graphite Impurities (Ref. 2).

Element	Concentration (ppm by wt.)
Ag	<0.2
B	0.101
Ca	9.28
Cd	<0.103
Cl	<3
Co	<0.13
Cr	1.81
Dy	<0.01
Eu	<0.01
Fe	2.95
Gd	<0.01
Li	<1
Mn	0.43
Ni	<1
S	<0.011
Ti	0.497
V	<0.433

Moderator Pebbles

Moderator pebble impurities are given in Table 1.1-14, and were obtained from the moderator pebble quality control records. Uncertainties for the moderator pebble impurities were not available, and values for fourteen elements contributing less than 0.1 % to the total boron equivalent were not given. The table does not include values for absorbed moisture in the pebbles. The quantity of moisture contained in the pebbles was measured at PSI by randomly selecting two moderator pebbles and heating them to 500 ºC under vacuum for five hours. Each pebble showed a weight loss of 0.02 g, 0.01 wt.% (Ref. 2).

Table 1.1-14. Moderator Pebble Impurities (Ref. 2).

Element	Concentration (ppm by wt.)
B	0.76
Ca	129
Cd	<0.6
Cl	18.64
Dy	0.065
Eu	0.13
Fe	5.9
Gd	0.040
Li	0.88
Ni	0.78
S	140
Si	35
Sm	0.086
Ti	10
V	13

Start-Up Source

The material properties of the start-up source were not available in the reference reports.

Detectors

The material properties of the detectors (six ionization chambers and two fission chambers) were not available in the reference reports.

Temperature Sensors

The material properties of the temperature sensors were not available in the reference reports.

1.1.3.2 Components Unique to Core 4

The following components are unique to core configuration 4.

Graphite Fillers

The total mass of the 21 cavity floor filler pieces was 85.60 kg (Ref. 2).

ZEBRA Control Rods

The ZEBRA control rods were not used in the experiments with Core 4.

Withdrawable Stainless Steel Control Rods

The inner tube of the withdrawable stainless steel control rods was St1.4301 (Table 1.1-15) and the outer tube was St1.4541 (Table 1.1-16). Both steels had a density of 7.9 g/cm^3 (Ref. 2).

Table 1.1-15. St1.4301 (Ref. 2).

Element	Composition (wt.%)
C	≤0.07
Si	≤1.0
Mn	≤2.0
Cr	17.0-20.0
Ni	9.0-11.5

Table 1.1-16. St1.4541 (Ref. 2).

Element	Composition (wt.%)
C	≤0.10
Si	≤1.0
Mn	≤2.0
Cr	17.0-19.0
Ni	9.0-11.5
Ti	≥x %C

Polyethylene Rods

Polyethylene rods were not used in the experiments with Core 4.

Copper Wire

Copper wire was not used in the experiments with Core 4.

Ambient Air

Ambient (hall) temperatures, air pressure, and humidity for HTR-PROTEUS critical experiments, Core 4, are provided in the following tables:

- Core 4.1 (reference state #1): Table 1.1-3
- Core 4.2 (reference state #1): Table 1.1-4
- Core 4.3 (reference state #1): Table 1.1-5

1.1.4 Temperature Data

Room (hall) and reflector temperatures for HTR-PROTEUS critical experiments, Core 4, are provided in the following tables (core temperatures were not measured):

- Core 4.1 (reference state #1): Table 1.1-3
- Core 4.2 (reference state #1): Table 1.1-4
- Core 4.3 (reference state #1): Table 1.1-5

The reactor was operated at room temperature with the power limited to 1 kW so that no active cooling systems were required.[a]

1.1.5 Additional Information Relevant to Critical and Subcritical Measurements

An estimate of excess reactivity, in units of dollars, was provided for each of the core configurations. The value of β_{eff} is provided for each case. The excess reactivity was provided in terms of individual component worths such that users could pick and choose which simplifications to incorporate into their models. Where possible, the component worths had been measured directly in the relevant configurations (indicated by **M** in the tables) but in many cases the values had to be calculated (**C**), estimated (**E**), or scaled from another configuration (**S**). Most reference component worth measurements were performed in Cores 1 and 5 (Ref. 1). These measurements represent deviations of the real-life assembly from an ideal, clean core configuration. The effects of these deviations are quantified; an example of how these measurements were performed was provided elsewhere for Core 1.[b] Reactivity corrections for Core 4, provided in the original references, are summarized in the following tables:

- Core 4.1 (reference state #1): Table 1.1-17
- Core 4.2 (reference state #2): Table 1.1-18
- Core 4.3 (reference state #3): Table 1.1-19

The worth of various core components was provided to allow for the development of simplified models for calculation of the HTR-PROTEUS experiments. The measured worths of the individual components are normally evaluated against the worths of the ZEBRA/control rods, which were carefully calibrated using the stable period technique, or against the autorod worth, which had been subsequently inter-calibrated with the ZEBRA/control rods (Ref. 3).

A small degree of inhomogeneity in the radial graphite reflector was inevitable. Axial holes were required for control and shutdown rod insertion and radial and axial holes for nuclear instrumentation. The C-Driver holes in the inner radial reflector, left over from the previous experiments, had to be filled with graphite rods. These rods were relatively easy to remove and useful in estimating the effect of missing graphite. Correction for the air gaps between the 27.5 mm ID C-Driver channels and the 26.5 mm OD graphite filler rods were calculated by V. D. Davidenko of the Kurchatov Institute using the Cristall code system (Ref. 3).

No explicit measurements were made to determine the worth of the four empty ZEBRA/control rod channels. The values reported in the tables were made on the basis of the results of the C-Driver hole measurements. For safety reasons, the worth of the eight safety and shutdown rod channels cannot be measured and their values were calculated at PSI using the TWODANT code. It was considered reasonable to include them in the calculational model, removing them from the reactivity excess list (Ref. 3).

---

[a] Köberl, O., Seiler, R., and Chawla, R., "Experimental Determination of the Ratio of 238U Capture to 235U Fission in LEU-HTR Pebble-Bed Configurations," *Nucl. Sci. Eng.*, **146**, 1-12 (2004).
[b] Williams, T., "HTR PROTEUS CORE 1: Reactivity Corrections for the Critical Balance," TM-41-93-20, Paul Scherrer Institut, Villigen, October 7, 1993.

The upper and lower axial reflectors were furnished with 33 “ventilation holes” to enable air-cooling of the core. The axial thermal flux peak is strongly shifted downwards and graphite density variations in the upper part of the lower axial reflector were of greater significance than those above. Unfortunately, for practical reasons, it was difficult to measure the effect in the lower reflector and satisfactory measurements could only be made in the upper axial reflector. In the upper reflector, measurements were made with 11 of the 33 holes plugged with graphite. Because full access to the ventilation holes in the lower axial reflector is impeded from below, it was not possible to measure their worth in the usual manner. At best, it was possible to partially fill some of the channels with graphite and linearly scale the effect to 33 filled channels. In some of the core configurations all of the coolant channels in the lower axial reflector were filled with graphite plugs (Ref. 3).

In all the deterministic cores, ~12 pebbles were directly over one of the 33 cooling channels in the lower axial reflector. To avoid pebble displacement in these cases, special aluminum plugs were developed to support the pebbles in Core 1. In later cores, simple graphite rods were used (Ref. 3).

The reactor start-up sources were normally in their “in” position during reactor operation. At low fluxes their reactivity effect is positive by virtue of the apparent enhanced neutron multiplication; at normal operating fluxes of $>10^7$ n/cm^2/s, their effect was negative due to parasitic neutron absorption in the source and casing. The start-up sources pass through horizontal aluminum guide tubes situated in the radial reflector at about the level of the cavity floor. The worth of these penetrations were also measured (Ref. 3).

The pulsed neutron source, when used for subcriticality measurements, was partially inserted into the lower axial reflector. Its reactivity worth was measured by replacing it with a plug of graphite of dimensions 250 mm × 120 mm Ø (Ref. 3).

The worth of one of the six ionization chambers compared with a graphite plug was measured by opening a plugged channel and inserting a spare ionization chamber. The worth of one of the two impulse channels in the outer radial reflector was also measured by means of filling a similar channel first with a replacement detector and then with a graphite plug (Ref. 3).

The temperature sensors were systematically removed from the system in order to assess their reactivity worths (Ref. 3).

The value of β_{eff} was calculated for each of the cores (Ref. 3).

Table 1-17. Core 4.1 (Reference State #1) Reactivity Corrections (Ref. 1 and 3).

Reactivity Corrections to Critical Loading	No.		Total ¢			Comments
Control Rest Insertion (1530)[a]	4	**M,S**	-44.9	±	5	Scaled from Core 5
Control Rod Channels[b]	4	**S**	-2.4	±	1	Scaled from Core 5
Autorod Rest Worth[c]	1	**S**	-9.8	±	0.3	Scaled from Core 1A
Autorod Insertion (660 mm)[c]	1	**S**	-2.1	±	0.3	Scaled from Core 1A
Autorod Channel[c]	1	**S**	-0.7	±	0.2	Scaled from Core 1A
Safety and Shutdown Rod Channels[c,d]	8	**C,S**	-30	±	10	Scaled from Core 1A
Empty Channels R2[b,e]	2	**S**	-3.0	±	0.3	Scaled from Core 5
Air Gaps in C-Driver Holes[f]	320	**C**	-10.3			
Channels in Upper Reflector[g]	34	**M**	-3.6	±	2.0	Core 1A value
Channels in Lower Reflector[g]	33	**M**	-23	±	10	Core 1Avalue
Aluminum Plugs in Lower Reflector[g]	12	**M**	-15.3	±	5	Core 1A value
Start-up Sources[c]	2	**S**	-3.6	±	0.1	Scaled from Core 1A
Start-up Source Penetrations	2	**M**	-1	±	0.1	Core 1A value
Pulsed Neutron Source and Missing Graphite[c]	1	**S**	-4.7	±	0.3	Scaled from Core 1[a]
Nuclear Instrumentation (Ionization)[c]	7	**S**	-10.7	±	2.0	Scaled from Core 1A
Nuclear Instrumentation (Fission)[c]	2	**S**	-0.9	±	0.6	Scaled from Core 1A
Temperature Instrumentation Reflector[c]	3	**S**	-17.4	±	2.0	Scaled from Core 1A
Total Correction			**183**	**±**	**16**	
Corrected k_{eff} (β_{eff} = 0.00723)			**1.0134**	**±**	**0.0011**	

(a) The control rods are fully inserted when 2500 mm is indicated. Their integral worths were measured using stable period measurements yielding a total bank worth of some 1.47 ± 0.04 dollars. In this case the differential worths were not measured and the reactivity associated with a particular insertion was calculated from a combination of the Core 5 S-Curves and the Core 4.1 integral worths – hence the larger than usual uncertainty.

(b) The Core 5 value had been scaled by the ratio of the control rod banks in Cores 4.1 and 5 (1.09) to yield an estimate for Core 4.1. Performing the same procedure with the Core 1 measurements yielded a very similar value for Core 4.1.

(c) The results measured in Core 1/1A were scaled by the ratio of the bank worths (1.27). In most cases the uncertainties were also increased.

(d) For safety reasons the worth of these eight channels cannot be measured and the values were calculated at PSI using the TWODANT code. In the table, the calculation made for Core 1 was scaled by the ratio of the control rod bank worths in Cores 1A and 4.1. Independent calculations by V. D. Davidenko of the Kurchatov Institute yielded a value of 19.8 cents for this core.

(e) R2 indicates the second ring of the C-Driver channels.

(f) Corrects for the air gaps between the 27.5 mm ID C-Driver channels and the 26.5 mm OD graphite filler rods. The value here was calculated by V. D. Davidenko of the Kurchatov Institute using the Cristall code system.

(g) Core 1 values taken but uncertainty increased.

Table 1-18. Core 4.2 (Reference State #1) Reactivity Corrections (Ref. 1 and 3).

Reactivity Corrections to Critical Loading	No.		Total ¢			Comments
Control Rod Insertion (1600 mm)[a]	4	**M,S**	-51.5	±	5	Scaled from Core 5
Control Rod Channels[b]	4	**S**	-2.4	±	1	Scaled from Core 5
Autorod Rest Worth[c]	1	**S**	-9.8	±	0.3	Scaled from Core 1A
Autorod Insertion (470 mm)[c]	1	**S**	-3.3	±	0.3	Scaled from Core 1A
Autorod Channel[c]	1	**S**	-0.7	±	0.2	Scaled from Core 1A
Safety and Shutdown Rod Channels[c,d]	8	**C,S**	-30	±	10	Scaled from Core 1A
Empty Channels R2[b,e]	2	**S**	-3.0	±	0.3	Scaled from Core 5
Air Gaps in C-Driver Holes[f]	320	**C**	-10.2			
Channels in Upper Reflector[g]	34	**M**	-3.6	±	2.0	Core 1A Value
Channels in Lower Reflector[g]	33	**M**	-23	±	10	Core 1A Value
Start-up Sources[c]	2	**S**	-3.6	±	0.01	Scaled from Core 1A
Start-up Source Penetrations	2	**M**	-1	±	0.1	Core 1A Value
Pulsed Neutron Source and Missing Graphite[c]	1	**S**	-4.7	±	0.3	Scaled from Core 1A
Nuclear Instrumentation (Ionization)[c]	7	**S**	-10.7	±	2.0	Scaled from Core 1A
Nuclear Instrumentation (Fission)[c]	2	**S**	-0.9	±	0.6	Scaled from Core 1A
Temperature Instrumentation Reflector[c,h]	3	**S**	-17.4	±	10	Scaled from Core 1A
Total Correction			**175.8**	**±**	**14**	
Corrected k_{eff} (β_{eff} = 0.00723)			**1.0129**	**±**	**0.001**	

(a) The control rods are fully inserted when 2500 mm is indicated. Their integral worths were measured using stable period measurements yielding a total bank worth of some 1.46 ± 0.04 dollars. In this case the differential worths were not measured and the reactivity associated with a particular insertion was calculated from a combination of the Core 5 S-Curves and the Core 4.2 integral worths – hence the larger than usual uncertainty.

(b) The Core 5 value had been scaled by the ratio of the control rod banks in Cores 4.1 and 5 (1.09) to yield an estimate for Core 4.2. Performing the same procedure with the Core 1 measurements yielded a very similar value for Core 4.2.

(c) The results measured in Core 1/1A were scaled by the ratio of the bank worths (1.27). In most cases the uncertainties were also increased.

(d) For safety reasons the worth of these eight channels cannot be measured and the values were calculated at PSI using the TWODANT code. Independent calculations by V. D. Davidenko of the Kurchatov Institute yielded a value of 16.6 cents for this core.

(e) R2 indicates the second ring of the C-Driver channels.

(f) Corrects for the air gaps between the 27.5 mm ID C-Driver channels and the 26.5 mm OD graphite filler rods. The value here was calculated by V. D. Davidenko of the Kurchatov Institute using the Cristall code system.

(g) Core 1 values taken but uncertainty increased.

(h) The temperature sensors in channels R2/47 and R2/15 had been pulled down to be 420 mm above the lower reactor support plate but there was no measurement for this position and so the uncertainty has been increased.

Table 1-19. Core 4.3 (Reference State #1) Reactivity Corrections (Ref. 1 and 3).

Reactivity Corrections to Critical Loading	No.		Total ¢			Comments
Control Rod Insertion (1620 mm)[a]	4	**M,S**	-56.5	±	5	Scaled from Core 5
Control Rod Channels[b]	4	**S**	-2.4	±	1	Scaled from Core 5
Autorod Rest Worth[c]	1	**S**	-9.8	±	0.3	Scaled from Core 1A
Autorod Insertion (500 mm)[c]	1	**S**	-3.1	±	0.3	Scaled from Core 1A
Autorod Channel[c]	1	**S**	-0.7	±	0.2	Scaled from Core 1A
Safety and Shutdown Rod Channels[c,e]	8	**C,S**	-30	±	10	Scaled from Core 1A
Empty Channels R2[b,e]	2	**S**	-3.0	±	0.3	Scaled from Core 5
Air Gaps in C-Driver Holes[f]	320	**C**	-10.3			
Channels in Upper Reflector[g]	34	**M**	-3.6	±	2.0	Core 1A Value
Channels in Lower Reflector[g]	33	**M**	-23	±	10	Core 1A Value
Start-up Sources[c]	2	**S**	-3.6	±	0.01	Scaled from Core 1A
Start-up Source Penetrations	2	**M**	-1	±	0.1	Core 1A Value
Pulsed Neutron Source and Missing Graphite[c]	1	**S**	-4.7	±	0.3	Scaled from Core 1A
Nuclear Instrumentation (Ionization)[c]	7	**S**	-10.7	±	2.0	Scaled from Core 1A
Nuclear Instrumentation (Fission)[c]	2	**S**	-0.9	±	0.6	Scaled from Core 1A
Temperature Instrumentation Reflector[c,h]	3	**S**	-17.4	±	10	Scaled from Core 1A
Total Correction			**180**	**±**	**14**	
Corrected k_{eff} (β_{eff} = 0.00723)			**1.0132**	**±**	**0.001**	

(a) The control rods are fully inserted when 2500 mm is indicated. Their integral worths were measured using stable period measurements yielding a total bank worth of some 1.49 ± 0.04 dollars. In this case the differential worths were not measured and the reactivity associated with a particular insertion was calculated from a combination of the Core 5 S-Curves and the Core 4.3 integral worths – hence the larger than usual uncertainty.

(b) The Core 5 value had been scaled by the ratio of the control rod banks in Cores 4.3 and 5 (1.09) to yield an estimate for Core 4.3. Performing the same procedure with the Core 1 measurements yielded a very similar value for Core 4.3.

(c) The results measured in Core 1/1A were scaled by the ratio of the bank worths (1.27). In most cases the uncertainties were also increased.

(d) For safety reasons the worth of these eight channels cannot be measured and the values were calculated at PSI using the TWODANT code. Independent calculations by V. D. Davidenko of the Kurchatov Institute yielded a value of 19.8 cents for this core.

(e) R2 indicates the second ring of the C-Driver channels.

(f) Corrects for the air gaps between the 27.5 mm ID C-Driver channels and the 26.5 mm OD graphite filler rods. The value here was calculated by V. D. Davidenko of the Kurchatov Institute using the Cristall code system.

(g) Core 1 values taken but uncertainty increased.

(h) The temperature sensors in channels R2/47 and R2/15 had been pulled down to be 420 mm above the lower reactor support plate but there was no measurement for this position and so the uncertainty has been increased.

1.2 Description of Buckling and Extrapolation Length Measurements

Buckling and extrapolation length measurements were made but have not yet been evaluated.

1.3 Description of Spectral Characteristics Measurements

Spectral characteristics measurements were not made.

1.4 Description of Reactivity Effects Measurements

Reactivity effects measurements were made but have not yet been evaluated.

1.5 Description of Reactivity Coefficient Measurements

Reactivity coefficient measurements were made but have not yet been evaluated.

1.6 Description of Kinetics Measurements

Kinetics measurements were made but have not yet been evaluated.

1.7 Description of Reaction-Rate Distribution Measurements

Reaction-rate distribution measurements were made but have not yet been evaluated.

1.8 Description of Power Distribution Measurements

Power distribution measurements were not made.

1.9 Description of Isotopic Measurements

Isotopic measurements were not made.

1.10 Description of Other Miscellaneous Types of Measurements

Other miscellaneous types of measurements were not made.

2.0 EVALUATION OF EXPERIMENTAL DATA

2.1 Evaluation of Critical and / or Subcritical Configuration Data

One benchmark experiment was evaluated in this report: Core 4. Core 4 represents the only configuration with random pebble packing in the HTR-PROTEUS series of experiments, and has a moderator-to-fuel pebble ratio of 1:1. Three random configurations were performed. The initial configuration, Core 4.1, was rejected because the method for pebble loading, separate delivery tubes for the moderator and fuel pebbles, may not have been completely random; this core loading was rejected by the experimenters. Cores 4.2 and 4.3 were loaded using a single delivery tube, eliminating the possibility for systematic ordering effects. The second and third cores differed slightly in the quantity of pebbles loaded (40 each of moderator and fuel pebbles), stacked height of the pebbles in the core cavity (0.02 m), withdrawn distance of the stainless steel control rods (20 mm), and withdrawn distance of the autorod (30 mm). The 34 coolant channels in the upper axial reflector and the 33 coolant channels in the lower axial reflector were open. Additionally, the axial graphite fillers used in all other HTR-PROTEUS configurations to create a 12-sided core cavity were not used in the randomly packed cores. Instead, graphite fillers were placed on the cavity floor, creating a quasi-conical, or funnel-like, base, to discourage ordering effects during pebble loading.

The benchmark specifications selected for Core 4 is a single configuration that represents the average pebble loading and stacked core height between configurations 4.2 and 4.3. Additionally, average withdrawn control rod and autorod positions were used. Treatment of any additional bias and bias uncertainty is discussed in Section 3.1.1.1.

The benchmark critical configurations for Core 4 will also be referred to as Case 1. Both methods of identification are utilized throughout the rest of this report to facilitate users with differing familiarities with HTR-PROTEUS and IRPhEP benchmark format.

Monte Carlo n-Particle (MCNP) version 5-1.60 calculations were utilized to estimate the biases and uncertainties associated with the experimental results in this evaluation. MCNP is a general-purpose, continuous-energy, generalized-geometry, time-dependent, coupled n-particle Monte Carlo transport code.[a] The Evaluated Neutron Data File library, ENDF/B-VII.0,[b] cross section data was also used in this evaluation. The statistical uncertainty in k_{eff} and Δk_{eff} is $\leq$0.00007 and $\leq$0.00010, respectively. Calculations were performed with 1,650 generations with 100,000 neutrons per generation. The k_{eff} estimates (with the first 150 generations skipped) are the result of 150,000,000 neutron histories.

Variations of the benchmark model provided in Section 3 were utilized with perturbations of the model parameters to estimate uncertainties in k_{eff} due to uncertainties in parameter values defining the benchmark experiment. Some perturbations required more detail than that retained in the benchmark model. More detailed models (Appendix C) were utilized to evaluate these uncertainties. Transformation from the detailed model to the benchmark model is described in Section 3.1.1.1. Where applicable, comparison of the upper and lower perturbation k_{eff} values to evaluate the uncertainty in the eigenvalue were utilized to minimize correlation effects, if any, induced by comparing all perturbations to the original benchmark model configuration, as discussed elsewhere.[c]

Unless specifically stated otherwise, all uncertainty values in this section correspond to 1σ. When the change in k_{eff} between the base case and the perturbed model (single-sided perturbation), or two

[a] X-5 Monte Carlo Team, "MCNP – a General Monte Carlo n-Particle Transport Code, version 5," LA-UR-03-1987, Los Alamos National Laboratory (2003).
[b] M. B. Chadwick, et al., "ENDF/B-VII.0: Next Generation Evaluated Nuclear Data Library for Nuclear Science and Technology," *Nucl. Data Sheets*, **107**: 2931-3060 (2006).
[c] D. Mennerdahl, "Statistical Noise for Nuclear Criticality Safety Specialists," *Trans. Am. Nucl. Soc.*, **101**: 465-466 (2009).

perturbed models (double-sided perturbation directly comparing an upper and a lower perturbation from the base case), is less than the statistical uncertainty of the Monte Carlo results, the changes in the variable are amplified, if possible, and the calculations repeated. The resulting calculated change is then scaled back, using a scaling factor, corresponding to the actual uncertainty, assuming that it is linear, which should be adequate for these changes in k_{eff}. Throughout Section 2, the difference in eigenvalues computed using the perturbation method described is denoted with Δk_p; the scaled 1σ uncertainty is denoted as Δk_{eff}. All Δk_{eff} uncertainties are considered to be absolute values whose magnitude applies both positively and negatively to the experimental k_{eff}, as shown in Tables 2.1-32 through 2.1-35. Negative signs are retained in other tables in Section 2, where the effective uncertainty is reported for a given uncertainty perturbation, to demonstrate whether the effect in k_{eff} was directly or indirectly proportional to the uncertainty.

Evaluated uncertainties ≤0.00010 are considered negligible because their calculated worth is within the statistical uncertainty of the Monte Carlo approach being utilized.

Elemental data such as molecular weights and isotopic abundances were taken from the 16th edition of the Chart of the Nuclides.[a] These values are summarized in Appendix E.

Milling and finishing of the graphite components to tight tolerances would be necessary to fit all the components of this assembly together. Small dimensional inconsistencies would result in increased void fractions between graphite components. The effect of these void fractions would be minor compared to the uncertainty in graphite density. The dimensions of some of the graphite parts used in this experiment series are often recorded with many significant digits. While the number of significant digits may not always represent the accuracy or precision of their respective measured value, it is assumed by the evaluator that an uncertainty of ±1 in the last reported significant digit should be adequate in evaluating the uncertainty in reported graphite dimensions. Similar discussion of tight manufacturing tolerances and the resultant small or negligible uncertainties can be found in other gas-cooled thermal reactor benchmarks (HTTR-GCR-RESR-001, -002, -003, and HTR10-GCR-RESR-001)

The total evaluated uncertainty in k_{eff} for this experiment is provided in Section 2.1.8; individual uncertainties are summed under quadrature to obtain the total uncertainty in the experimental k_{eff}.

When evaluating parameters such as measured diameters, heights, and mass, all parts of a given type are perturbed at the same time: e.g., the uranium mass in all fuel pebbles is simultaneously increased or decreased. Then the calculated uncertainty is reduced by the square root of the number of components perturbed, representative of a random uncertainty. For many of these uncertainties, there is insufficient information available to evaluate what portion of the total evaluated uncertainty is systematic instead of random. All uncertainties involving the perturbation of multiple assembly components are treated as 15% systematic in this evaluation, unless otherwise specified.

This assumption provides a basic prediction of the effect on k_{eff}. Most systematic uncertainties should be below 50 % of the total uncertainty and above the historic approach of ignoring the unknown systematic components (i.e., treat it with a 0 % probability). In actuality, careful experimenters may have an unknown systematic uncertainty that is approximately 10-15 % of their total reported uncertainty. Because significant effort had gone into the development of benchmark quality HTR-PROTEUS experiments, a systematic uncertainty of 15 % is assumed. Evaluated uncertainties are listed as calculated, such that the readers may themselves adjust results according to some desired systematic-to-random uncertainty ratio.

The following evaluated uncertainties would have both systematic and random uncertainties (Table 2.1-1). Many of these uncertainties are negligible without adjusting the computed value to account for

[a] E. M. Baum, H. D. Knox, and T. R. Miller, *Nuclides and Isotopes: 16th Edition*, Knolls Atomic Power Laboratory (2002).

multiple assembly components (i.e., treating the uncertainty as 100 % systematic is still negligible). The systematic and random components are only evaluated in more detail when the evaluated uncertainty (assuming 100 % systematic) is not negligible (>0.00010).

Table 2.1-1. Summary of Uncertainties with Systematic and Random Components.

• Radial Reflector – C-Driver Positions – C-Driver Hole Diameter – ZEBRA Rod Hole Positions – ZEBRA Rod Hole Diameter – ZEBRA Hole Filler Diameter – ZEBRA Hole Filler Length – Safety/Shutdown Rod Positions – Safety/Shutdown Rod Hole Diameter – C-Driver Plug Diameter – C-Driver Plug Length • Upper Axial Reflector – Coolant Channel Positions – Coolant Channel Diameter – Plug Diameter – Plug Length • Lower Axial Reflector – Coolant Channel Positions – Coolant Channel Diameter – Plug Diameter – Plug Length • Safety/Shutdown Rods – Borated Steel Rod Diameter – Borated Steel Rod Length – Steel Tube Diametrical Thickness – Steel Tube Length	• Fuel Pebbles – Kernel Radius – Buffer Thickness – IPyC Thickness – SiC Thickness – OPyC Thickness – Fuel Zone Radius – Pebble Radius – Total Uranium Mass – Total Carbon Mass • Moderator Pebbles – Radius – Mass • Graphite Fillers – Cavity Floor Height – Coolant Channel Positions – Coolant Channel Diameter • Stainless Steel Control Rods – Inner Tube Diametrical Thickness – Outer Tube Diametrical Thickness – Length of Tubes and End Plugs • Measurements – Safety/Shutdown Rod Positions – Withdrawable Control Rod Positions – Core Height

2.1.1 Streamlining the Uncertainty Analysis

A comprehensive uncertainty analysis was performed for the initial HTR-PROTEUS configurations, Cores 1, 1A, 2, and 3 (PROTEUS-GCR-EXP-001). The evaluated uncertainty for many of the perturbed parameters were determined to be negligible (≤0.00010 Δk), resulting in a much shorter list of uncertainties actually contributing to the total uncertainty (see Section 2.1.22 of PROTEUS-GCR-EXP-001). Further evaluation of Cores 9 and 10 (PROTEUS-GCR-EXP-004) and 5 through 8 (PROTEUS-GCR-EXP-003) supported the fact that ignoring the contribution of uncertainties ≤0.00030 Δk of the total uncertainty could also be considered negligible due to the contributions from some of the more significant uncertainties. A summary of negligible uncertainties pertinent to the current benchmark configurations is provided in Table 2.1-2; these uncertainties were not evaluated as their contribution to the total uncertainty in the benchmark configurations is judged to be negligible. Table 2.1-3 contains a list of uncertainties that are individually evaluated in this report. Uncertainties relating to the ZEBRA control rods and associated holes were not evaluated as they were only pertinent in Core 1. Uncertainties in the graphite cavity floor fillers were included in this analysis because they are unique to Core 4 . Uncertainties in pebble packing and the core height were included as well evaluation of the uncertainty due to random packing of the pebbles, the stacked height of the core, and graphite cavity floor filler pieces, as they are unique to this core configuration.

Table 2.1-2. Summary of Negligible Uncertainties Not Evaluated for Core 4.

- Concrete
  - Thickness
  - Density
  - Composition
- Steel Plate Pedestal
  - Thickness
  - Density
  - Composition
- Radial Reflector
  - Inner Diameter
  - Outer Diameter
  - Height
  - C-Driver Hole Positions
  - C-Driver Hole Diameter
  - Autorod Hole Position
  - Autorod Hole Diameter
  - ZEBRA Rod Hole Positions
  - ZEBRA Rod Hole Diameter
  - ZEBRA Hole Filler Diameter
  - ZEBRA Hole Filler Length
  - ZEBRA Hole Filler Density
  - ZEBRA Hole Filler Impurity Content
  - Safety/Shutdown Rod Positions
  - Safety/Shutdown Rod Hole Diameter
  - Thermal Column Width
  - Thermal Column Depth
  - Thermal Column Height
  - Safety Ring Vertical Thickness
  - Safety Ring Diametrical Thickness
  - Safety Ring Density
  - Safety Ring Composition
  - C-Driver Plug Diameter
  - C-Driver Plug Length
  - C-Driver Plug Density
  - C-Driver Plug Impurities
- Upper Axial Reflector
  - Cylinder Diameter
  - Annulus Inner Diameter
  - Annulus Outer Diameter
  - Annulus Geometry
  - Height
  - Graphite Mass
  - Graphite Impurity Content
  - Coolant Channel Positions
  - Coolant Channel Diameter
  - Plug Diameter
  - Plug Length
  - Plug Density
  - Plug Impurity Content
  - Aluminum Density
- Lower Axial Reflector
  - Cylinder Diameter
  - Annulus Inner Diameter
  - Annulus Outer Diameter
  - Height
  - Cylinder Density
  - Annulus Density
  - Cylinder Impurity Content
  - Annulus Impurity Content
  - Coolant Channel Positions
  - Coolant Channel Diameter
  - Plug Diameter
  - Plug Length
  - Plug Density
  - Plug Impurity Content
  - Source Position Diameter
  - Source Position Length
  - Source Plug Diameter
  - Source Plug Length
  - Source Plug Density
  - Source Plug Impurity Content
- Safety/Shutdown Rods
  - Borated Steel Rod Diameter
  - Borated Steel Rod Length
  - Borated Steel Density
  - Boron Content of Borated Steel
  - Borated Steel Composition
  - Steel Tube Diametrical Thickness
  - Steel Tube Length
  - Steel Tube Density
  - Steel Tube Composition
  - Shock Damper Dimensions
  - Shock Damper Mass
  - Shock Damper Composition
- Autorod
  - Copper Wedge Thickness
  - Copper Wedge Length
  - Copper Wedge Density
  - Copper Wedge Composition
  - Orientation of Copper Wedge
  - Tube Thickness
  - Tube Length
  - Tube Density
  - Tube Composition

Table 2.1-2 (cont'd.). Summary of Negligible Uncertainties Not Evaluated for Core 4.

• Fuel Pebbles – Quantity of Pebbles – TRISO Random Packing – Kernel Radius – Buffer Thickness – IPyC Thickness – SiC Thickness – OPyC Thickness – Fuel Zone Radius – Pebble Radius – ^{234}U Isotopic Content – ^{236}U Isotopic Content – ^{238}U Isotopic Content – Total Carbon Mass – Total Pebble Mass – Kernel Density – Buffer Density – IPyC Density – SiC Density – OPyC Density – Kernel Impurity Content – Buffer Impurity Content – IPyC Impurity Content – SiC Impurity Content – OPyC Impurity Content – Pebble Water Content – Oxygen-to-Uranium Ratio	• Moderator Pebbles – Quantity of Pebbles – Radius – Mass – Water Content • Stainless Steel Control Rods – Inner Tube Diametrical Thickness – Outer Tube Diametrical Thickness – Length of Tubes and End Plugs – Inner Tube Density – Outer Tube Density – Inner Tube Composition – Outer Tube Composition • Measurements – Measurement of k_{eff} – Autorod Position – Safety/Shutdown Rod Positions – Withdrawable Control Rod Positions – Temperature • Ambient Air – Temperature – Pressure – Humidity • Isotopic Abundance of Boron

Table 2.1-3. Summary of Uncertainties Evaluated for Core 4.

• Radial Reflector – Density – Impurity Content • Upper Axial Reflector – Location – Aluminum Support Structure Dimensions – Aluminum Composition • Fuel Pebbles – Pebble Packing Fraction – Pebble Random Packing – ^{235}U Isotopic Content – Pebble Uranium Mass – Fueled Zone Impurity Content – Unfueled Zone Impurity Content	• Moderator Pebbles – Impurity Content • Graphite Fillers – Cavity Floor Inner Equivalent Diameter – Cavity Floor Outer Equivalent Diameter – Cavity Floor Height – Cavity Floor Coolant Channel Positions – Cavity Floor Coolant Channel Diameter – Cavity Floor Mass – Cavity Floor Impurities • Measurements – Stacked Pebble Height

2.1.2 Radial Reflector

2.1.2.1 Graphite Density

The graphite for the majority of the system, which includes much of the radial reflector and thermal column, was reported to have a density of 1.76 ± 0.01 g/cm^3 (Table 1.1-6), obtained from reactor-based measurements. Measurement of 28 graphite samples resulted in an apparent average density of 1.763 ± 0.012 g/cm^3. A value of 1.76 ± 0.012 g/cm^3 (1σ) was selected to represent the graphite utilized in the radial reflector and thermal column, using the reported average density from the construction of the assembly and the larger uncertainty obtained from apparent density measurements. All graphite (excluding pebbles) used in the HTR-PROTEUS experiments are assumed to have the same density uncertainty unless otherwise specified.

The density of the radial reflector surrounding the core, and the thermal column, was 1.76 g/cm^3. The uncertainty in the density was 0.012 g/cm^3 (1σ). A double-sided perturbation was performed in which the density was perturbed by ±0.036 g/cm^3 to estimate the uncertainty in k_{eff} due to the uncertainty in the density of the radial reflector. Half of the differences between the calculated upper and lower perturbed values were then scaled to obtain the 1σ uncertainty. Results are shown in Table 2.1-4.

Table 2.1-4. Effect of Uncertainty in Graphite Density.

Case (Core)	Deviation	Δk_p	±	$\sigma_{\Delta kp}$	Scaling Factor	Δk_{eff} (1σ)	±	$\sigma_{\Delta keff}$
1 (4)	±0.036 g/cm^3	0.00313	±	0.00005	3	0.00104	±	0.00002

2.1.2.2 Graphite Impurities

Various values were reported for the nominal absorption cross section or boron content for the graphite material used in the core (Table 1.1-6). Subtraction of the absorption cross section of graphite (~3.5 mbarn/atom) allows for estimation of the equivalent boron content (EBC) using nominal boron data (3,840,000 mbarn/atom ^{10}B, 19.9 % ^{10}B in B_{nat}).[a] These values, however, are low since they do not account for the water or air content absorbed into the graphite. Table 1.1-7 with its accompanying text provides some insight into the evaluated water content. Pulsed neutron source measurements were performed to obtain global impurity measurements for the entire core that included moisture content and intergranular nitrogen from the air. These measurements were performed in the empty PROTEUS graphite reflectors and were initially evaluated using diffusion theory.[b] Later Monte Carlo methods were used to evaluate the measured data to provide a nominal ^{10}B concentration of 2.69 ± 0.16 (assumed units of mbarn/atom), which corresponds to 0.2696 and 0.2591 ppma in the radial and axial reflectors, respectively.[c] The average EBC is 1.33 ppm (by at.%). The uncertainty in the initial reported concentration (±0.16 mbarn/atom) is propagated to obtain an uncertainty in the EBC of ±0.08 ppma (1σ). All graphite (excluding pebbles) used in the HTR-PROTEUS experiments are assumed to have the same impurity content and uncertainty unless otherwise specified.

[a] E. M. Baum, H. D. Knox, and T. R. Miller, *Nuclides and Isotopes: 16th Edition*, Knolls Atomic Power Laboratory (2002).
[b] Williams, T., Mathews, D., and Yamane, T., "Measurement of the Absorption Properties of the HTR-PROTEUS Reflector Graphite by Means of a Pulsed-Neutron Technique," TM-41-93-34, Paul Scherrer Institut, Villigen, October 3, 1995.
[c] Difilippo, F. C., "Applications of Monte Carlo Simulations of Thermalization Processes to the Nondestructive Assay of Graphite," *Nucl. Sci. Eng.*, **133**, 163-177 (1999).

The impurity content of the radial reflector surrounding the core and the thermal column was 1.33 ppm (EBC by atom percent). The uncertainty in the impurity content was 0.08 ppma (1σ). A double-sided perturbation was performed in which the impurity content was perturbed by ±0.24 ppma to estimate the uncertainty in k_{eff} due to the uncertainty in the impurity content of the radial reflector. Half of the differences between the calculated upper and lower perturbed values were then scaled to obtain the 1σ uncertainty. Results are shown in Table 2.1-5.

Table 2.1-5. Effect of Uncertainty in Graphite Impurity Content.

Case (Core)	Deviation	Δk_p	±	$\sigma_{\Delta kp}$	Scaling Factor	Δk_{eff} (1σ)	±	$\sigma_{\Delta keff}$
1 (4)	±0.24 ppma	-0.00312	±	0.00005	3	-0.00104	±	0.00002

2.1.3 Upper Axial Reflector

2.1.3.1 Location above Core

The bottom surface of the graphite in the upper axial reflector is located 1893 mm above the top surface of the lower axial reflector, creating a core cavity with a height of 1893 mm. This value is obtained by calculating the difference between reported heights in Figure 1.1-1. Elsewhere it has been reported that this height is 1863 mm.[a] It is believed that this latter value was reported incorrectly. The suspended position of the upper axial reflector was measured to within 3 to 5 mm.[b]

The location of the upper axial reflector above the inside bottom of the core cavity is 1893 mm. The uncertainty in this location was assumed to be 5 mm (bounding limit with uniform probability distribution). A double-sided perturbation was performed in which the location was perturbed by ±15 mm to estimate the uncertainty in k_{eff} due to the uncertainty in the location of the upper axial reflector. Half of the differences between the calculated upper and lower perturbed values were then scaled to obtain the 1σ uncertainty. Results are shown in Table 2.1-6.

Table 2.1-6. Effect of Uncertainty in the Location of the Upper Axial Reflector.

Case (Core)	Deviation	Δk_p	±	$\sigma_{\Delta kp}$	Scaling Factor	Δk_{eff} (1σ)	±	$\sigma_{\Delta keff}$
1 (4)	±15 mm	-0.00067	±	0.00005	$3\sqrt{3}$	-0.00013	±	0.00001

2.1.3.2 Aluminum Dimensions

A detailed model was prepared (see Appendix C) where the aluminum support structure for the upper axial reflector (see Figures 1.1-4 and 1.1-6) was included with the geometry and dimensions modeled as identical as possible to those provided in the figures. Components of the aluminum support structure were included below the upper surface of the upper axial reflector. Uncertainty in the exact geometry is assumed to be negligible since the effective bias for compacting the curved surface below the graphite components of the reflector was negligible (see Section 3.1.1.1). An uncertainty was assumed of 1 mm in the thickness of all aluminum sheet material used to manufacture the structural support for the upper

[a] Difilippo, F. C., "Monte Carlo Calculations of Pebble Bed Benchmark Configurations of the PROTEUS Facility," *Nucl. Sci. Eng.*, **143**, 240-253 (2003).
[b] Personal communication with Oliver Köberl at PSI (October 26, 2011).

axial reflector. Due to the difficulty in exactly modeling the dimensions of all aluminum components, this uncertainty is treated as systematic and total aluminum mass was not conserved.

The uncertainty in dimensions of the aluminum support structure was assumed to be 1 mm (bounding limit with uniform probability distribution). A single-sided perturbation was performed in which all thicknesses were simultaneously decreased by 2 mm (material replaced by void) to estimate the uncertainty in k_{eff} due to the uncertainty in the dimensions of the aluminum support structure. The calculated results were then scaled to obtain the 1σ uncertainty. The total mass of the aluminum was not conserved. Results are shown in Table 2.1-7.

Table 2.1-7. Effect of Uncertainty in Aluminum Dimensions.

Case (Core)	Deviation	Δk_p	±	$\sigma_{\Delta kp}$	Scaling Factor	Δk_{eff} (1σ)	±	$\sigma_{\Delta keff}$
1 (4)	-2 mm	-0.00237	±	0.00010	$2\sqrt{3}$	-0.00068	±	0.00003

2.1.3.3 Aluminum Composition

The composition specifications for Peraluman-300 is provided in Table 1.1-8. The composition values listed as less than a given value are taken at half this maximum value in the nominal material composition. The aluminum content is adjusted such that the total composition adds up to 100 %. The nominal composition used for evaluation of the uncertainty in the composition of the safety ring is in Table 2.1-8.

A double-sided perturbation was performed in which the plate composition was perturbed by minimizing and maximizing the aluminum content in the Peraluman, while simultaneously maximizing or minimizing the other elemental constituents within the specified limits, to estimate the uncertainty in k_{eff} due to the uncertainty in the composition of the aluminum support structure for the upper axial reflector. Half of the differences between the calculated upper and lower perturbed values were then scaled to obtain the 1σ uncertainty assuming a bounding limit with uniform probability distribution. Results are shown in Table 2.1-9.

Table 2.1-8. Composition of the Peraluman-300.

Element	Minimum wt.%	Maximum wt.%	Nominal wt.%	Nominal Atoms/barn-cm
B	--	0.001	0.0005	7.3807E-07
Mg	--	3.1	1.55	1.0177E-03
Al	Balance		97.344	5.7575E-02
Si	0.4	0.4	0.4	2.2729E-04
Mn	--	0.5	0.25	7.2621E-05
Fe	0.3	0.3	0.3	8.5730E-05
Cu	0.05	0.05	0.05	1.2557E-05
Zn	0.1	0.1	0.1	2.4398E-05
Ga	--	0.01	0.005	1.1444E-06
Cd	--	0.001	0.0005	7.0983E-08
Total	--	--	100	5.9018E-02

Table 2.1-9. Effect of Uncertainty in Support Structure Composition.

Case (Core)	Deviation	Δk_p	±	$\sigma_{\Delta kp}$	Scaling Factor	Δk_{eff} (1σ)	±	$\sigma_{\Delta keff}$
1 (4)	Min/Max Al	0.00065	±	0.00005	√3	0.00038	±	0.00003

2.1.4 Fuel Pebbles

2.1.4.1 Quantity of Pebbles

Exact quantities of fuel and moderator pebbles were placed in the cores. There is no associated uncertainty. The number of fuel pebbles reported for core configuration 4 is summarized in Table 2.1-10.

Table 2.1-10. Number of Fuel Pebbles.

Case (Core)	# Fuel Pebbles
1 (4)	4920

2.1.4.2 Pebble Packing Fraction

The pebbles were randomly packed for the Core 4 configurations of HTR-PROTEUS. A reference value for the random packing of pebbles in the HTR-PROTEUS assembly is 0.61.[a] The random packing of solid spheres has been recorded with the lowest packing fraction of 0.5236, and densest theoretical regular packing, rhombohedral or hexagonal close-packed, of 0.7405 (the latter of which was used in the finite core Core 1, 1A, 2, and 3; see PROTEUS-GCR-EXP-001). Further delineation of random packing includes the following descriptions:[b]

1. Very loose random packing: obtained when the fluid velocity in a fluidized bed is slowly reduced, the sedimentation of spheres settle to a packing fraction of 0.56.
2. Loose random packing: obtained when spheres individually roll into place over similarly placed spheres, individual random hand-packing, or by dropping the spheres into a container as loose mass. Typical packing fractions are between 0.59 and 0.60.
3. Poured random packing: obtained when spheres are poured into a container. Typical packing fractions are between 0.609 and 0.625.
4. Close random packing: obtained when a bed of spheres is vibrated or shaken down vigorously. Typical packing fractions are between 0.625 and 0.641.

The poured random packing method most closely matches the process for packing the Core 4 configurations. Some redistribution of pebbles was performed by hand in an effort to level the final core height. More recent theoretical studies indicate that the maximum packing fraction achievable is approximately 0.634,[c] which is slightly greater than the packing fraction obtained for this experiment and unachievable as the entire PROTEUS core was not shaken in order to increase the pebble packing.

[a] Difilippo, F. C., "Monte Carlo Calculations of Pebble Bed Benchmark Configurations of the PROTEUS Facility," *Nucl. Sci. Eng.*, **143**, 240-253 (2003).
[b] Dullien, F. A. L., *Porous Media: Fluid Transport and Pore Structure*, 2nd ed., Academic Press, Inc., San Diego, CA (1992).
[c] C. Song, P. Wang, H. A. Makse, "A Phase Diagram for Jammed Matter," *Nature*, **453**, 629-632 (2008).

Comparison of the packing fraction between Cores 4.2 and 4.3 indicate a difference of ~0.003 (a decrease in core height by 0.02 m, and a decrease in the number of pebbles by 80). This effect is slightly smaller than the uncertainty in the packing fraction that can be attributed to an arbitrary uncertainty in the core height of 0.01 m, which is approximately ±0.004.

The packing fraction for the core configuration was computed by taking the total volume of pebbles within the core cavity (assumed diameter of 6.000 cm) and dividing by the total core volume within the nearly cylindrical cavity, the pebble stack height, and the bottom of the cavity (comprised of the top of the lower axial reflector and the cavity floor filler pieces). The packing fraction is approximately 61 vol.% (see Table 2.1-11). Uncertainty in the packing fraction is due to the small uncertainties in the diameters of the pebbles and dimensions of the graphite reflector, which are negligible contributors, and the uncertainty in the stacked height of the pebbles within the core cavity, which is evaluated in Section 2.1.7.1.

Table 2.1-11. Pebble Packing Fraction.

Case (Core)	Total # Pebbles	Pebble Volume (m^3)	Pebble Stack Height (m)	Core Volume (m^3)	Packing Fraction (vol.%)[(a)]
1 (4)	9840	~1.1129	1.51	~1.8271	~60.91

(a) A nominal packing fraction for random pebbles is ~0.61.

2.1.4.3 Pebble Random Packing

In Core 4, the pebbles were randomly loaded into the PROTEUS core cavity; their exact positions are unknown. The actual packing fraction of the core is at the lower end of the range of typical packing fraction values for randomly loaded pebbles (see Section 2.1.4.2). Although the PEBBLES code[a] was utilized in the analysis of the HTR10 reactor (see Section 2.1.39 of HTR10-GCR-RESR-001), it was unable to effectively generate randomly packed pebble distributions within the bounding limits of the core cavity's quasi-conical bottom (see Figure 2.1-3) and measured stacked pebble height.

An automated process was developed in which layers of pebbles were "dropped" within the confines of the core cavity region (see Figures 3.1-13 and 4.1-2) using a quasi-random method. The random pebble placement model uses a "radial" pitch to create a single layer of pebbles in a hexagonal array to fill the cross-section of the reactor vessel. An axial pitch is used to stack the next layer of pebbles, which is also in a hexagonal array but has been shifted so that bottoms of the pebbles in this layer are centered in the "valleys" formed by the pebbles in the previous layer, tentatively forming a hexagonal close-packed lattice (see PROTEUS-GCR-EXP-001) but with gaps from randomly displaced pebbles and a looser packing fraction (see Figure 4.1-3). The process is randomized by adding a displacement perturbation to each of the pebble's coordinates. The magnitude of the perturbation is equal to the distance between pebbles in each coordinate direction times a user specified constant. The value to be added to each coordinate is determined by a random number that is normalized to give a value with uniform probability between -1 and +1 times the perturbation magnitude. The process continues by adding layers until a desired height or fill factor is reached. If this is not achieved then the process is iterated by varying the radial and axial pitches to satisfy the desired height or fill factor with the added constraint that each layer is complete and the number of pebbles is as close as possible to the exact number of specified pebbles. The exact number of pebbles is obtained by either increasing the magnitude of the displacement perturbations, which causes pebble intersections that are removed by the process, and/or by randomly deleting the excess number of pebbles. Finally, the specified number of fuel and graphite pebbles are

[a] A. M. Ougouag and J. J. Cogliati, "Methods for Modeling the Packing of Fuel Elements in Pebble Bed Reactors," Mathematics and Computations, Supercomputing, Reactor Physics and Nuclear and Biological Applications, Palais des Papes, Avignon, France, September 12-15 (2005).

randomly assigned from the entire distribution of pebbles. This approach for simulating pebble packing in the core is thought to roughly reproduce the experimental method of pouring pebbles into the core cavity and then hand-leveling the pebble stack throughout the loading process. The code used to simulate the random packing of pebbles was compared against the PEBBLES code for the HTR10 reactor (HTR10-GCR-RESR-001) during its review process; there were no significant differences in the calculated results obtained when using one code or the other to simulate the random pebble packing.

The uncertainty in the random packing of the pebbles was assessed by varying the random seed for the packing simulation, effectively changing the positions of each pebble and the localized moderator-to-fuel pebble ratios throughout the core. Six additional pebble arrangements were compared to the original model (see MCNP input deck in Appendix A.1.8 for exact pebble locations), which were generated by changing the random seed used in the packing simulation. Results are shown in Table 2.1-12. Packing configuration 1, which is provided as sample MCNP5 input for the benchmark model in Appendix A.1 and a detailed model in Appendix C, was used for the analysis of the uncertainties in this experiment.

Table 2.1-12. Pebble Random Packing Evaluation.[(a)]

Packing Configuration	k_{MCNP}	σ
1 (input in App. A.1)	1.02165	0.00007
2	1.02241	0.00007
3	1.02231	0.00007
4	1.02219	0.00007
5	1.02195	0.00007
6	1.02181	0.00007
7	1.02109	0.00007
Average	1.02192	0.00045

(a) Calculations were performed with control rods fully withdrawn.

2.1.4.4 Isotopic Content (Mass) ^{235}U

The mass and uncertainty of each uranium isotope in a fuel pebble was reported in Table 1.1-1. The isotopic content of the fuel would have been measured and the mass of each isotope calculated based upon the total uranium mass within each pebble. The isotopic content (in wt.%) of each isotope was computed for both the uranium metal and UO_2 fuel kernel (see Table 2.1-13).

The mass of ^{235}U reported was 1.000 g per pebble (Table 1.1-1). The uncertainty in the ^{235}U mass was 0.010 g (~0.17 wt.%, 1σ). A double-sided perturbation was performed in which the ^{235}U mass was perturbed by ±0.030 g (~0.50 wt.%) to estimate the uncertainty in k_{eff} due to the uncertainty in the isotopic content of ^{235}U. To conserve total uranium mass, the ^{238}U mass was adjusted. Half of the differences between the calculated upper and lower perturbed values were then scaled to obtain the 1σ uncertainty. Results are shown in Table 2.1-14.

Table 2.1-13. Isotopic Composition of Uranium.

Isotope/Element	Mass (g)	Uranium Metal Composition (wt.%)	UO_2 Composition (wt.%)
^{234}U	0.008	0.134	0.118
^{235}U	1.000	16.762	14.77
^{236}U	0.005	0.084	0.074
^{238}U	4.953	83.020	73.155
O	--	--	11.87
Impurities	--	--	0.013
Total	5.966	100.000	100.000

Table 2.1-14. Effect of Uncertainty in the ^{235}U Content.

Case (Core)	Deviation	Δk_p	±	$\sigma_{\Delta kp}$	Scaling Factor	Δk_{eff} (1σ)	±	$\sigma_{\Delta keff}$
1 (4)	±0.030 g (~0.50 wt.%)	0.00755	±	0.00005	3	0.00252	±	0.00002

2.1.4.5 Uranium Mass

Table 1.1-1 reports a mass uncertainty in the fuel of ±0.060 g, which appears to be a sum of the uncertainties in the ^{235}U and ^{238}U masses and equates to a mass density uncertainty in the UO_2 fuel of approximately 0.11 g/cm^3. However, this table also reports the uncertainty in the UO_2 density as ±0.04 g/cm^3, almost a factor of 3 smaller. The table has footnotes for some of the uncertainties to explain the confidence level of the measured parameters; however, no additional information is provided for the uranium fuel mass or UO_2 density. A fuel mass of 5.966 g (UO_2 density of 10.88 g/cm^3) was selected for the fuel kernels and the larger uncertainty of 0.060 g (0.11 g/cm^3) selected to represent the 1σ uncertainty in the uranium mass.

The total mass of uranium per fuel pebble was 5.966 g (Table 1.1-1). The uncertainty in the mass was 0.060 g (0.068 g UO_2, 0.11 g/cm^3, 1σ). A double-sided perturbation was performed in which the uranium dioxide density was perturbed by ±0.12 g/cm^3 to estimate the uncertainty in k_{eff} due to the uncertainty in the uranium mass per fuel pebble. Half of the differences between the calculated upper and lower perturbed values were then scaled to obtain the 1σ uncertainty. The radius of the UO_2 kernels and the oxygen-to-uranium ratio was held constant. Results are shown in Table 2.1-15.

The calculated Δk_{eff} uncertainty was adjusted to account for random and systematic components of the total uncertainty. The systematic component is assumed to represent 15 % of the total uncertainty; the random component is negligible due to the perturbation of a large quantity of objects. The final adjusted Δk_{eff} uncertainty is therefore only the preserved systematic uncertainty.

Table 2.1-15. Effect of Uncertainty in the Fuel Pebble Uranium Mass.

Case (Core)	Deviation	Δk_p	±	$\sigma_{\Delta kp}$	Scaling Factor[(a)]	Δk_{eff} (1σ)	±	$\sigma_{\Delta keff}$	Systematic Component of Δk_{eff} (1σ)
1 (4)	±0.065 g (0.12 g/cm^3)	0.00225	±	0.00005	12/11	0.00206	±	0.00005	0.00031

(a) The scaling factor converts the perturbation uncertainty of 0.12 g/cm^3, which represents the reported 3σ uncertainty in the UO_2 mass density to the 0.11 g/cm^3 1σ uncertainty in the mass density based upon the reported uncertainty in the uranium mass measurements.

2.1.4.6 Fueled Zone Impurities

The reported impurity content for the fuel pebbles is listed in Table 1.1-13. The composition values listed as less than a given value are taken at half this maximum value in the nominal material composition. The fueled zone composition (graphite region within the pebble surrounding the TRISO particles) is adjusted such that the total composition adds up to 100 %. The nominal impurity content used for evaluation of the uncertainty in the fueled zone impurities is in Table 2.1-16.

The nominal fueled zone impurity content is shown in Table 2.1-16. The selected uncertainty in each impurity was 50 % of the nominal value (1σ). A double-sided perturbation was performed in which all impurities were simultaneously perturbed by ±50 % to estimate the uncertainty in k_{eff} due to the uncertainty in the fueled zone impurity content. Half of the differences between the calculated upper and lower perturbed values were then scaled to obtain the 1σ uncertainty.

The scaling factor was obtained by first determining the equivalent boron content (EBC) of each impurity based upon their concentration in the graphite and their respective ASTM EBC factor.[a] The ratio of the equivalent boron content for each individual impurity to the total EBC was calculated; most ratios were small compared to the dominant impurities of boron (~41 %) and lithium (~30 %). Sample perturbations were performed to confirm that perturbations of the dominant impurities produced uncertainties in k_{eff}, divided by the total uncertainty obtained by perturbing all impurities simultaneously, would produce ratios approximately equal to the EBC ratios. The EBC ratios for all the graphite impurities were combined taking the square root of the sum of the squares to obtain a scaling factor of 53 %, which is needed to convert the additive perturbation of impurity content into one representing the quadrative summation expected for perturbing each impurity individually by 50 %. Results are shown in Table 2.1-17.

[a] ASTM C1233-03, "Standard Practice for Determining Equivalent Boron Contents of Nuclear Materials," ASTM International, West Conshohocken, PA (2009).

Table 2.1-16. Fuel Pebble Impurities.

Element	Minimum ppm (wt.%)	Maximum ppm (wt.%)	Nominal ppm (wt.%)
Ag	--	0.2	0.1
B	0.101	0.101	0.101
Ca	9.28	9.28	9.28
Cd	--	0.103	0.0515
Cl	--	3	1.5
Co	--	0.13	0.065
Cr	1.81	1.81	1.81
Dy	--	0.01	0.005
Eu	--	0.01	0.005
Fe	2.95	2.95	2.95
Gd	--	0.01	0.005
Li	--	1	0.5
Mn	0.43	0.43	0.43
Ni	--	1	0.5
S	--	0.011	0.0055
Ti	0.497	0.497	0.497
V	--	0.433	0.2165
Total	--	--	18.0215

Table 2.1-17. Effect of Uncertainty in the Fueled Zone Impurities.

Case (Core)	Deviation	Δk_p	±	$\sigma_{\Delta kp}$	Scaling Factor	Δk_{eff} (1σ)	±	$\sigma_{\Delta keff}$
1 (4)	±50 %	-0.00028	±	0.00005	1/0.53	-0.00015	±	0.00003

2.1.4.7 Unfueled Zone Impurities

The reported impurity content for the fuel pebbles is listed in Table 1.1-13. It is assumed that the unfueled zone impurities are the same as the fueled zone impurities in Section 2.1.4.6. The composition values listed as less than a given value are taken at half this maximum value in the nominal material composition. The unfueled zone composition (graphite shell surrounding the fueled zone of the pebble) is adjusted such that the total composition adds up to 100 %. The nominal impurity content used for evaluation of the uncertainty in the unfueled zone impurities is in Table 2.1-16.

The nominal unfueled zone impurity content is shown in Table 2.1-16. The selected uncertainty in each impurity was 50 % of the nominal value (1σ). A double-sided perturbation was performed in which all impurities were simultaneously perturbed by ±50 % to estimate the uncertainty in k_{eff} due to the uncertainty in the unfueled zone impurity content. Half of the differences between the calculated upper and lower perturbed values were then scaled to obtain the 1σ uncertainty.

The scaling factor was obtained by first determining the equivalent boron content (EBC) of each impurity based upon their concentration in the graphite and their respective ASTM EBC factor.[a] The ratio of the equivalent boron content for each individual impurity to the total EBC was calculated; most ratios were small compared to the dominant impurities of boron (~41 %) and lithium (~30 %). Sample perturbations were performed to confirm that perturbations of the dominant impurities produced uncertainties in k_{eff}, divided by the total uncertainty obtained by perturbing all impurities simultaneously, would produce ratios approximately equal to the EBC ratios. The EBC ratios for all the graphite impurities were combined taking the square root of the sum of the squares to obtain a scaling factor of 53 %, which is needed to convert the additive perturbation of impurity content into one representing the quadrative summation expected for perturbing each impurity individually by 50 %. Results are shown in Table 2.1-18.

Table 2.1-18. Effect of Uncertainty in the Unfueled Zone Impurities.

Case (Core)	Deviation	Δk_p	±	$\sigma_{\Delta kp}$	Scaling Factor	Δk_{eff} (1σ)	±	$\sigma_{\Delta keff}$
1 (4)	±50 %	-0.00024	±	0.00005	1/0.53	-0.00013	±	0.00003

2.1.5 Moderator Pebbles

2.1.5.1 Quantity of Pebbles

Exact quantities of fuel and moderator pebbles were placed in the cores. There is no associated uncertainty. The number of moderator pebbles reported for core configuration 4 is given in Table 2.1-19. The number of moderator pebbles is exactly the same as the number of fuel pebbles.

Table 2.1-19. Number of Moderator Pebbles.

Case (Core)	# Moderator Pebbles
1 (4)	4920

[a] ASTM C1233-03, "Standard Practice for Determining Equivalent Boron Contents of Nuclear Materials," ASTM International, West Conshohocken, PA (2009).

2.1.5.2 Impurities

The reported impurity content for the moderator pebbles is listed in Table 1.1-14. The composition values listed as less than a given value are taken at half this maximum value in the nominal material composition. The moderator pebble composition is adjusted such that the total composition adds up to 100 %. The nominal impurity content used for evaluation of the uncertainty in the unfueled zone impurities is in Table 2.1-20.

The nominal moderator pebble impurity content is shown in Table 2.1-20. The selected uncertainty in each impurity was 50 % of the nominal value (1σ). A double-sided perturbation was performed in which all impurities were simultaneously perturbed by ±50 % to estimate the uncertainty in k_{eff} due to the uncertainty in the moderator pebble impurity content. Half of the differences between the calculated upper and lower perturbed values were then scaled to obtain the 1σ uncertainty.

The scaling factor was obtained by first determining the equivalent boron content (EBC) of each impurity based upon their concentration in the graphite and their respective ASTM EBC factor.[a] The ratio of the equivalent boron content for each individual impurity to the total EBC was calculated; most ratios were small compared to the dominant impurities of boron (~47 %), chlorine (~16 %) and gadolinium (~11 %). Sample perturbations were performed to confirm that perturbations of the dominant impurities produced uncertainties in k_{eff}, divided by the total uncertainty obtained by perturbing all impurities simultaneously, would produce ratios approximately equal to the EBC ratios. The EBC ratios for all the graphite impurities were combined taking the square root of the sum of the squares to obtain a scaling factor of 52 %, which is needed to convert the additive perturbation of impurity content into one representing the quadrative summation expected for perturbing each impurity individually by 50 %. Results are shown in Table 2.1-21.

Table 2.1-20. Moderator Pebble Impurities.

Element	Minimum ppm (wt.%)	Maximum ppm (wt.%)	Nominal ppm (wt.%)
B	0.76	0.76	0.76
Ca	129	129	129
Cd	--	0.6	0.3
Cl	18.64	18.64	18.64
Dy	0.065	0.065	0.065
Eu	0.13	0.13	0.13
Fe	5.9	5.9	5.9
Gd	0.040	0.040	0.040
Li	0.88	0.88	0.88
Ni	0.78	0.78	0.78
S	140	140	140
Si	35	35	35
Sm	0.086	0.086	0.086
Ti	10	10	10
V	13	13	13
Total	--	--	354.581

[a] ASTM C1233-03, "Standard Practice for Determining Equivalent Boron Contents of Nuclear Materials," ASTM International, West Conshohocken, PA (2009).

Table 2.1-21. Effect of Uncertainty in the Moderator Pebble Impurities.

Case (Core)	Deviation	Δk_p	±	$\sigma_{\Delta kp}$	Scaling Factor	Δk_{eff} (1σ)	±	$\sigma_{\Delta keff}$
1 (4)	50 %	-0.00333	±	0.00005	1/0.52	-0.00173	±	0.00003

2.1.6 Graphite Fillers

2.1.6.1 Cavity Floor Inner Equivalent Diameter

The set of graphite cavity floor fillers is comprised of 21 finely machined graphite blocks. These blocks are placed in a radial pattern surrounding the top of the central cylinder of the lower axial reflector, approximating a nearly circular annulus (Figure 1.1-15). The set of fillers forms an irregularly-shaped icosikaihenagon (21-sided polygon). Available information regarding the dimensions of the cavity floor fillers (captured in Figure 2.1-1 from Figure 1.1-15) were utilized to estimate the location of the vertices to form the annular shape (see Figure 2.1-2). A perfect polygon could not be generated using all the dimensions provided. Various dimensions had to be estimated from available information with adjustments made to complete the annulus. Possible gaps in assembly may have contributed to slight measurement discrepancies. It should also be noted that the interstitial vertex on the largest wedge was removed from the calculations. The impact of dimensional discrepancies is negligible.

The dimensions shown in Figure 2.1-2 were used to calculate the total area encompassed by the inner polygon (~0.20 m^2) and then the radius and diameter of a circle encompassing this equivalent area (~250 and ~499 mm, respectively). The dimensions of the cavity floor filler pieces modeled as a single annulus are provided in Figure 2.1-3.

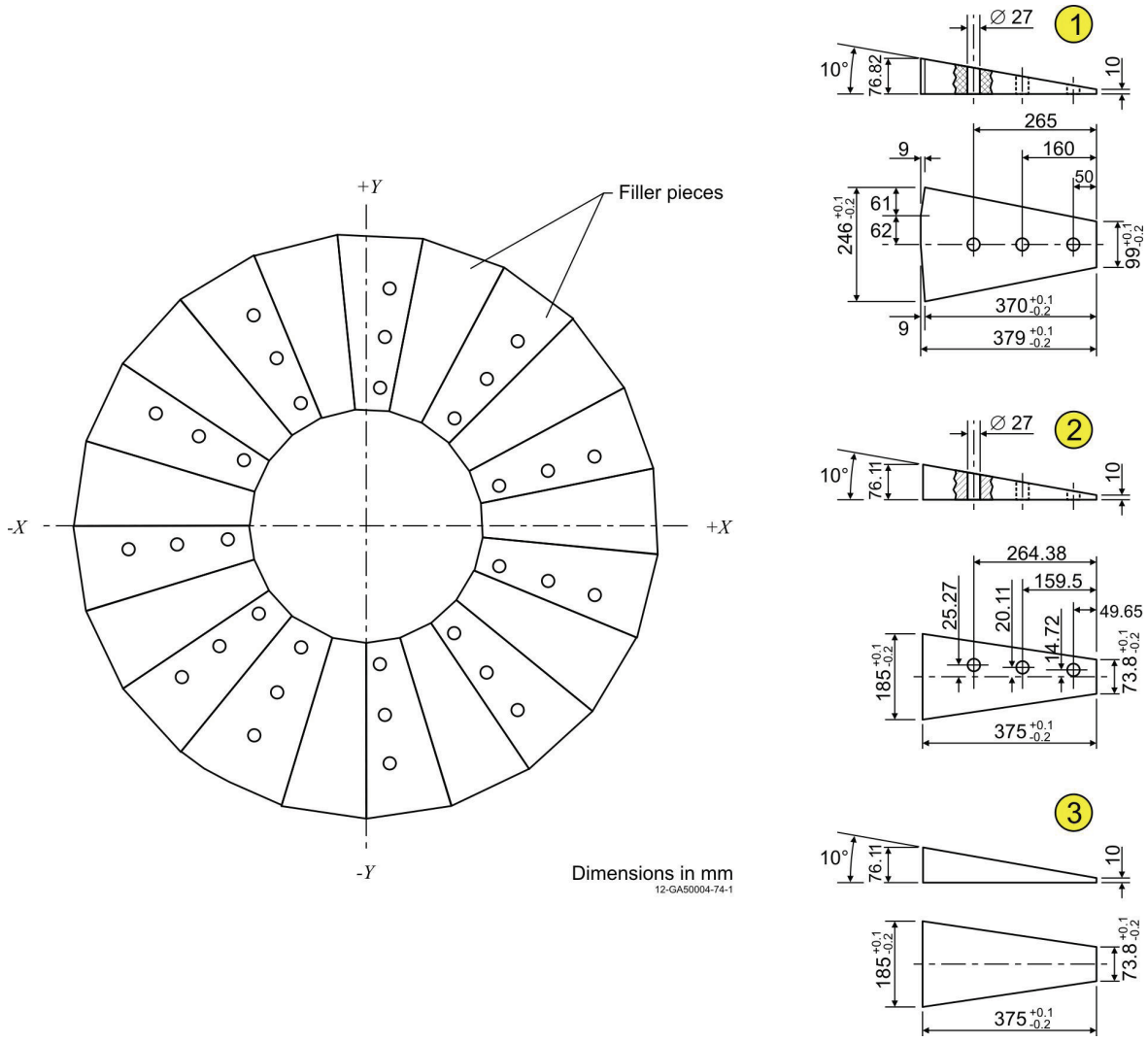

Figure 2.1-1. Cavity Floor Filler Pieces (Redrawn from Figure 1.1-15).

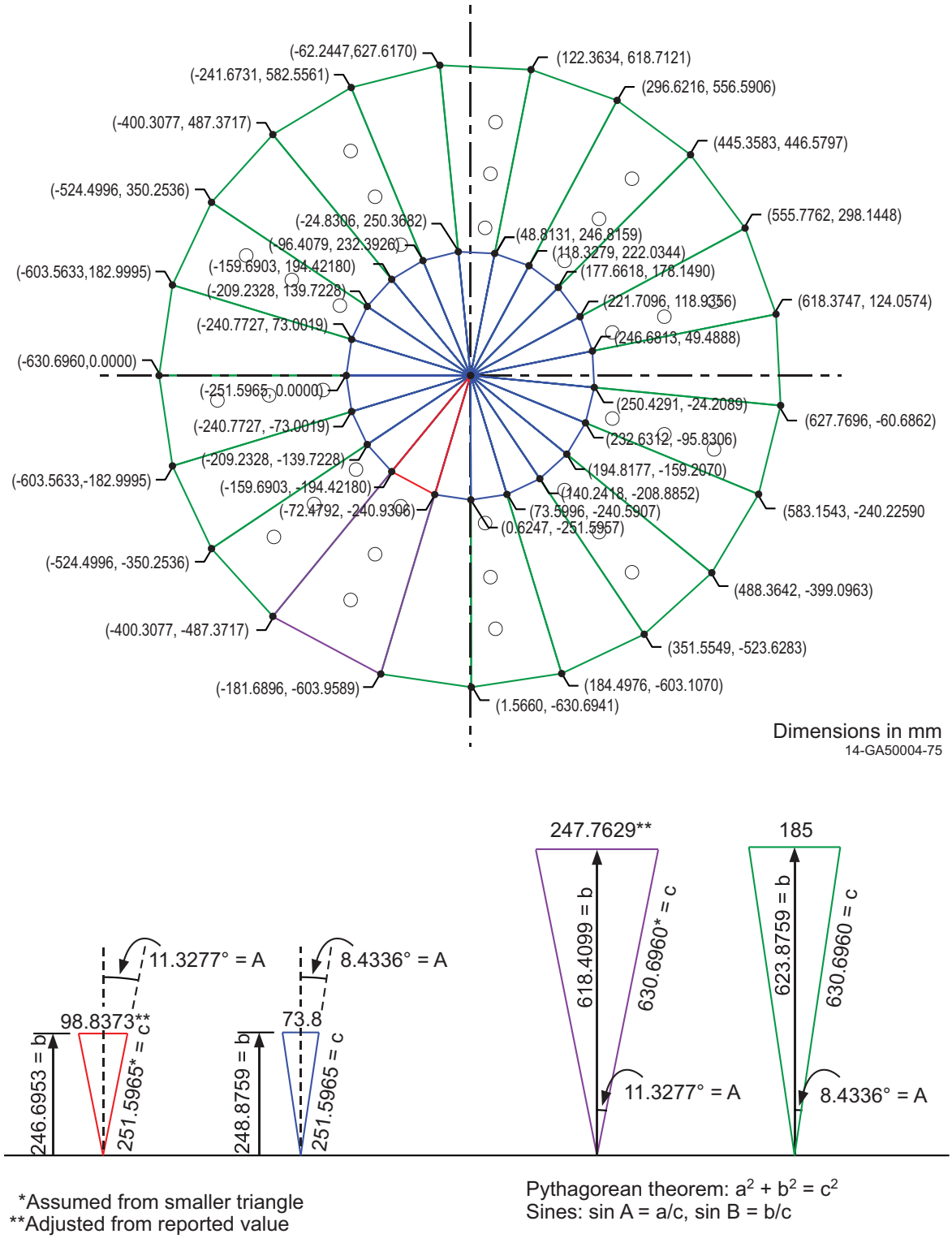

Figure 2.1-2. Vertices and Dimensions of the Cavity Floor Filler Pieces.

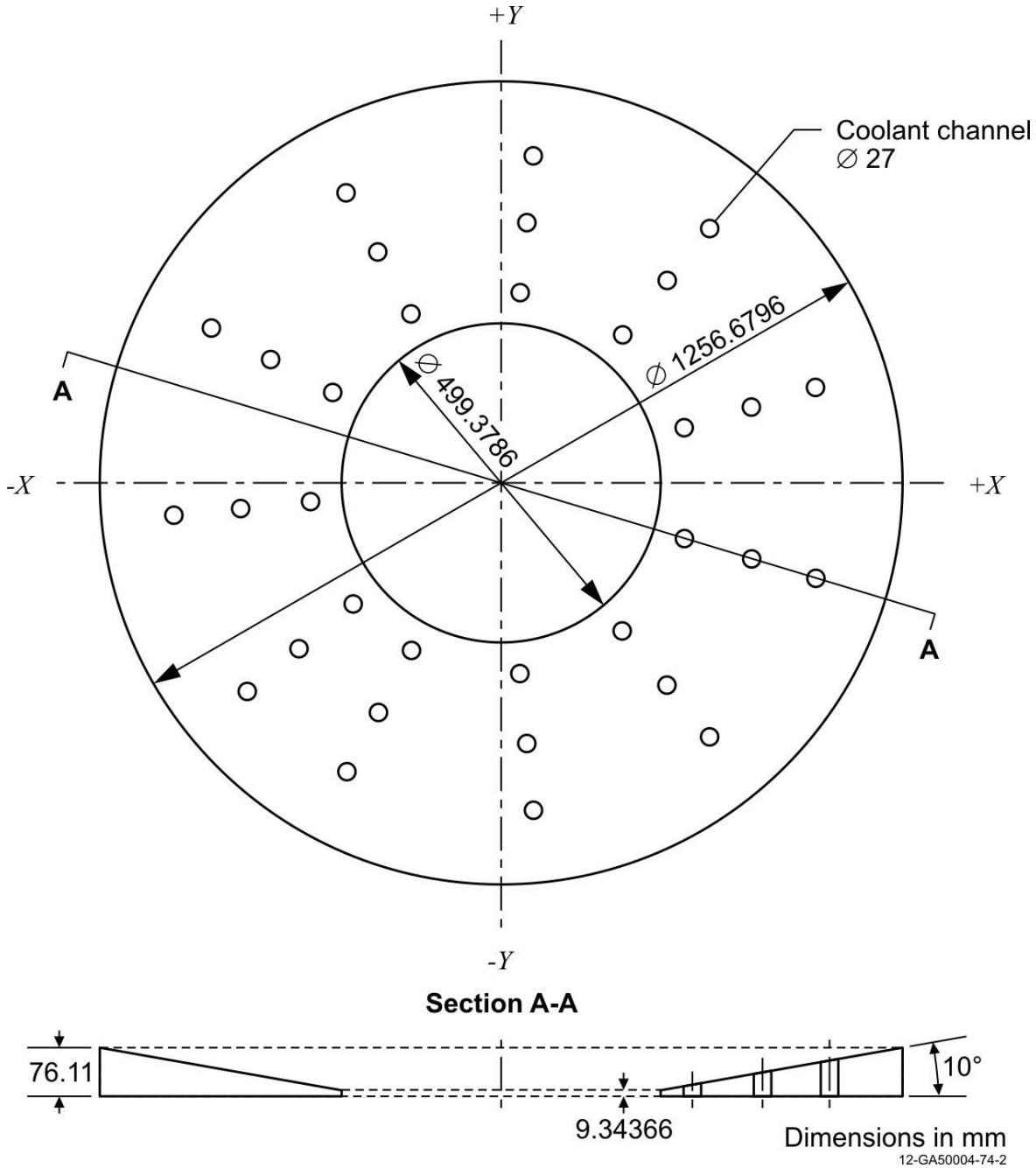

Figure 2.1-3. Dimensions of the Cavity Floor Filler Pieces Modeled as a Single Annulus.

The calculated inner equivalent diameter of the cavity floor filler pieces is ~499 mm. The uncertainty in the diameter was assumed to be 1 mm (bounding limit with uniform probability distribution). A double-sided perturbation was performed in which the diameter was perturbed by ±3 mm to estimate the uncertainty in k_{eff} due to the uncertainty in inner equivalent diameter of the cavity floor filler pieces. Half of the calculated results were then scaled to obtain the 1σ uncertainty. Results are shown in Table 2.1-22. The calculated uncertainty is negligible (≤0.00010).

Table 2.1-22. Effect of Uncertainty in Inner Equivalent Diameter.

Case (Core)	Deviation	Δk_p	±	$\sigma_{\Delta kp}$	Scaling Factor	Δk_{eff} (1σ)	±	$\sigma_{\Delta keff}$
1 (4)	±3 mm	0.00005	±	0.00005	3√3	0.00001	±	0.00001

2.1.6.2 Cavity Floor Outer Equivalent Diameter

The dimensions shown in Figure 2.1-2 were used to calculate the total area encompassed by the outer polygon describing the cavity floor filler pieces (~1.23 m^2) and then the radius and diameter of a circle encompassing this equivalent area (~626 and ~1252 mm, respectively). However, to simplify the benchmark model, the outer diameter was extended to match the inner equivalent diameter of the radial reflector, which has a radius and diameter of ~628 and ~1257 mm, respectively (see Figure 2.1-3).

The outer equivalent diameter of the cavity floor filler pieces is ~1257 mm. The uncertainty in the diameter was assumed to be 2 mm (bounding limit with uniform probability distribution). A single-sided perturbation was performed in which the diameter was decreased by 6 mm to estimate the uncertainty in k_{eff} due to the uncertainty in outer equivalent diameter of the cavity floor filler pieces. The calculated results were then scaled to obtain the 1σ uncertainty. Results are shown in Table 2.1-23. The calculated uncertainty is negligible (≤0.00010).

Table 2.1-23. Effect of Uncertainty in Outer Equivalent Diameter.

Case (Core)	Deviation	Δk_p	±	$\sigma_{\Delta kp}$	Scaling Factor	Δk_{eff} (1σ)	±	$\sigma_{\Delta keff}$
1 (4)	-6 mm	0.00008	±	0.00010	3√3	0.00002	±	0.00002

2.1.6.3 Cavity Floor Height

Figures 2.1-1 and 2.1-3 provide the height of the quasi-conical polyhedron/annulus. Any uncertainty in the height would be much less than 1 mm, and the impact on the slope would also be insignificant. Perturbation of the height of the cavity floor filler pieces was not performed as the impact on the uncertainty in k_{eff} would be negligible, as the total measured mass of the graphite would be conserved and only minimally redistributed beneath the pebbles in model calculations. Therefore, the uncertainty in the height of the cavity floor filler pieces is judged to be negligible (≤0.00010).

2.1.6.4 Cavity Floor Coolant Channel Positions

The radial location of the 33 typically open coolant channels are reported to have radial distances from the core center of 300, 410, and 515 mm, representing the 1st, 3rd, and 5th rings (see Figures 1.1-2b and 1.1-7) for the lower axial reflector. It is assumed that the channels in the cavity floor filler pieces are located in the same positions both radially and azimuthally (as shown in Figure 1.1-15). Equidistant holes within a ring are 11.25° apart in the lower axial reflector. The exact positions of the channels in the cavity floor filler pieces is provided in Table 3.1-5 Due to the uncertainty in the exact radial placement of each coolant channel ring, an uncertainty of ±5 mm is assumed sufficient to encompass that uncertainty. This uncertainty also encompasses the uncertainty in the angular placement within a ring (assumed negligible). The positions of the channels were perturbed independently from the channels located in the upper and lower axial.

The positions of the coolant channel holes within the cavity floor filler pieces were approximately 300, 410, and 515 mm radially from the core center. The uncertainty in these positions was 5 mm (bounding limit with uniform probability distribution). A double-sided perturbation was performed in which all positions were simultaneously perturbed by ±15 mm to estimate the uncertainty in k_{eff} due to the uncertainty in the positions of the coolant channel holes within the cavity floor filler pieces. Half of the calculated results were then scaled to obtain the 1σ uncertainty. Results are shown in Table 2.1-24. The calculated uncertainty is negligible (≤0.00010).

Table 2.1-24. Effect of Uncertainty in Coolant Channel Positions.

Case (Core)	Deviation	Δk_p	±	$\sigma_{\Delta kp}$	Scaling Factor	Δk_{eff} (1σ)	±	$\sigma_{\Delta keff}$
1 (4)	±15 mm	-0.00002	±	0.00005	3√3	<0.00001	±	0.00001

2.1.6.5 Cavity Floor Coolant Channel Diameter

The diameter of the coolant channel holes within the cavity floor filler pieces was 27 mm. The uncertainty in hole diameter was assumed to be 1 mm (bounding limit with uniform probability distribution). A double-sided perturbation was performed in which the diameter of all positions were simultaneously perturbed by ±3 mm to estimate the uncertainty in k_{eff} due to the uncertainty in the diameter of the coolant channel holes within the cavity floor filler pieces. Half of the calculated results were then scaled to obtain the 1σ uncertainty. Results are shown in Table 2.1-25. The calculated uncertainty is negligible (≤0.00010).

Table 2.1-25. Effect of Uncertainty in Coolant Channel Hole Diameter.

Case (Core)	Deviation	Δk_p	±	$\sigma_{\Delta kp}$	Scaling Factor	Δk_{eff} (1σ)	±	$\sigma_{\Delta keff}$
1 (4)	±3 mm	-0.00002	±	0.00005	3	<0.00001	±	0.00001

2.1.6.6 Cavity Floor Mass

The total mass of the 21 cavity floor filler pieces was 85.60 kg (estimated mass density of ~1.7551 g/cm^3). The uncertainty in the mass was assumed to be 0.01 kg (0.0002 g/cm^3, bounding limit with uniform probability distribution). A double-sided perturbation was performed in which the total mass was perturbed by ±0.03 kg (0.0062 g/cm^3) to estimate the uncertainty in k_{eff} due to the uncertainty in the mass of the cavity floor filler pieces. Half of the calculated results were then scaled to obtain the 1σ uncertainty. Results are shown in Table 2.1-26. The calculated uncertainty is negligible (≤0.00010).

Table 2.1-26. Effect of Uncertainty in the Mass of the Cavity Floor Filler Pieces.

Case (Core)	Deviation	Δk_p	±	$\sigma_{\Delta kp}$	Scaling Factor	Δk_{eff} (1σ)	±	$\sigma_{\Delta keff}$
1 (4)	±0.03 kg (0.0062 g/cm^3)	-0.00003	±	0.00005	3√3	<0.00001	±	0.00001

2.1.6.7 Cavity Floor Impurities

It is assumed that the EBC of 1.33 ± 0.08 ppm (by at.%), discussed in Section 2.1.2.2, sufficiently described the impurity content in the cavity floor filler pieces.

The impurity content of the cavity floor filler pieces was 1.33 ppm (EBC by atom percent). The uncertainty in the impurity content was 0.08 ppma (1σ). A double-sided perturbation was performed in which the impurity content was perturbed by ±0.24 ppma to estimate the uncertainty in k_{eff} due to the uncertainty in the impurity content of the cavity floor filler pieces. Half of the calculated results were then scaled to obtain the 1σ uncertainty. Results are shown in Table 2.1-27. The calculated uncertainty is negligible (≤0.00010).

Table 2.1-27. Effect of Uncertainty in the Impurity Content of the Cavity Floor Filler Pieces.

Case (Core)	Deviation	Δk_p	±	$\sigma_{\Delta kp}$	Scaling Factor	Δk_{eff} (1σ)	±	$\sigma_{\Delta keff}$
1 (4)	±0.24 ppma	-0.00007	±	0.00005	3	-0.00002	±	0.00002

2.1.7 Experimental Measurements

2.1.7.1 Randomly Loaded Pebble Height

The pebbles were randomly packed for the Core 4 configurations of HTR-PROTEUS. Fuel and moderator pebbles were alternatively added to the core cavity using a single delivery pipe for core loadings 4.2 and 4.3 (core loading 4.1 was rejected due to the inability to quantify the loading bias due to the use of a dual-tube delivery system). The top surface of the pebble bed was lightly flattened following each loading step. A rigid rod was placed on top of the pebbles to assist in the measurement of the core height. The core height for the benchmark model is 1.51 m. An arbitrary 1σ uncertainty of 1 cm was assigned to the height of the Core 4 configurations by the original experimenters. Nominal core parameters regarding the core height and packing fraction are reported in Table 2.1-11.

As discussed in Section 2.1.4.2, the difference in the pebble packing fraction between Cores 4.2 and 4.3 was ~0.003, and was attributed to a decrease in pebble loading by 80 and a decrease in core height by 2 cm. Adjusting the core height by ±1 cm, while maintaining the core pebble loading constant, incurs a packing fraction uncertainty of ±0.004. This value is more than twice the uncertainty obtained by comparing Cores 4.2 and 4.3 and estimating the core height perturbation of ±1 cm to represent a packing fraction uncertainty of ±0.0015. Therefore, an uncertainty of ±0.4 cm is presumed to more adequately represent the true uncertainty in the core height, incurring an uncertainty in the packing fraction of approximately ±0.0016.

The uncertainty in the core height is a correlated function of the uncertainty in the diameter of the individual pebbles, the uncertainty in the dimensions of core cavity geometry, and the packing fraction, where the packing fraction would be the quantity derived from the geometric properties of both core cavity and pebbles. The uncertainty in the pebble radii is very small and found to have a negligible impact on the total experimental uncertainty for the other HTR-PROTEUS core configurations (see PROTEUS-GCR-EXP-001, -003, and -004). A separate uncertainty analysis was performed to investigate the impact of the uncertainty in the core stack height while retaining all other core parameters constant, effectively restacking the random distribution of pebbles within the core and perturbing the core packing fraction (see Section 2.1.4.3). Essentially, the more loosely-packed the pebbles are within the core cavity, the higher they must be stacked; this is because the dimensions of the cavity floor and the

cylindrical wall remain constant and the pebble stack needs to "expand" upward to accommodate the extra volume of air. In the actual experiments, the pebbles were rearranged such that the top of the pebble stack was nearly level; a level top was retained for the pebble stack in the uncertainty analysis as well.

The stacked pebble height in the core was 151 cm. The uncertainty in the height was estimated to be 0.4 cm (packing fraction uncertainty of ±0.0016). A double-sided perturbation was performed in which the stacked pebble height was perturbed by ±1 cm to estimate the uncertainty in k_{eff} due to the uncertainty in the core height. A different pebble arrangement was generated for each perturbation in the stacked pebble height. The quantity of pebbles within the core, and all other core cavity dimensions, were held constant. Half of the differences between the calculated upper and lower perturbed values were then scaled to obtain the 1σ uncertainty. Results are shown in Table 2.1-28.

Because of the potential for non-linearity in the response of Δk with core height, an additional perturbation analysis was performed including additional calculated perturbation points at ±2 cm. A polynomial fit was performed to estimate the uncertainty in k_{eff} due to the uncertainty in the core height of ±0.4 cm. Once again, a different pebble arrangement was generated for each perturbation of the stacked pebble height while the quantity of pebbles within the core, and all other core cavity dimensions, were held constant. The calculated result from this second evaluation of the uncertainty in the stacked pebble height is provided in Table 2.1-28; this uncertainty includes the additional uncertainty incurred through use of the derived polynomial fit equation. It is slightly lower than the uncertainty obtained via the linear adjustment. The uncertainty obtained via the polynomial analysis is selected to represent the total uncertainty in the experiment due to the uncertainty in the stacked pebble height.

Table 2.1-28. Effect of Uncertainty in the Stacked Pebble Height.

Case (Core)	Deviation	Δk_p	±	$\sigma_{\Delta kp}$	Scaling Factor	Δk_{eff} (1σ)	±	$\sigma_{\Delta keff}$
1 (4)	±1 cm (PF ±0.0016) [linear]	-0.00089	±	0.00005	5/2	-0.00035	±	0.00002
1 (4)	±2 cm (PF ±0.0032) [poly fit]	NA			NA	-0.00020		--

2.1.8 Total Experimental Uncertainty

A compilation of the total evaluated uncertainty in the critical configurations of Core 4 (Case 1) of the HTR-PROTEUS experiments is provided in Table 2.1-29. As discussed earlier, uncertainties that are not treated as 100 % systematic, because perturbation analyses were simultaneously applied to multiple components are treated as 15 % systematic (to preserve some uncertainty due to possible, yet unknown, systematic effects) and 85 % random. The random portion of the uncertainty is then divided by the square root of the number of perturbed components, and is negligible for most uncertainties. The total evaluated uncertainty is the root-sum square of all individual uncertainties. A graphical representation of the primary sources of uncertainty is shown in Figure 2.1-4.

Uncertainties ≤0.00010 are reported as negligible (neg) and those that do not apply to a given configuration because they are not used or included as part of the evaluation of a different uncertainty are marked as not applicable (NA). The most significant contribution to the overall uncertainty is the fuel enrichment and the impurity content of the moderator pebbles. All uncertainties providing at least 0.05 %Δk_{eff} are highlighted in Table 2.1-29. The uncertainties in the experimental critical configurations for Core 4 was evaluated and determined to be acceptable.

Table 2.1-29. Summary of Evaluated Uncertainties in HTR-PROTEUS Case 1 (Core 4).

Perturbed Parameter	Parameter Value	1σ Uncertainty	Δk_{eff} (1σ)
Radial Reflector Density (g/cm^3)	1.76	0.012	0.00104
Radial Reflector Impurities (ppma EBC)	1.33	0.08	0.00104
Location of Upper Axial Reflector (mm)	1893	5 / √3	0.00013
Upper Axial Aluminum Dimensions (mm)	Figure 1.1-4	1 / √3	0.00068
Upper Axial Aluminum Composition	Table 2.1-8	1 / √3	0.00038
Pebble Random Packing	See Section 2.1.4.3		0.00045
^{235}U Isotopic Content (wt.%)	~16.762	~0.17	0.00252
Fuel Pebble Uranium Mass (g)	5.966	0.060	0.00031
Fueled Zone Impurities (ppm)	Table 2.1-16	50 %	0.00015
Unfueled Zone Impurities (ppm)	Table 2.1-16	50 %	0.00013
Moderator Pebble Impurities (ppm)	Table 2.1-20	50 %	0.00173
Cavity Floor Inner Equivalent Diameter (mm)	~499	1 / √3	neg
Cavity Floor Outer Equivalent Diameter (mm)	~1257	1 / √3	neg
Cavity Floor Height (mm)	10 to ~76	<<1	neg
Cavity Floor Coolant Channel Positions (mm)	300, 410, 515	5 / √3	neg
Cavity Floor Coolant Channel Diameter (mm)	27	1 / √3	neg
Cavity Floor Mass (kg)	85.60	0.01 / √3	neg
Cavity Floor Impurities (ppma EBC)	1.33	0.08	neg
Stacked Pebble Height (m)	1.51	0.004	0.00020
Total Experimental Uncertainty	**--**	**--**	**0.00354**

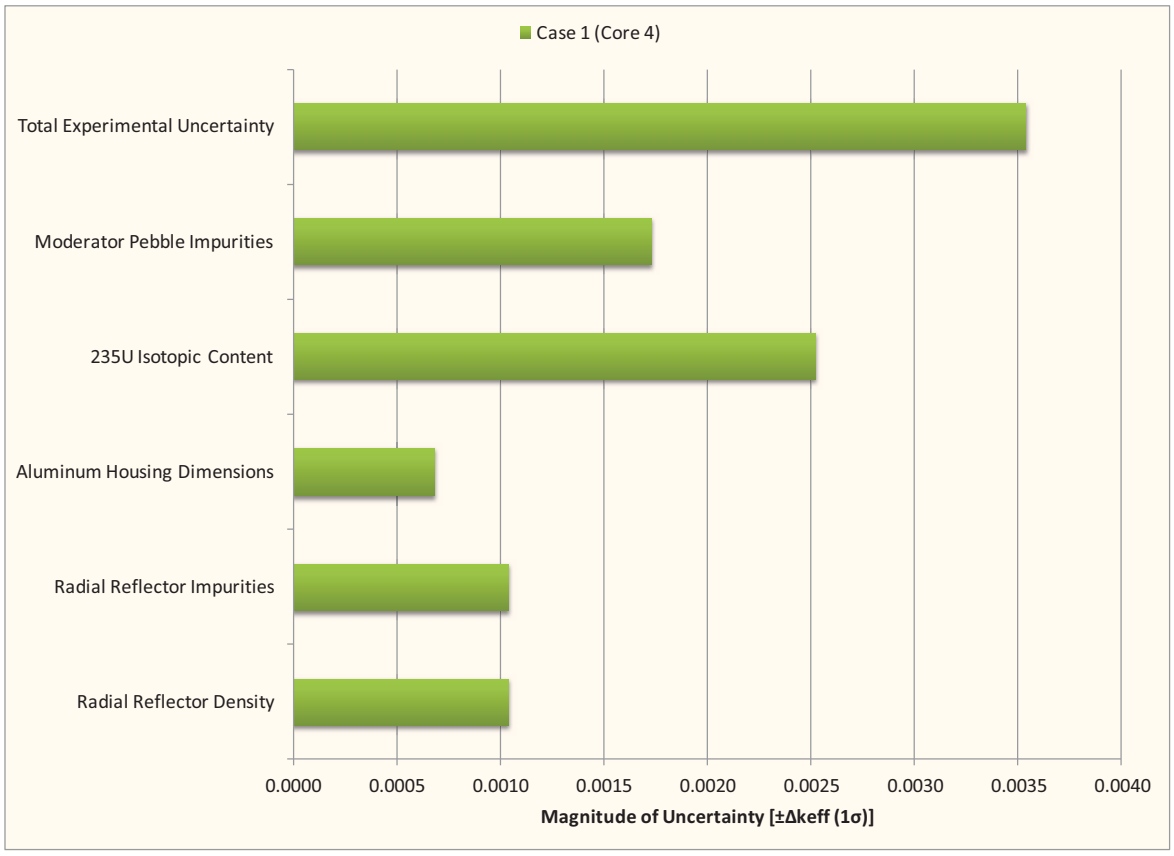

Figure 2.1-4. Graphical Representation of Primary Uncertainties in HTR-PROTEUS, Core 4.

2.2 Evaluation of Buckling and Extrapolation Length Data

Buckling and extrapolation length measurements were made but have not yet been evaluated.

2.3 Evaluation of Spectral Characteristics Data

Spectral characteristics measurements were not made.

2.4 Evaluation of Reactivity Effects Data

Reactivity effects measurements were made but have not yet been evaluated.

2.5 Evaluation of Reactivity Coefficient Data

Reactivity coefficient measurements were made but have not yet been evaluated.

2.6 Evaluation of Kinetics Measurements Data

Kinetics measurements were made but have not yet been evaluated.

2.7 Evaluation of Reaction-Rate Distributions

Reaction-rate distribution measurements were made but have not yet been evaluated.

2.8 Evaluation of Power Distribution Data

Power distribution measurements were not made.

2.9 Evaluation of Isotopic Measurements

Isotopic measurements were not made.

2.10 Evaluation of Other Miscellaneous Types of Measurements

Other miscellaneous types of measurements were not made.

3.0 BENCHMARK SPECIFICATIONS

3.1 Benchmark-Model Specifications for Critical and / or Subcritical Measurements

One benchmark experiment was evaluated in this report: Core 4. Core 4 represents the only configuration with random pebble packing in the HTR-PROTEUS series of experiments, and has a moderator-to-fuel pebble ratio of 1:1. Three random configurations were performed. The initial configuration, Core 4.1, was rejected because the method for pebble loading, separate delivery tubes for the moderator and fuel pebbles, may not have been completely random; this core loading was rejected by the experimenters. Cores 4.2 and 4.3 were loaded using a single delivery tube, eliminating the possibility for systematic ordering effects. The second and third cores differed slightly in the quantity of pebbles loaded (40 each of moderator and fuel pebbles), stacked height of the pebbles in the core cavity (0.02 m), withdrawn distance of the stainless steel control rods (20 mm), and withdrawn distance of the autorod (30 mm). The 34 coolant channels in the upper axial reflector and the 33 coolant channels in the lower axial reflector were open. Additionally, the axial graphite fillers used in all other HTR-PROTEUS configurations to create a 12-sided core cavity were not used in the randomly packed cores. Instead, graphite fillers were placed on the cavity floor, creating a quasi-conical, or funnel-like, base, to discourage ordering effects during pebble loading.

The benchmark specifications selected for Core 4 is a single configuration that represents the average pebble loading and stacked core height between configurations 4.2 and 4.3. Additionally, average withdrawn control rod and autorod positions were used. Treatment of any additional bias and bias uncertainty is discussed in Section 3.1.1.1.

The benchmark critical configurations for Core 4 will also be referred to as Case 1. Both methods of identification are utilized throughout the rest of this report to facilitate users with differing familiarities with HTR-PROTEUS and IRPhEP benchmark format.

The HTR-PROTEUS configurations consist of a thick annular graphite reflector surrounding a pair of thick axial graphite reflectors that sandwich a core cavity region containing fuel and moderator pebbles (see Figures 3.1-16 and 3.1-23). Most core configurations in the HTR-PROTEUS experimental series included exact placement of the pebbles; this is not the case with this benchmark report, where Case 1 (Core 4) was generated with random pebble placement in the core cavity region. Penetrations in the graphite reflectors were provided for control rods and instrumentation; typically these holes were filled with graphite plugs or filler pieces when not in use.

Case 1 (Core 4) represented the only critical experiment with random pebble loading. The core could be compared with the columnar hexagonal point-on-point packed configurations (Cores 9 and 10) with the same moderator:fuel pebble ratio of 1:1 (see PROTEUS-GCR-EXP-004).

3.1.1 Description of the Benchmark Model Simplifications

Various simplifications were necessary to prepare benchmark model specifications for the critical core configurations. Experimental measurements were performed or estimated based on experimental measurements for a variety of simplifications (see Section 1.1.5), since the original intent of this experimental series was to provide benchmark quality experiments that could be easily modeled. Only a selection of the measured simplifications was retained as biases to be applied to the benchmark models (see Table 3.1-1). Some of the core features were retained in the models to reduce the total effective bias, since they could be modeled easily. The retained measured biases generally represent simplifications of the benchmark models where insufficient information existed to reproduce the measurement with a calculation or reverse the simplification by adding more detail to the benchmark model. Simplifications that were simulated in the original reference reports (also reported in Section 1.1.5) were not retained, but instead recalculated.

Significant simplifications in assembly geometries and compositions were investigated for the first HTR-PROTEUS cores: 1, 1A, 2, and 3 (PROTEUS-GCR-EXP-001). Those simplifications that yielded small (≤0.00100 Δk) or negligible (≤0.00010 Δk) biases that were incorporated into the other benchmark models are now also included in this benchmark model (see Table 3.1-3). Biases calculated for the removal of control rods, coolant channels in the axial reflectors, removal of upper axial reflector aluminum support structure, and voiding of air were large and considered unacceptable for the benchmark models of Cores 1, 1A, 2, and 3. Therefore, these simplifications were not performed and the features were retained in the benchmark model of Core 4.

3.1.1.1 Evaluation of Benchmark Model Biases

A summary of the experimentally measured reactivity corrections utilized for the benchmark model is provided in Table 3.1-1 for Case 1 (Core 4). The values for Case 1 were obtained from Tables 1.1-17 through 1.1-19. The calculated β_{eff} value is 0.00723 for Case 1. The reported β_{eff} value was used to convert the reactivity corrections and their associated uncertainties from their original measured reactivities in units of ¢ into Δk; it was assumed that there was an additional bias uncertainty due to the use of the reported β_{eff} values of 5% (1σ) of the reported value (~0.00036 $\Delta\beta_{eff}$). Many of the measurement biases were used directly, since sufficient information was not available to include most of them in the models.

The autorod position for the benchmark model of Case 1 (Core 4) was obtained by taking the average of the reported autorod positions for Cores 4.2 and 4.3. The position of the withdrawable control rods was also obtained by taking the average of the reported control rod positions for Cores 4.2 and 4.3. An additional bias uncertainty was calculated to be 4.6¢, as the change in the control rod and autorod positions was relatively small. No additional bias or bias uncertainty was added for using an averaged quantity of moderator and fuel pebbles or an averaged core height; any additional bias uncertainty is assumed to be included within that already assessed for using averaged control rod positions or within the experimental uncertainty assessed for this core configuration.

Some of the C-Driver channels in the 2nd and 3rd rings of the radial reflector contained instrumentation instead of graphite rods. The effect of filling these empty positions with graphite rods was measured.

Start-up sources with associated penetrations were used in HTR-PROTEUS. The effect of removing these sources and filling the penetrations with graphite was measured.

Instrumentation and detectors in the core were removed and the effect was measured.

Typically 33 coolant channels in the lower axial reflector and 34 coolant channels in the upper axial reflector were empty during many of the HTR-PROTEUS experiments, as was performed experimentally with Core 4.

Table 3.1-1. Experimentally Determined Reactivity Corrections for Case 1 (Core 4).

Measured Effect	Reactivity Correction ρ¢	±	σ	Reactivity Correction Δk	±	σ
Averaged Core Configuration	0	±	4.6	--	±	0.00033
Empty Channels in Ring 2 of Radial Reflector	3	±	0.3	0.00022	±	0.00002
Start-Up Sources	3.6	±	0.01	0.00026	±	0.00001
Start-Up Source Penetrations	1	±	0.1	0.00007	±	0.00001
Pulsed Neutron Source and Missing Graphite	4.7	±	0.3	0.00034	±	0.00003
Nuclear Instrumentation (Ionization)	10.7	±	2.0	0.00077	±	0.00015
Nuclear Instrumentation (Fission)	0.9	±	0.6	0.00006	±	0.00004
Temperature Instrumentation in Radial Reflector	17.4	±	10	0.00125	±	0.00073
Total (Reported β_{eff} = 0.00723)[(a)]	41.30	±	11.21	0.00297	±	0.00081

(a) Assumed uncertainty in β_{eff} of 5% (1σ).

Additional biases were evaluated for the benchmark simplifications of Cores 1, 1A, 2, and 3 (PROTEUS-GCR-EXP-001); a summary of the biases is listed in Table 3.1-2. The effective bias for most of the individually calculated biases were negligible compared to the statistical uncertainty for Cores 1, 1A, 2, and 3, except for the bias for homogenizing the radial reflector; therefore, individual calculations were not performed for Core 4, and only a summary of the simplifications is provided with the total effective bias for incorporation of these simplifications in the benchmark models. The effective simplification bias was computed by comparing calculated eigenvalues obtained with MCNP5 input decks (Appendix A) of the benchmark models described in Section 3 and detailed models (Appendix C).

Simplifications to the benchmark models include the removal of many of the assembly components external to the large radial reflector, such as the concrete walls, steel support pedestal, and thermal column (Figures 1.1-1, 1.1-3, and 1.1-9). Experimental measurements confirmed that room return effects were negligible for this series of experiments and therefore deemed unnecessary in the benchmark models.

The safety/shutdown rods and the aluminum shock dampers (Figure 1.1-9) were removed from the benchmark models. The eight channels for these rods were retained in the models (Figure 1.1-2b). Since the safety/shutdown rods were fully withdrawn from the core, their removal from the benchmark models was effectively negligible.

The radial reflector was homogenized with the C-Driver channels, and graphite plugs in the C-Driver channels (Figures 1.1-2 and 1.1-3). Only penetrations for control rod use were retained: withdrawable control rods, safety/shutdown rods, and autorod. The withdrawable control rods were placed in four of the C-Driver channels in ring 5 of the radial reflector. The ZEBRA rod channels from the initial core, Core 1, were filled with graphite plugs. Radial reflector simplifications facilitate ease of modeling these benchmark configurations. The outer and inner 22-sided polygon surfaces of the radial reflector were converted to cylindrical surfaces.

The graphite fillers placed on the cavity floor were also converted from a polyhedral geometry to an annulus with a 10º slope (see Section 2.1.6); the holes for the 33 coolant channels were retained and mass was conserved. The resultant bias is judged to be negligible.

The safety ring (Figure 1.1-4) is removed from the benchmark model and the aluminum support structure of the upper axial reflector was simplified such that the aluminum spherical surfaces (Figures 1.1-4 and 1.1-6) are modeled as an aluminum disc, 1-cm-thick, retaining the outer diameter of the aluminum

structure (104.2 cm). The aluminum support structure was a complex entity and very difficult to model with exact detail.

The lower axial reflector was simplified by cylinderizing the graphite annulus and filling the small source gap with graphite (Figure 1.1-7). As with simplification of the radial reflector, removal of the exact location of vertices for the multifaceted polygons used to generate this core by using cylindrical representations greatly simplifies modeling of these benchmark configurations.

All pebbles in the models have a radius of 3.000 cm. The mass of the pebbles was conserved and the resultant bias is negligible.

Impurities in the TRISO particles are removed from the models.

A standard air composition was used for all models with a temperature of 20°C, pressure of 980 mbar, and 50 % humidity. Neon, helium, and krypton are not included in the benchmark model; the bias for their removal is negligible.

Table 3.1-2. Calculated Simplification Biases.

• Removal of Concrete Walls • Removal of Steel Support Pedestal • Removal of Thermal Column • Removal of Safety/Shutdown Rods – Includes Shock Dampers • Cylinderization of Radial Reflector – Outer and inner 22-sided polygon surfaces converted to cylindrical surfaces • Cylinderization of Cavity Floor Graphite Fillers • Removal of Safety Ring • Homogenization of Radial Reflector – Remove All Penetrations Except Those for Control Rods • Simplify Aluminum Support Structure of Upper Axial Reflector • Cylinderize Lower Axial Reflector Annulus • Fill Source Gap with Graphite • Model All Pebbles with a Radius of 3.000 cm • Remove UO_2 Impurities in the TRISO Kernels • Remove Impurities in the TRISO Layers • Use a Standard Air Composition for All Models – Remove Ne, He, and Kr from Air Composition • Top ends of copper wire not bent (Core 6 only)			
Case (Core)	1 (4)		
Bias (Δk)	0.00094	±	0.00010

The total bias for each benchmark configuration (Table 3.1-3) is obtained by summation of the experimentally measured corrections (Table 3.1-1) with the computed simplification bias (Table 3.1-2). The total bias uncertainties are obtained by summing under quadrature the individual bias uncertainties. For example, for Case 1 (Core 4), the measured correction of 0.00297 ± 0.00081 Δk (Table 3.1-1) is added to the calculated simplification bias of 0.00094 ± 0.00010 Δk (Table 3.1-2) to obtain a total simplification bias for the benchmark model of 0.00391 ± 0.00082 Δk (Table 3.1-3).

Table 3.1-3. Total Benchmark Bias (Δk).

Case (Core)	1 (4)
Measured Corrections	0.00297 ± 0.00081
Calculated Simplifications	0.00094 ± 0.00010
Total Bias	**0.00391 ± 0.00082**

3.1.2 Dimensions

3.1.2.1 Radial Reflector

The graphite radial reflector (Figure 3.1-1) is an annulus with an equivalent inner radius of 62.83398 cm, an equivalent outer radius of 163.76986 cm, and a height of 330.4 cm. Penetrations in the radial reflector are provided for eight safety/shutdown rods, an autorod, and four withdrawable control rods. These holes axially penetrate completely through the radial reflector with the x,y positions provided in Table 3.1-4 and shown in Figure 3.1-2. While the penetrations for the safety/shutdown rods are preserved in the benchmark model, the rods themselves are not included.

Table 3.1-4. Penetrations in Radial Reflector (dimensions in cm).

Penetration Purpose	x-Coordinate	y-Coordinate	Hole Diameter
Safety/Shutdown Rod Hole 1	-38.45	56.57	4.5
Safety/Shutdown Rod Hole 2	32.74	-60.05	4.5
Safety/Shutdown Rod Hole 3	57.17	37.55	4.5
Safety/Shutdown Rod Hole 4	-53.23	-42.95	4.5
Safety/Shutdown Rod Hole 5	67.19	-12.82	4.5
Safety/Shutdown Rod Hole 6	-66.98	13.87	4.5
Safety/Shutdown Rod Hole 7	19.31	65.62	4.5
Safety/Shutdown Rod Hole 8	-13.87	-66.98	4.5
Autorod Hole	17.36	-87.29	5.5
Withdrawable Control Rod Hole 1	-83.70	34.67	2.743
Withdrawable Control Rod Hole 2	34.67	83.70	2.743
Withdrawable Control Rod Hole 3	83.70	-34.67	2.743
Withdrawable Control Rod Hole 4	-34.67	-83.70	2.743

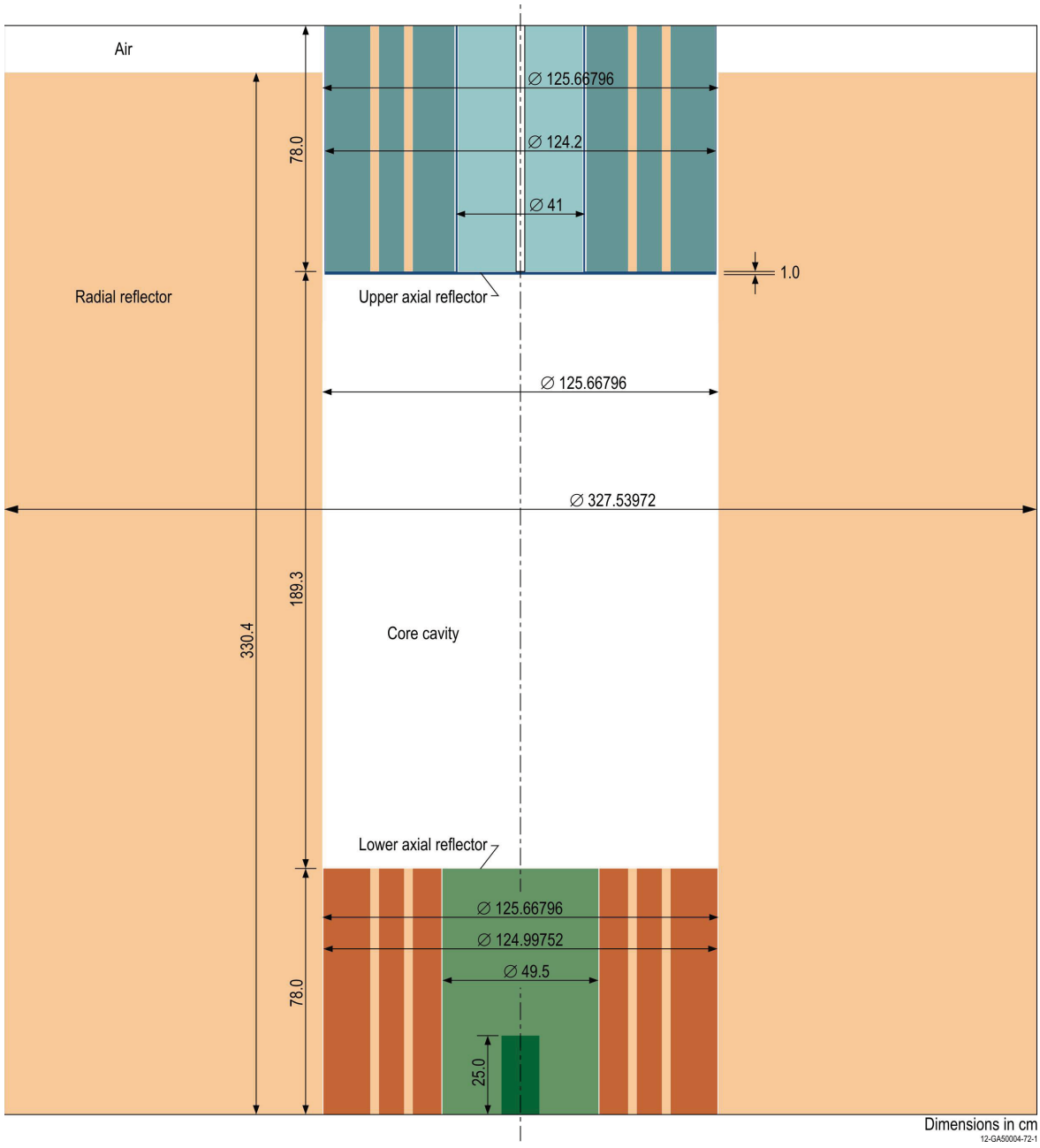

Figure 3.1-1. Radial and Axial Reflectors Surrounding Core Cavity Region.

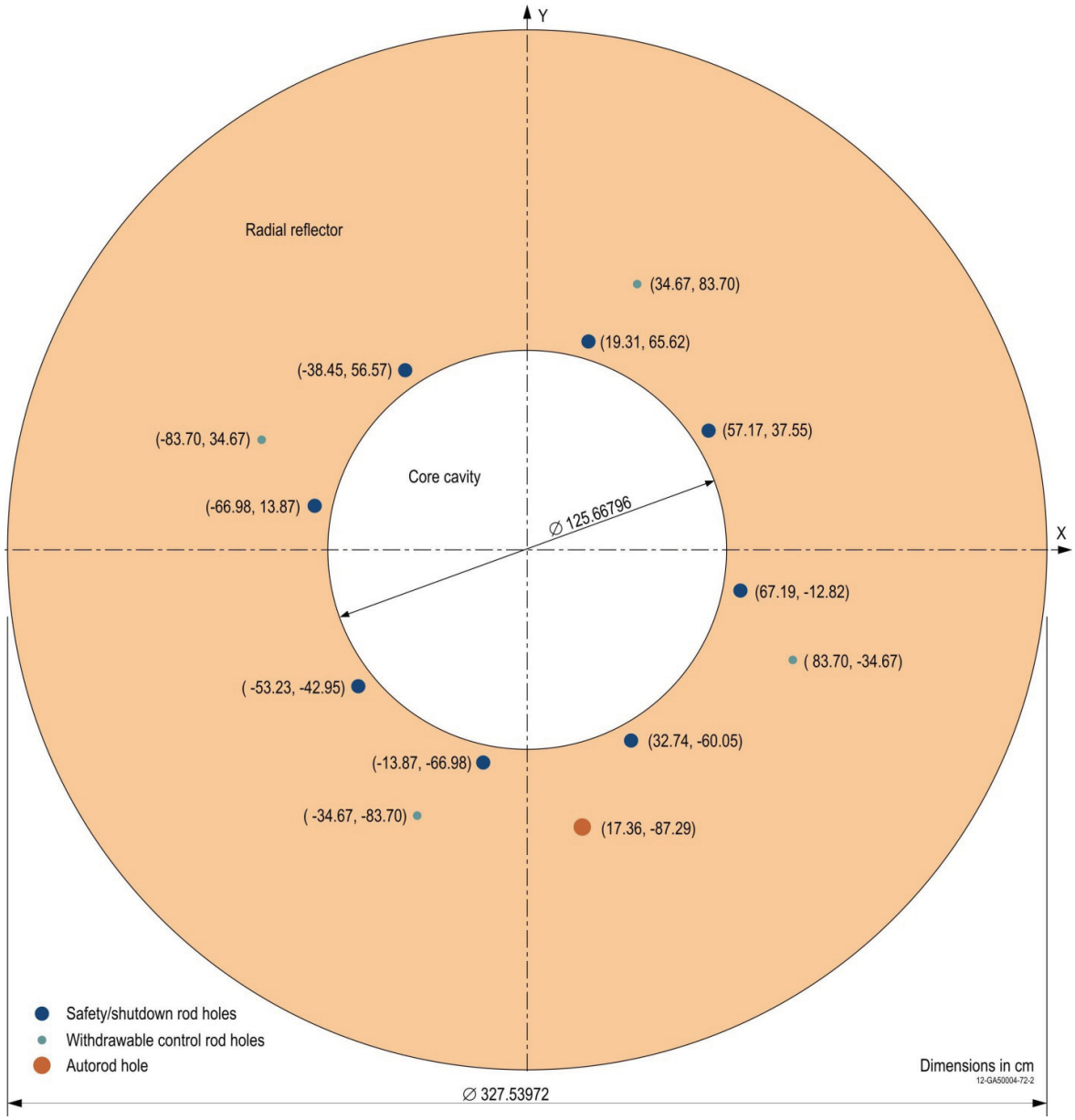

Figure 3.1-2. Radial Reflector Surrounding Core Cavity Region.

3.1.2.2 Upper Axial Reflector

The upper axial reflector consists of a graphite cylinder (radius of 19.7 cm) with a single coolant channel (diameter of 2.743 cm) and a graphite annulus (inner radius of 20.93 cm and outer radius of 61.7 cm) with 160 coolant channels (diameters of 2.743 cm) distributed equally and uniformly spaced within 5 annular locations with distances of 30.0, 35.5, 41.0, 46.25, and 51.5 cm radially from the center of the reflector (see Figure 3.1-3 and Table 3.1-5). Of the 161 channels, 127 are filled with graphite plugs (diameter of 2.65 cm), as noted in Table 3.1-5 with a "Y". The height of all graphite components is 78.0 cm. An aluminum structure supports the graphite components of the upper axial reflector with an inner annular sheet (19.8 cm inner radius and 20.5 cm outer radius) separating the graphite annulus and cylinder and another outer annular sheet (61.8 cm inner radius and 62.1 cm outer radius) surrounding the entire axial reflector. Air gaps exist between the graphite and aluminum portions of the reflector. The thickness of the aluminum structure below the graphite is 1.0 cm. The bottom of the graphite in the upper axial reflector rests 189.3 cm above the top of the lower axial reflector. The inside radius of the radial reflector surrounding the upper axial reflector is 62.83398 cm.

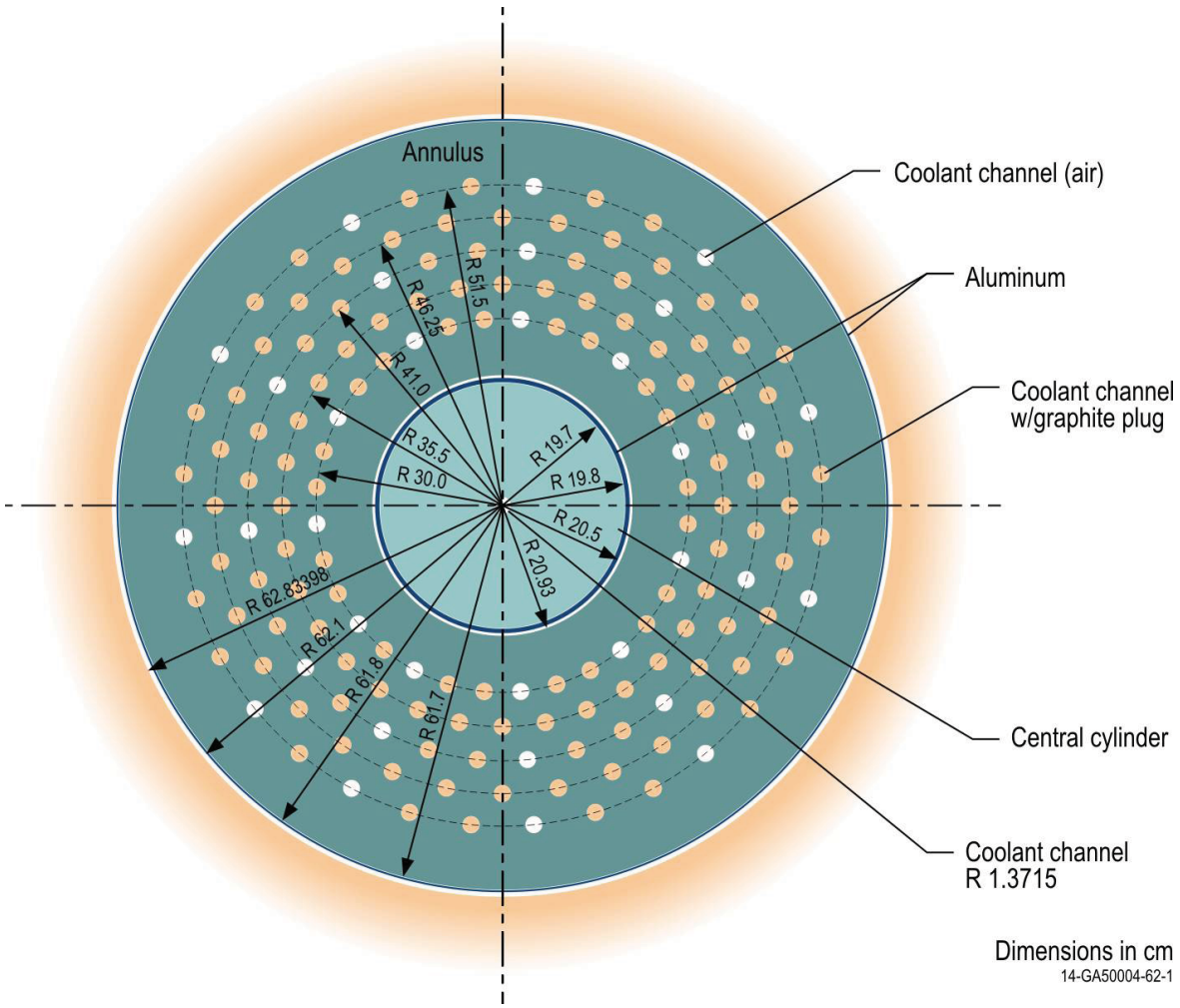

Figure 3.1-3. Upper Axial Reflector.

Table 3.1-5. Penetration Coordinates in the Axial Reflectors and Cavity Floor Filler Pieces (dimensions in cm).

Ring	1			2			3		
Position	**x**	**y**	**Plug?[(a)]**	**x**	**y**	**Plug?[(a)]**	**x**	**y**	**Plug?[(a)]**
1	-29.86	2.94	Y	-34.82	6.93	Y	-39.23	11.90	Y
2	-28.71	8.71	Y	-32.80	13.59	Y	-36.16	19.33	N
3	-26.46	14.14	N	-29.52	19.72	Y	-31.69	26.01	Y
4	-23.19	19.03	Y	-25.10	25.10	Y	-26.01	31.69	Y
5	-19.03	23.19	Y	-19.72	29.52	Y	-19.33	36.16	N
6	-14.14	26.46	N	-13.59	32.80	Y	-11.90	39.23	Y
7	-8.71	28.71	Y	-6.93	34.82	Y	-4.02	40.80	Y
8	-2.94	29.86	Y	0.00	35.50	Y	4.02	40.80	N
9	2.94	29.86	N	6.93	34.82	Y	11.90	39.23	Y
10	8.71	28.71	Y	13.59	32.80	Y	19.33	36.16	Y
11	14.14	26.46	Y	19.72	29.52	Y	26.01	31.69	N
12	19.03	23.19	N	25.10	25.10	Y	31.69	26.01	Y
13	23.19	19.03	Y	29.52	19.72	Y	36.16	19.33	Y
14	26.46	14.14	Y	32.80	13.59	Y	39.23	11.90	N
15	28.71	8.71	N	34.82	6.93	Y	40.80	4.02	Y
16	29.86	2.94	Y	35.50	0.00	Y	40.80	-4.02	Y
17	29.86	-2.94	Y	34.82	-6.93	Y	39.23	-11.90	N
18	28.71	-8.71	N	32.80	-13.59	Y	36.16	-19.33	Y
19	26.46	-14.14	Y	29.52	-19.72	Y	31.69	-26.01	Y
20	23.19	-19.03	Y	25.10	-25.10	Y	26.01	-31.69	N
21	19.03	-23.19	N	19.72	-29.52	Y	19.33	-36.16	Y
22	14.14	-26.46	Y	13.59	-32.80	Y	11.90	-39.23	Y
23	8.71	-28.71	Y	6.93	-34.82	Y	4.02	-40.80	N
24	2.94	-29.86	N	0.00	-35.50	Y	-4.02	-40.80	Y
25	-2.94	-29.86	Y	-6.93	-34.82	Y	-11.90	-39.23	Y
26	-8.71	-28.71	Y	-13.59	-32.80	Y	-19.33	-36.16	N
27	-14.14	-26.46	N	-19.72	-29.52	Y	-26.01	-31.69	Y
28	-19.03	-23.19	Y	-25.10	-25.10	Y	-31.69	-26.01	N
29	-23.19	-19.03	N	-29.52	-19.72	Y	-36.16	-19.33	Y
30	-26.46	-14.14	Y	-32.80	-13.59	Y	-39.23	-11.90	Y
31	-28.71	-8.71	Y	-34.82	-6.93	Y	-40.80	-4.02	N
32	-29.86	-2.94	N	-35.50	0.00	Y	-40.80	4.02	Y

Table 3.1-5 (cont'd.). Penetration Coordinates in the Axial Reflectors and Cavity Floor Filler Pieces (dimensions in cm).

Ring	4			5		
Position	**x**	**y**	**Plug?[(a)]**	**x**	**y**	**Plug?[(a)]**
1	-42.73	17.70	Y	-45.42	24.28	N
2	-38.46	25.70	Y	-39.81	32.67	Y
3	-32.70	32.70	Y	-32.67	39.81	Y
4	-25.70	38.46	Y	-24.28	45.42	N
5	-17.70	42.73	Y	-14.95	49.28	Y
6	-9.02	45.36	Y	-5.05	51.25	Y
7	0.00	46.25	Y	5.05	51.25	N
8	9.02	45.36	Y	14.95	49.28	Y
9	17.70	42.73	Y	24.28	45.42	Y
10	25.70	38.46	Y	32.67	39.81	N
11	32.70	32.70	Y	39.81	32.67	Y
12	38.46	25.70	Y	45.42	24.28	Y
13	42.73	17.70	Y	49.28	14.95	N
14	45.36	9.02	Y	51.25	5.05	Y
15	46.25	0.00	Y	51.25	-5.05	Y
16	45.36	-9.02	Y	49.28	-14.95	N
17	42.73	-17.70	Y	45.42	-24.28	Y
18	38.46	-25.70	Y	39.81	-32.67	Y
19	32.70	-32.70	Y	32.67	-39.81	N
20	25.70	-38.46	Y	24.28	-45.42	Y
21	17.70	-42.73	Y	14.95	-49.28	Y
22	9.02	-45.36	Y	5.05	-51.25	N
23	0.00	-46.25	Y	-5.05	-51.25	Y
24	-9.02	-45.36	Y	-14.95	-49.28	Y
25	-17.70	-42.73	Y	-24.28	-45.42	N
26	-25.70	-38.46	Y	-32.67	-39.81	Y
27	-32.70	-32.70	Y	-39.81	-32.67	N
28	-38.46	-25.70	Y	-45.42	-24.28	Y
29	-42.73	-17.70	Y	-49.28	-14.95	Y
30	-45.36	-9.02	Y	-51.25	-5.05	N
31	-46.25	0.00	Y	-51.25	5.05	Y
32	-45.36	9.02	Y	-49.28	14.95	Y

(a) This column notes whether a graphite plug is (marked by "Y") or is not (marked by "N") located within the coolant channel. Coolant channels marked by "N" also represent the position of the 33 coolant channels in the cavity floor graphite filler.

3.1.2.3 Lower Axial Reflector

The lower axial reflector consists of a graphite cylinder (radius of 24.75 cm) containing a removable source plug and a graphite annulus (equivalent inner radius of 25.05171 cm and equivalent outer radius of 62.71754 cm) with 160 coolant channels (diameter of 2.742 cm) with the same XY positions as the upper axial reflector (see Figure 3.1-4 and Table 3.1-5). As shown in Figure 3.1-4, 33 channels were empty, matching the 33 open channels in the upper axial reflector. The height of all graphite components, except the source plug, is 78.0 cm. The source plug is located at the bottom of the graphite cylinder along its axis and has a radius of 6.0 cm and height of 25.0 cm, located within a hole in the graphite cylinder with the same dimensions. The inside radius of the radial reflector surrounding the lower axial reflector is 62.83398 cm.

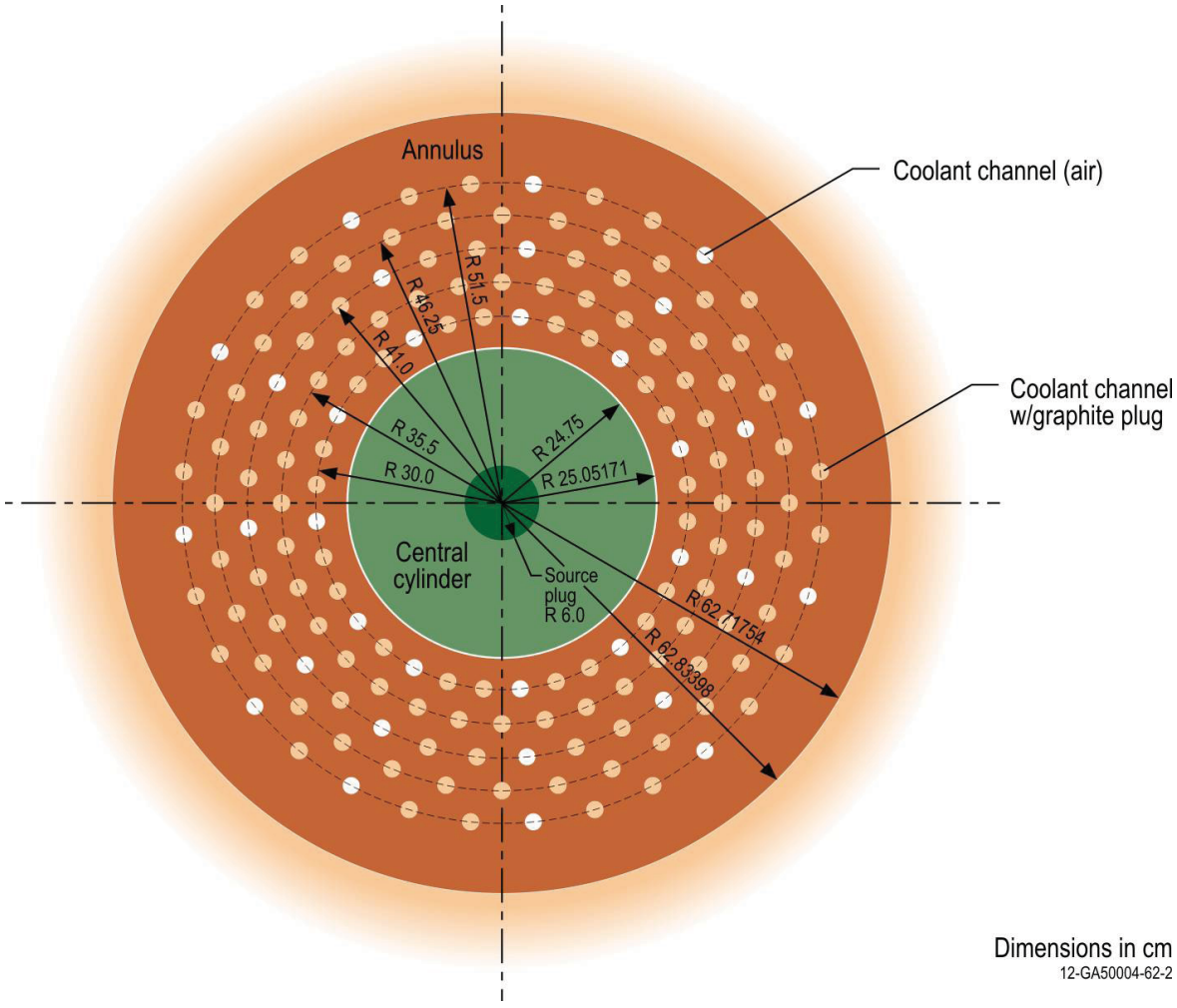

Figure 3.1-4. Lower Axial Reflector.

3.1.2.4 Autorod

The autorod (Figures 3.1-5 and 3.1-6) consists of an aluminum guide tube (inner diameter of 4 cm and outer diameter of 4.4 cm) running the full length of its penetration in the radial reflector. A copper wedge can be raised or lowered within the tube for fine reactivity control of the assembly. The copper wedge has a thickness of 0.3 cm and a length of 230 cm. The top of the wedge has a width of 3.9 cm and tapers to a point at the bottom of the wedge. The XY position of the autorod compared to the core is shown in Figure 3.1-2 with the orientation shown in Figure 3.1-5. When fully inserted, the tip of the autorod is located 7.5 cm below the bottom of the radial reflector. The autorod is considered fully "withdrawn" in its uppermost position of 100.0 cm above its fully inserted position (see Figure 3.1-6). The distance the autorod is withdrawn from the fully inserted position for each core configuration is provided in Table 3.1-6.

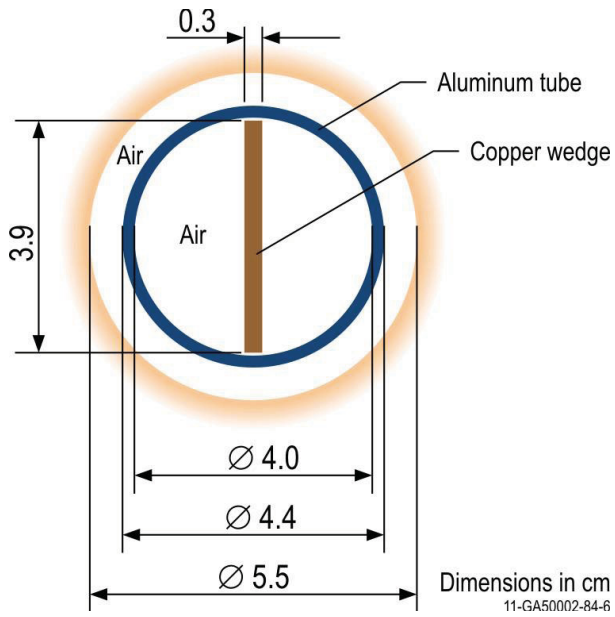

Figure 3.1-5. Top View of Autorod.

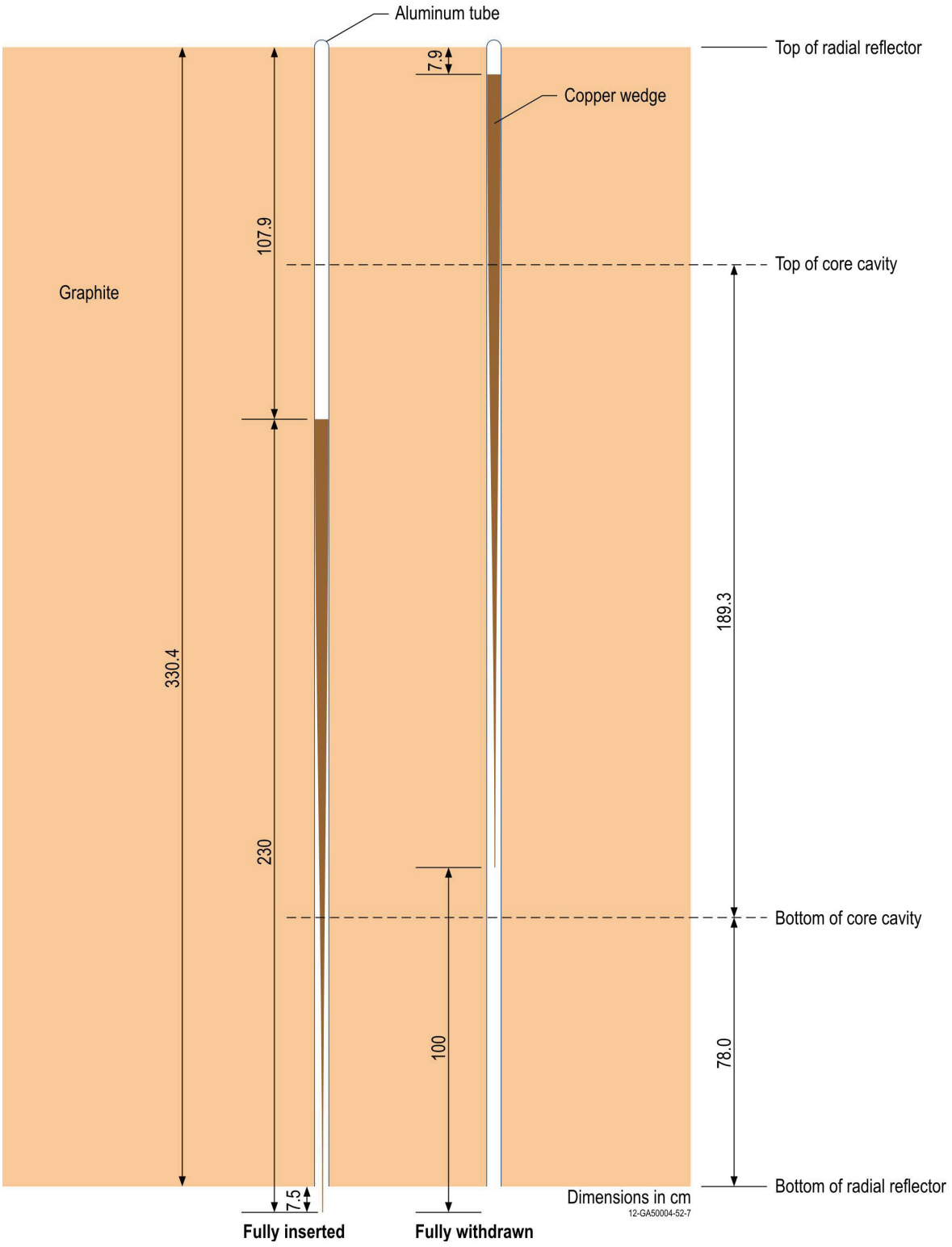

Figure 3.1-6. Autorod Vertical Position within Axial Reflector.

Table 3.1-6. Control Rod Positions (distance in cm).

Case (Core)	**1 (4)**
Control Rod	**Withdrawn Distance**
Safety/Shutdown Rod 1	NA
Safety/Shutdown Rod 2	NA
Safety/Shutdown Rod 3	NA
Safety/Shutdown Rod 4	NA
Safety/Shutdown Rod 5	NA
Safety/Shutdown Rod 6	NA
Safety/Shutdown Rod 7	NA
Safety/Shutdown Rod 8	NA
Autorod	48.5
Withdrawable Control Rod 1	89.0
Withdrawable Control Rod 2	89.0
Withdrawable Control Rod 3	89.0
Withdrawable Control Rod 4	89.0

3.1.2.5 Fuel Pebbles

The graphite fuel pebbles have a diameter of 6.000 cm. A total of 9394 TRISO particles are randomly distributed within the graphite matrix of the fueled zone (diameter of 4.700 cm) of each fuel pebble (Figure 3.1-7). The fuel pebbles are randomly distributed within the core cavity. Each TRISO particle consists of four layers surrounding a UO_2 kernel. The fuel kernel has a diameter of 0.0502 cm. A graphite buffer layer (thickness of 0.00915 cm) surrounds the fuel kernel. An inner pyrolytic carbon (IPyC) layer (thickness of 0.00399 cm), SiC layer (thickness of 0.00353 cm), and outer pyrolytic carbon (OPyC) layer (thickness of 0.00400 cm) then each, in succession, surround the growing TRISO particle, as shown in Figure 3.1-7.

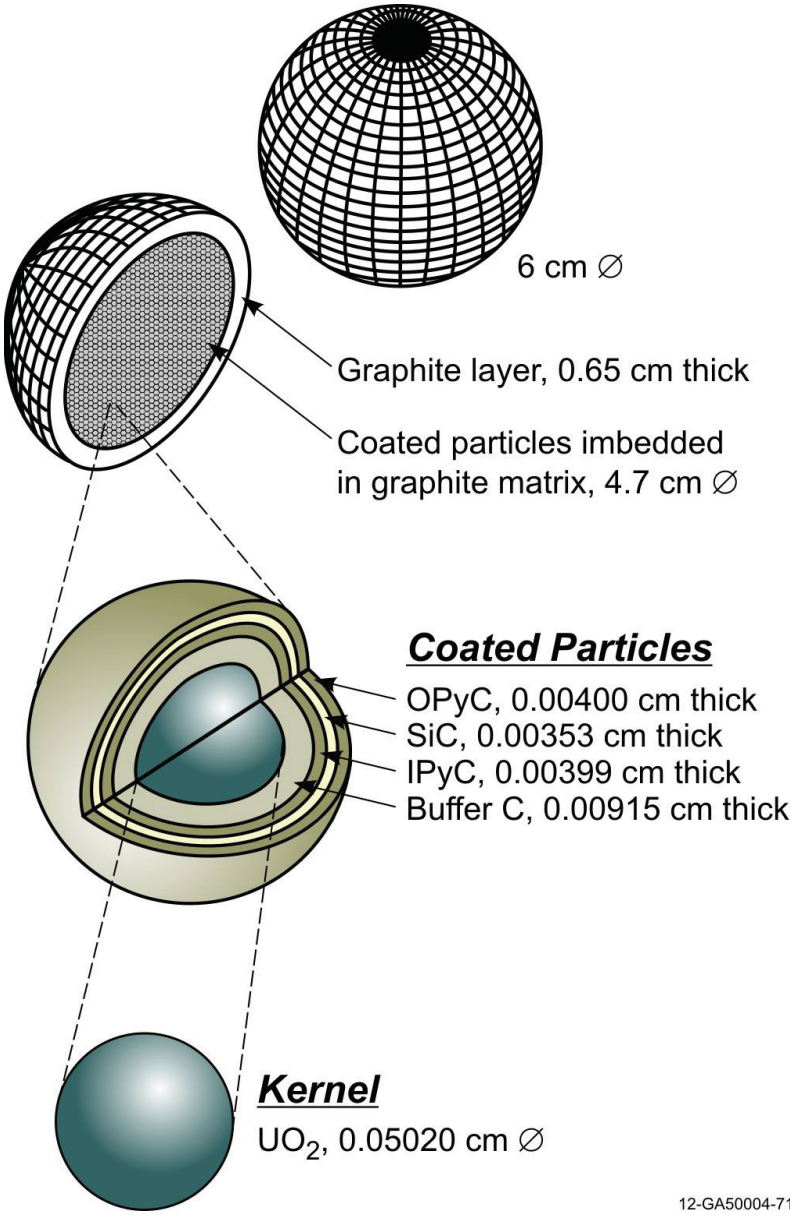

Figure 3.1-7. Fuel Pebble and TRISO Particle.

3.1.2.6 Moderator Pebbles

The graphite moderator pebbles have a diameter of 6.000 cm. They are randomly distributed within the core cavity.

3.1.2.7 Withdrawable Stainless Steel Control Rods

The withdrawable control rods (Figures 3.1-8 through 3.1-10) are comprised of two concentric stainless steel tubes with end plugs. The inner tube has an inner diameter of 0.95 cm and an outer diameter of 1.35 cm. The outer tube has an inner diameter of 1.4 cm and an outer diameter of 2.2 cm. Both tubes have a total length of 215.0 cm. The dimensions for the end plugs are shown in Figure 3.1-9. The stainless steel control rods are completely inserted into the core when the bottom surface of the bottom end plug is located 75.5 cm above the bottom of the radial reflector; they are completely withdrawn when raised 249.4 cm from the fully inserted position (see Figure 3.1-10). A graphite plug (diameter of 2.65 cm and height of 73.0 cm) is located in the bottom of each penetration for the withdrawable control rods. The withdrawn positions of the withdrawable control rods are provided in Table 3.1-6.

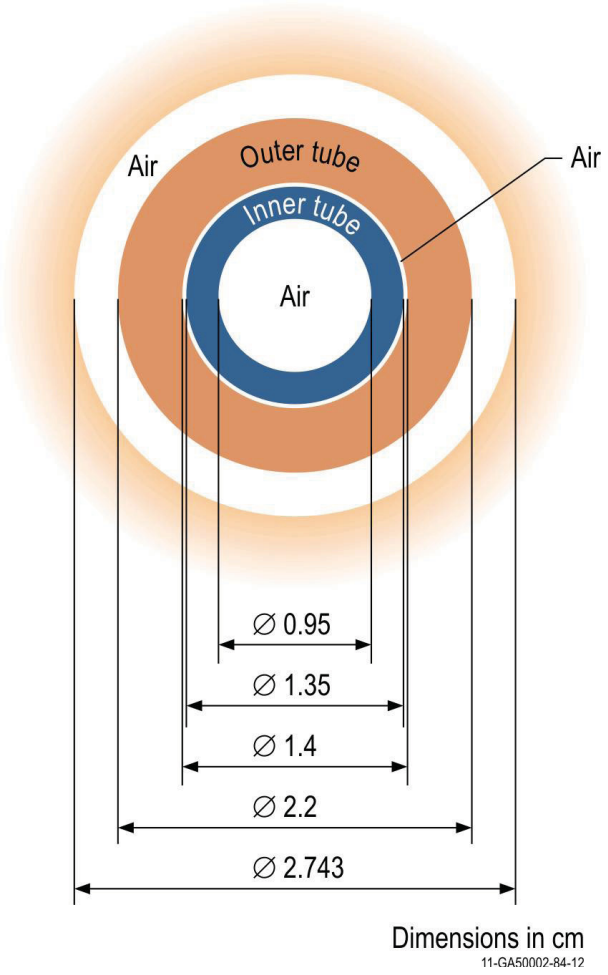

Figure 3.1-8. Top View of Withdrawable Control Rod.

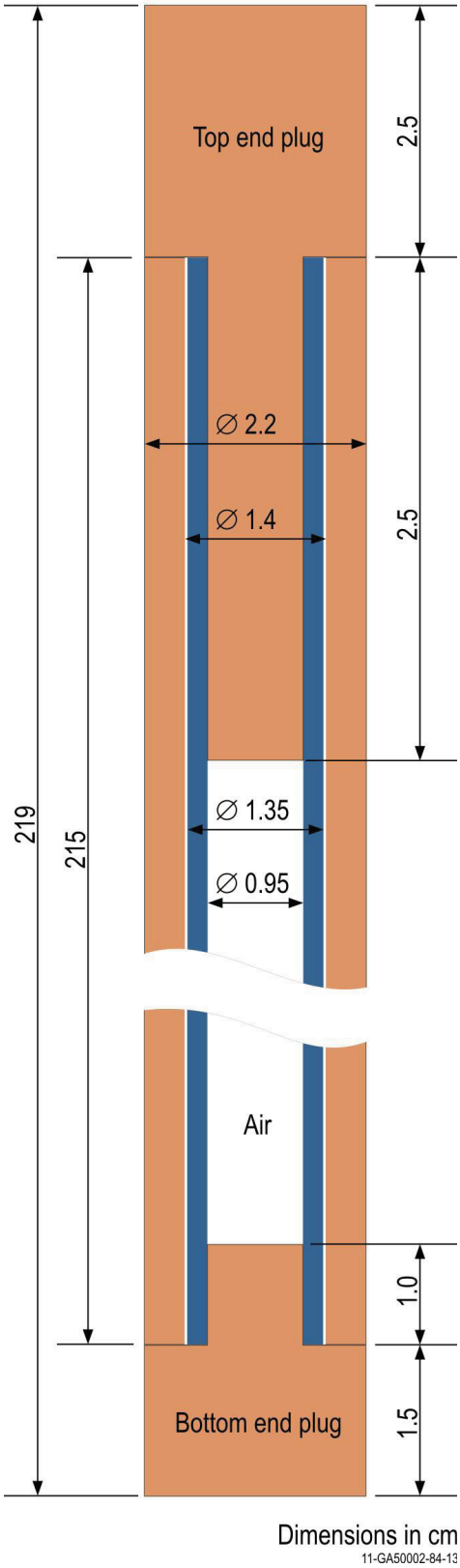

Figure 3.1-9. Axial View of Withdrawable Control Rod.

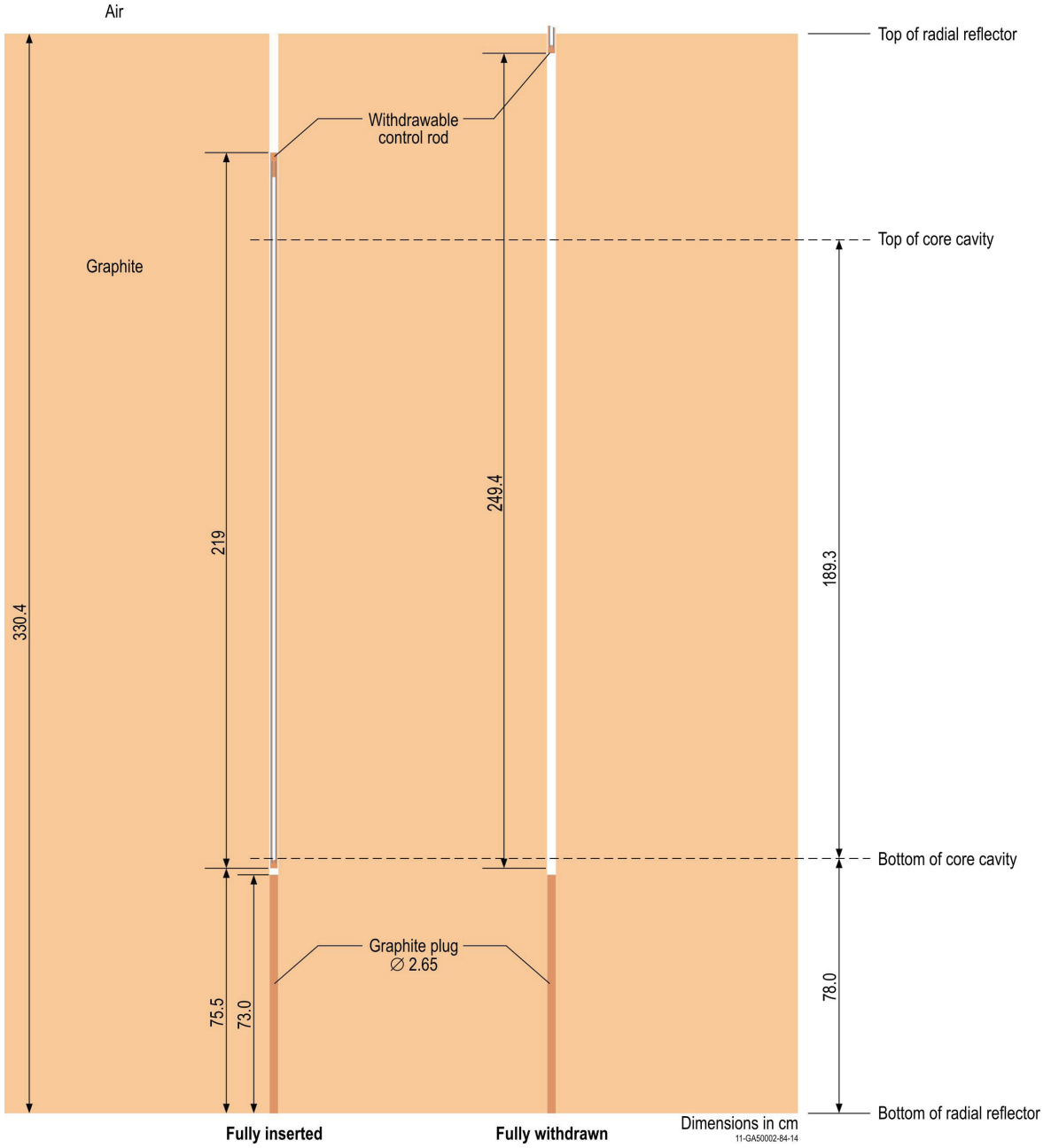

Figure 3.1-10. Withdrawable Control Rod Vertical Position within Axial Reflector.

3.1.2.8 Graphite Cavity Floor Filler

A graphite cavity floor filler was utilized to create a quasi-conical bottom to the core cavity. It had a 10º slope extending from the cavity wall, as shown in Figures 3.1-11 and 3.1-12. The coordinates of the 33 coolant channels in the cavity floor filler are marked with an "N" in Table 3.1-5. These coolant channels are not plugged; they contain air.

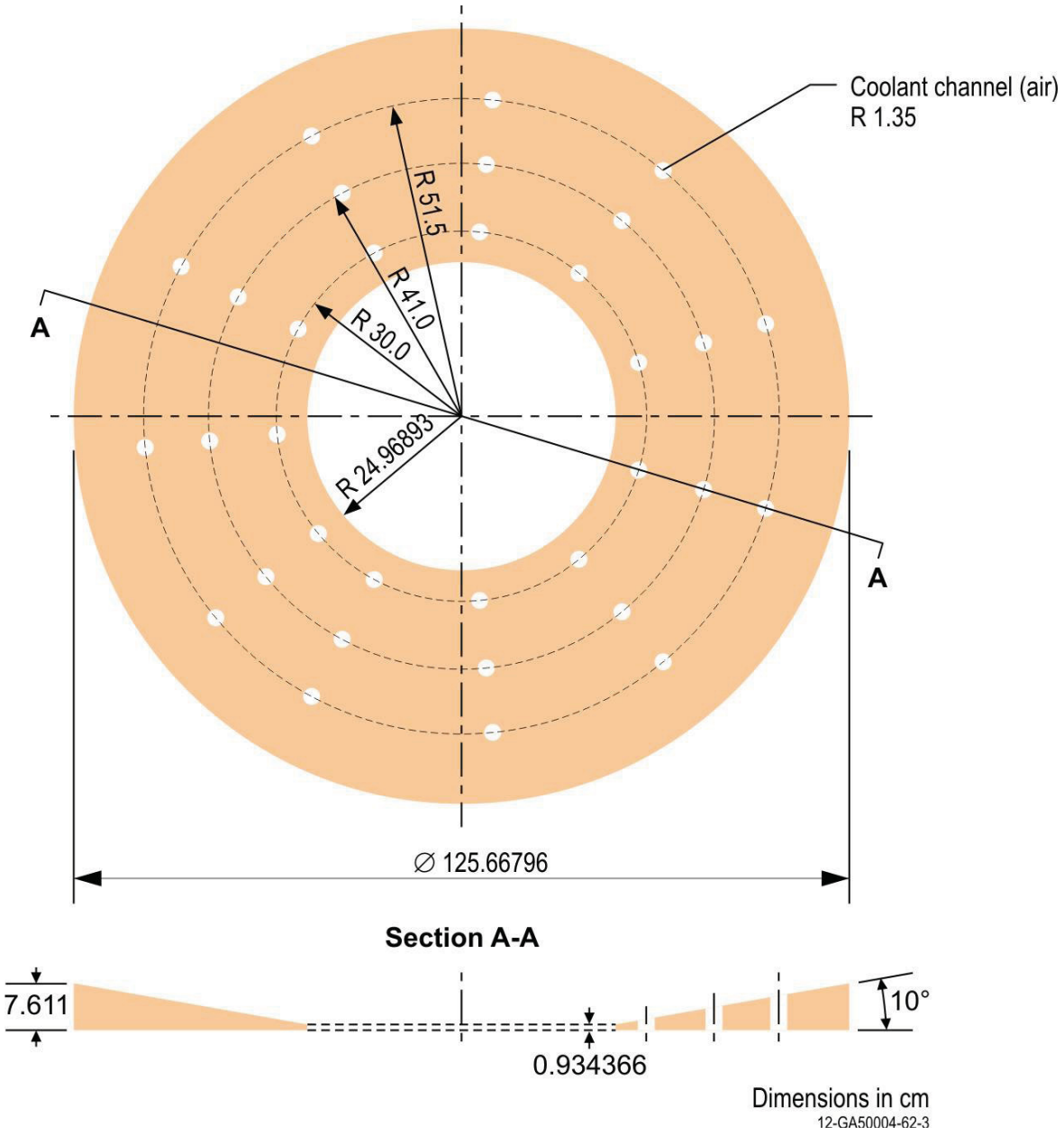

Figure 3.1-11. Graphite Cavity Floor Filler.

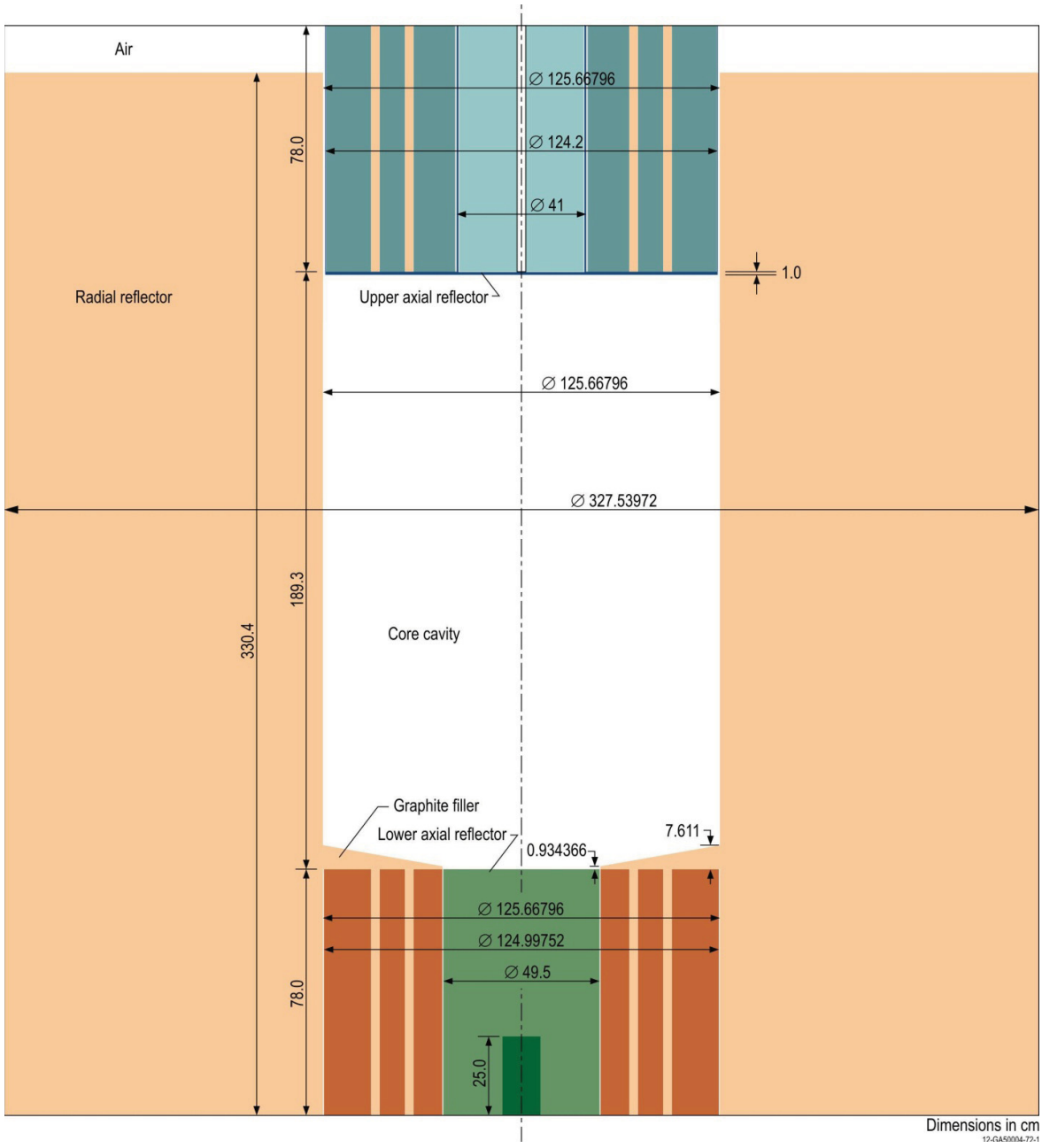

Figure 3.1-12. Graphite Reflectors and Cavity Floor Filler Surrounding Core Cavity Region.

3.1.2.9 Ambient Air

Air is located in any gaps, holes, or penetrations within the benchmark model that does not contain the graphite reflectors, graphite plugs, aluminum support structure, pebbles, lattice supports, or control rods.

3.1.2.10 Core Configurations

Information corresponding to the loading of the randomly packed configuration is provided in Table 3.1-7 with additional visualization of the core in Figure 3.1-13.

Table 3.1-7. Additional Core Configuration Parameters.

Case	Core	# Fuel Pebbles	# Moderator Pebbles	# Pebble Layers	Core Height (m)	# Polyethylene Rods	Associated Figure
1	4	4920	4920	NA	1.51	NA	3.1-13

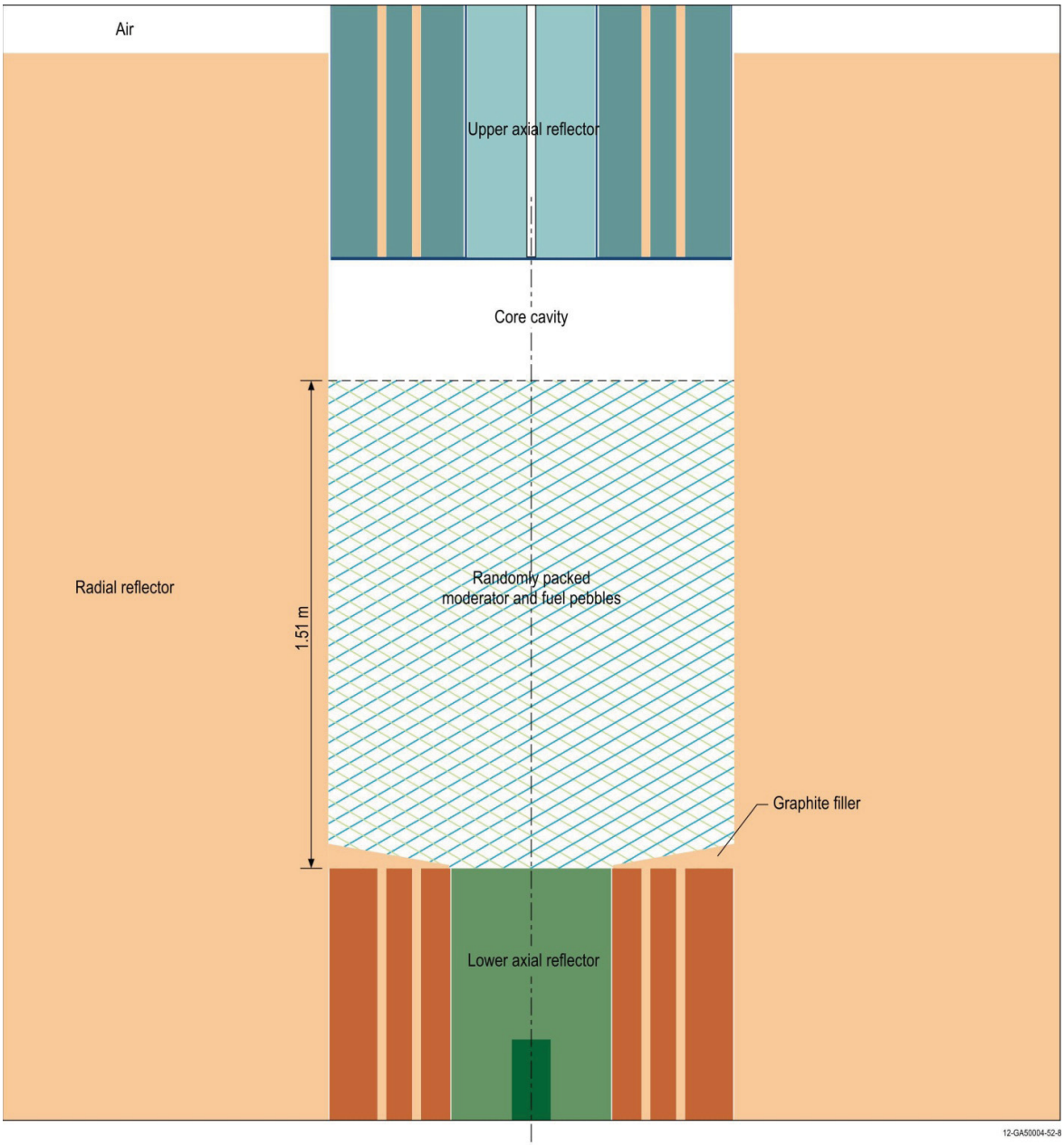

Figure 3.1-13. Vertical Core Profile.

3.1.3 Material Data

3.1.3.1 Radial Reflector

The homogenized (see Section 3.1.1.1) graphite radial reflector has the compositions in Table 3.1-8. The graphite in the radial reflector has 1.33 ppm EBC (by at.%), which equates to a nominal ^{10}B concentration of 2.69 mbarn/atom.

Table 3.1-8. Radial Reflector Graphite Composition.

Isotope/Element	Atoms/barn-cm
^{10}B	2.3261E-08
^{11}B	9.3627E-08
C	8.7886E-02
Total	8.7886E-02
Mass Density (g/cm^3)	1.752827

3.1.3.2 Upper Axial Reflector

The upper axial reflector graphite is comprised of three compositions, depending on the component of the assembly (see Table 3.1-9). The support structure into which the graphite material is placed is Peraluman-300 (Table 3.1-10).

Table 3.1-9. Upper Axial Reflector Graphite Composition (see Figure 3.1-3).

Component	Cylinder	Annulus	Plugs
Isotope/Element	**Atoms/barn-cm**	**Atoms/barn-cm**	**Atoms/barn-cm**
^{10}B	2.3235E-08	2.3368E-08	2.3356E-08
^{11}B	9.3524E-08	9.4059E-08	9.4011E-08
C	8.7789E-02	8.8291E-02	8.8245E-02
Total	8.7789E-02	8.8291E-02	8.8245E-02
Mass Density (g/cm^3)	1.750896	1.760901	1.76

Table 3.1-10. Upper Axial Reflector Peraluman-300 Support Structure Composition.

Isotope/Element	Atoms/barn-cm
^{10}B	1.4688E-07
^{11}B	5.9119E-07
Mg	1.0177E-03
Al	5.7575E-02
Si	2.2729E-04
Mn	7.2621E-05
Fe	8.5730E-05
Cu	1.2557E-05
Zn	2.4398E-05
Ga	1.1444E-06
Cd	7.0983E-08
Total	5.9018E-02
Mass Density (g/cm^3)	2.65

3.1.3.3 Lower Axial Reflector

The lower axial reflector graphite is comprised of two compositions, depending on the component of the assembly (see Table 3.1-11).

Table 3.1-11. Lower Axial Reflector Graphite Composition.

Component	Cylinder	Annulus / Source Plug
Isotope/Element	**Atoms/barn-cm**	**Atoms/barn-cm**
^{10}B	2.3223E-08	2.3356E-08
^{11}B	9.3476E-08	9.4011E-08
C	8.7744E-02	8.8245E-02
Total	8.7744E-02	8.8245E-02
Mass Density (g/cm^3)	1.75	1.76

3.1.3.4 Autorod

The autorod consists of copper wedge (Table 3.1-12) within an aluminum guide tube (Table 3.1-13).

Table 3.1-12. Autorod Copper (Type C110) Wedge Composition.

Element	Atoms/barn-cm
Cu	8.4206E-02
O	6.6923E-05
Ag	3.7224E-06
S	1.2522E-05
Ni	6.8410E-06
Fe	7.1900E-06
Total	8.4303E-02
Mass Density (g/cm^3)	8.89

Table 3.1-13. Autorod Aluminum (Type 1100) Tube Composition.

Element	Atoms/barn-cm
Si	2.8947E-04
Fe	1.4558E-04
Cu	3.1984E-05
Mn	7.3991E-06
Zn	1.2429E-05
Co	6.8975E-05
Ni	6.9257E-05
Sn	3.4242E-05
Al	5.9087E-02
Total	5.9746E-02
Mass Density (g/cm^3)	2.70

3.1.3.5 Fuel Pebbles

The UO_2 fuel used for the TRISO kernels has the composition provided in Table 3.1-14. The compositions of the additional SiC and graphite layers surrounding the kernel to form the TRISO particle are in Table 3.1-15. The fuel pebble graphite matrix surrounding the TRISO particles in the fueled zone and forming the outer unfueled layer has the composition shown in Table 3.1-16.

Table 3.1-14. UO_2 Fuel Kernel Composition.

Isotope/Element	**Atoms/barn-cm**
O	4.8612E-02
^{234}U	3.3079E-05
^{235}U	4.1172E-03
^{236}U	2.0499E-05
^{238}U	2.0135E-02
Total	7.2917E-02
Mass Density (g/cm^3)	10.88

Table 3.1-15. TRISO SiC and Graphite Layer Compositions.

Layer	**Buffer**	**IPyC**	**SiC**	**OPyC**
Isotope/Element	**Atoms/barn-cm**	**Atoms/barn-cm**	**Atoms/barn-cm**	**Atoms/barn-cm**
C	5.2640E-02	9.5254E-02	4.8055E-02	9.4752E-02
Si	--	--	4.8055E-02	--
Total	5.2640E-02	9.5254E-02	9.6110E-02	9.4752E-02
Mass Density (g/cm^3)	1.05	1.90	3.20	1.89

Table 3.1-16. Fuel Pebble Graphite Composition.

Isotope/Element	Atoms/barn-cm
C	8.6842E-02
Ag	9.6706E-10
^{10}B	1.9393E-09
^{11}B	7.8061E-09
Ca	2.4154E-07
Cd	4.7791E-10
Cl	4.4135E-08
Co	1.1505E-09
Cr	3.6312E-08
Dy	3.2097E-11
Eu	3.4322E-11
Fe	5.5104E-08
Gd	3.3169E-11
^{6}Li	5.7034E-09
^{7}Li	6.9441E-08
Mn	8.1647E-09
Ni	8.8864E-09
S	1.7893E-10
Ti	1.0831E-08
V	4.4334E-09
H	1.1581E-05
O	5.7904E-06
Total	8.6859E-02
Mass Density (g/cm^3)	1.732204

3.1.3.6 Moderator Pebbles

The composition of the graphite moderator pebbles is in Table 3.1-17.

Table 3.1-17. Moderator Pebble Graphite Composition.

Isotope/Element	Atoms/barn-cm
C	8.4434E-02
^{10}B	1.4193E-08
^{11}B	5.7130E-08
Ca	3.2656E-06
Cd	2.7077E-09
Cl	5.3343E-07
Dy	4.0583E-10
Eu	8.6793E-10
Fe	1.0719E-07
Gd	2.5808E-10
^{6}Li	9.7630E-09
^{7}Li	1.1887E-07
Ni	1.3483E-08
S	4.4297E-06
Si	1.2644E-06
Sm	5.8029E-10
Ti	2.1196E-07
V	2.5891E-07
H	1.1263E-05
O	5.6317E-06
Total	8.4461E-02
Mass Density (g/cm^3)	1.684743

3.1.3.7 Withdrawable Control Rods

The withdrawable control rods consist of an inner stainless steel tube (Table 3.1-18) held within an outer stainless steel tube with end plugs (Table 3.1-19).

Table 3.1-18. Control Rod Stainless Steel (Type St1.4301) Tube Composition.

Element	Atoms/barn-cm
C	1.3864E-04
Si	8.4696E-04
Mn	8.6597E-04
Cr	1.6927E-02
Ni	8.3083E-03
Fe	5.9391E-02
Total	8.6477E-02
Mass Density (g/cm^3)	7.9

Table 3.1-19. Control Rod Stainless Steel (Type St1.4541) Tube and End Plug Composition.

Element	Atoms/barn-cm
C	1.9805E-04
Si	8.4696E-04
Mn	8.6597E-04
Cr	1.6469E-02
Ni	8.3083E-03
Ti	4.9695E-05
Fe	5.9761E-02
Total	8.6499E-02
Mass Density (g/cm^3)	7.9

3.1.3.8 Graphite Cavity Floor Fillers

The composition of the graphite fillers placed on the cavity floor is in Table 3.1-20.

Table 3.1-20. Graphite Cavity Floor Filler Composition.

Isotope/Element	Atoms/barn-cm
^{10}B	2.3214E-08
^{11}B	9.3439E-08
C	8.7709E-02
Total	8.7709E-02
Mass Density (g/cm^3)	1.749294

3.1.3.9 Ambient Air

The composition of the ambient air is in Table 3.1-21. The air has a temperature of 293 K, pressure of 980 mbar, and 50 % humidity.

Table 3.1-21. Ambient Air Composition.

Element	Atoms/barn-cm
H	5.7098E-07
N	3.7362E-05
O	1.0326E-05
Ar	2.2345E-07
C	9.1319E-09
Total	4.8492E-05
Mass Density (g/cm^3)	0.00115932

3.1.4 Temperature Data

The benchmark model temperature is 293 K.

3.1.5 Experimental and Benchmark-Model k_{eff} and / or Subcritical Parameters

The experimental k_{eff} was approximately at unity, maintained at delayed critical with the 1σ uncertainty summarized in Section 2.1.8. Simplification biases and uncertainties, as discussed in Section 3.1.1.1 were applied to the benchmark model. The benchmark k_{eff} is shown in Table 3.1-22. The uncertainty in the benchmark k_{eff} value is obtained by summing under quadrature the total experimental uncertainty (Table 2.1-29) and the total bias uncertainty (Table 3.1-3).

Table 3.1-22. Experimental and Benchmark Eigenvalues, Bias, and Uncertainties.

		Experimental			Bias			Benchmark		
Case	Core	k_{eff}	±	σ	Δk	±	σ	k_{eff}	±	σ
1	4	1.0000	±	0.0035	0.0039	±	0.0008	1.0039	±	0.0036

3.2 Benchmark-Model Specifications for Buckling and Extrapolation-Length Measurements

Buckling and extrapolation length measurements were made but have not yet been evaluated.

3.3 Benchmark-Model Specifications for Spectral Characteristics Measurements

Spectral characteristics measurements were not made.

3.4 Benchmark-Model Specifications for Reactivity Effects Measurements

Reactivity effects measurements were made but have not yet been evaluated.

3.5 Benchmark-Model Specifications for Reactivity Coefficient Measurements

Reactivity coefficient measurements were made but have not yet been evaluated.

3.6 Benchmark-Model Specifications for Kinetics Measurements

Kinetics measurements were made but have not yet been evaluated.

3.7 Benchmark-Model Specifications for Reaction-Rate Distribution Measurements

Reaction-rate distribution measurements were made but have not yet been evaluated.

3.8 Benchmark-Model Specifications for Power Distribution Measurements

Power distribution measurements were not made.

3.9 Benchmark-Model Specifications for Isotopic Measurements

Isotopic measurements were not made.

3.10 Benchmark-Model Specifications for Other Miscellaneous Types of Measurements

Other miscellaneous types of measurements were not made.

4.0 RESULTS OF SAMPLE CALCULATIONS

4.1 Results of Calculations of the Critical or Subcritical Configurations

The benchmark models described in Section 3 were modeled using MCNP5 (see Appendix A.1 for sample input deck for Case 1) and ENDF/B-VII.0 neutron cross section data. Random particles are not easily modeled in MCNP, therefore all 9394 TRISO particles were modeled within a cubic lattice with sides 0.1758 cm in length. All TRISO particles are completely contained within the fueled region of the fuel pebbles (see Figure 4.1-1); this was verified by visually inspecting each layer in a visual editor. The effect of random particle placement was determined to be essentially negligible relative to a regular array of particles in a fuel pebble (see Section 2.1.9.4 of PROTEUS-GCR-EXP-001).[a]

The fuel and moderator pebbles were randomly placed within the core cavity as discussed in Section 2.1.4.3. Figures 4.1-2 and 4.1-3 provide sample cross section views of the core configuration containing randomly distributed pebbles. Some locations are empty, or devoid, of pebbles, which occurs when pebbles are randomly packed. The total packing fraction in the core is conserved.

Monte Carlo calculations were performed with 1,650 generations with 100,000 neutrons per generation. The k_{eff} estimates are based on 150 skipped generations and a total of 150,000,000 neutron histories each. Calculated eigenvalues are shown in Table 4.1-1. The calculated eigenvalue is greater than the benchmark value by almost 2 %, within approximately a 5σ uncertainty. Comparison of the results of sample calculations for all eleven HTR-PROTEUS critical configurations indicates that there is definitely a difference in the benchmark model or calculation method for the randomly packed core that is unaccounted for. While the overall uncertainty in this benchmark model is comparable to the uncertainty in the deterministic cores, the difference between the MCNP5 calculations and the benchmark values has approximately doubled.

The packing fraction of a randomly loaded pebble-bed depends on various parameters: the ratio of pebble diameter to core diameter, and the denseness of the packing itself, which also includes the change in packing density with time due to effects such as gravity. The packing fraction is not constant throughout the core, typically at a higher density near the radial core center, with a reduction of up to 0.25 at the pebble/wall interface. The truly random portion of the core would be the centermost region (~5× the pebble diameter).[b] Furthermore, while the void fraction (1 - packing fraction) decreases, on average, towards the center of the core, the local void fraction has some variability, especially towards the pebble/wall interface.[c] Therefore, while the core-averaged packing fraction is retained, the simulation of the localized packing fractions throughout the core may impact the final calculated results. The sensitivity of the calculation of k_{eff} for this benchmark configuration to the localized packing fraction, especially near the pebble/wall interface, is currently unknown.

Most of the features for the randomly-packed core configuration of HTR-PROTEUS are identical to those in the deterministically-packed cores (PROTEUS-GCR-EXP-001, -003, and -004). The experimentally measured worths, calculated biases, and calculated uncertainties are also correlated between the eleven critical benchmark configurations. It is concluded that the benchmark specifications provided in this report are correct. However, there may be a computational error in how the random pebbles are simulated for the MCNP calculation results provided below. Additional analyses with computational methods capable of evaluating randomly packed cores would provide further insight into this discrepancy.

---

[a] Uner, C. and Seker, V., "Monte Carlo Criticality Calculations for a Pebble Bed Reactor with MCNP," *Nucl. Sci. Eng.*, **149**, 131-137 (2005).
[b] Kugeler, K. and Schulten, R., *Hochtemperaturtechnik*, Springer Verlag, Berlin (1989) [In German].
[c] El-Wakil, M. M., *Nuclear Energy Conversion*, American Nuclear Society, La Grange, Illinois (1982).

Models developed by Difilippo using MCNP4C with ENDF/B-VI (DLC-189) neutron cross sections did not include Case 1 (Core 4).[a] As noted in PROTEUS-GCR-EXP-001, the models by Difilippo include water content within the graphite reflectors. Evaluation of the water content indicates that the small quantity has a negligible impact on the neutron scattering and only provides additional negative reactivity (~100 pcm) to the system. However, the addition of water absorption seems to be incorrect as the analysis of the equivalent boron content in the graphite reflectors should have already included absorption from water contained within the graphite blocks.

Monte Carlo calculations of k_{eff} for graphite-moderated reactors and assemblies typically compute greater than the benchmark values, as seen for the High Temperature Engineering Test Reactor (HTTR-GCR-RESR-001, -002, and -003), the HTR-10 Pebble-Bed Reactor (HTR10-GCR-RESR-001), and the other HTR-PROTEUS configurations (PROTEUS-GCR-EXP-001, -003, and -004). Computations of the ASTRA critical facility with the MCU-REA1 code agree well with the benchmark k_{eff} (ASTRA-GCR-EXP-001) but calculate high when using MCNP.[b] The MCU computer program was developed to include a special feature to evaluate systems with double-heterogeneity, such as TRISO particles in a HTGR.[c] The computational bias using MCNP is on the order of 1-2 % greater than the benchmark values. The HTTR configurations are closer to 2 % and it has been previously discussed that the bias is possibly due to uncertainties in the impurity content of the graphite blocks[d,e] and a need to increase the thermal neutron capture cross section of carbon.[f]

Additional calculations using MONK10(DEV) and ENDF/B-VII.0 were provided by David Hanlon from AMEC. Multiple runs (10 per mode) were performed using two different Modes: 0 and 2. In Mode 0 (see Figure 4.1-4), the core volume is initially filled with a close-packed hexagonal array of pebbles, which would have a packing fraction of ~0.74 in an infinite array. Random groups of four pebbles in a tetrahedral configuration were removed and replaced by a single pebble at the center of the original location. The regularity of the original array is perturbed and the packing fraction is effectively reduced. The number of sites is determined by the packing fraction requested in the input. In Mode 2 (see Figure 4.1-5), the core volume is filled with layers of pebbles in a hexagonal array with each layer sitting optimally on top of the one directly below it such that a given pebble touches three pebbles in the supporting layer beneath it. The requested packing fraction is achieved by opening the pitch within the layers. This regular form is considered physically unrealistic as it contains many streaming paths. It is included to allow investigation of the effects. The MONK PBMR hole geometry could not be used for this experimental configuration as the code was designed to handle a much greater ratio of core size to fuel pebble diameter.

A number of batch calculations were performed, with the statistical uncertainty of ±0.0005 Δk (±50 pcm) for a single run. Each of the 10 calculations per mode had a different starting random number seed for the Monte Carlo tracking processes, and another, different, fixed random number seed for arranging the spheres within the container. The standard deviation about the mean k_{eff} for the 10 calculations was approximately ±0.005 Δk (±500 pcm) which could not be further reduced by increasing the number of calculations. This variation is believed to be a fundamental uncertainty associated with the packing

[a] Difilippo, F. C., "Monte Carlo Calculations of Pebble Bed Benchmark Configurations of the PROTEUS Facility," *Nucl. Sci. Eng.*, **143**, 240-253 (2003).
[b] Z. Zibi and F. Albornoz, "Validating the MCNP Modelling of the ASTRA Critical Facility," *Proc. HTR 2010*, Prague, Czech Republic, October 18-20, 2010.
[c] N. N. Ponomarev-Stepnoi, et al., "Using the MCU Computer Program to Analyze the Results of Critical Experiments with HTGR Fuel Pellets on ASTRA Testing Stand," *Atomic Energy*, **97**, pp. 669-677 (2004).
[d] K. Yamashita, et al., "Startup Core Physics Tests of High Temperature Engineering Test Reactor (HTTR), (I)," *J. At. Energy Soc. Jpn.*, **42**, pp. 30-42 (2000) [in Japanese].
[e] N. Fujimoto, et al., "Startup Core Physics Tests of High Temperature Engineering Test Reactor (HTTR) (II)," *J. At. Energy Soc. Jpn.*, **42**, pp. 458-464 (2000) [in Japanese].
[f] S. Shimakawa, M. Goto, S. Nakagawa, and Y. Tachibana, "Impact of Capture Cross-Section of Carbon on Nuclear Design for HTGRs," *Proc. HTR 2010*, Prague, Czech Republic, October 18-20, 2010.

Mode adopted, and cannot be further reduced by converging the individual calculations. A small part of this variation is due to two components: namely actual total mass of fuel present in the random distribution of sphere, and the achieved ratio of fuel to moderator pebbles. The random component of fuel/moderator pebble placement also introduces uncertainty into the calculated results. In the MONK calculations, one specifies the size of the container into which the spheres are placed, the proportion of each sphere type (in this case 50:50), and the desired packing fraction (in this case 0.60898). Volume estimates of the material present in 10 of the MONK calculations for each mode indicate an uncertainty in the range of approximately ±100 pebbles of each type in the core. This leads to a variation of approximately ±4% in the fuel-to-moderator pebble ratio. For Mode 0, the average fuel to moderator sphere ratio is 1.006, and 0.988 for Mode 2. The significance of these differences is unclear as the actual average value for k_{eff} calculated for each Mode is very similar. Furthermore, where the difference between the calculated k_{eff} between Mode 0 and Mode 2 is negligible, and the uncertainty is each mode is similar, the uncertainty in the fuel-to-moderator ratio is believed to have a small impact on the total calculation uncertainty. Calculated results are provided in Table 4.1-2.[a] The MONK10(DEV) calculations are within 0.5% (2σ) of the benchmark k_{eff} values. Due to the larger, quantified, statistical uncertainty in the MONK calculations, the benchmark and MCNP5 results are within ~2σ of the MONK results.

An additional MONK calculation was performed using the explicit pebble locations utilized in the MCNP input deck (see Appendix A) for the MCNP results provided in Table 4.1-2. The only difference being that the location of the fuel and moderator pebbles were randomized while still maintaining the exact 1:1 moderator-to-fuel pebble ratio and quantity of pebbles within the core. The final result is provided in Table 4.1-2, which is within 1σ of the other MONK results, and between the MONK and MCNP results.

A comparison of the calculated eigenvalues for the MCNP5 and MONK10(DEV) quite possibly indicates that the modeling uncertainty in the MCNP5 analysis may be quite sizeable but currently not quantified. As discussed previously in this section, additional analyses could provide further insight into the challenges and limitations encountered when modeling nuclear systems containing randomly-distributed pebbles.

[a] Personal communications with Paul Smith and David Hanlon at AMEC (February 5, 2013).

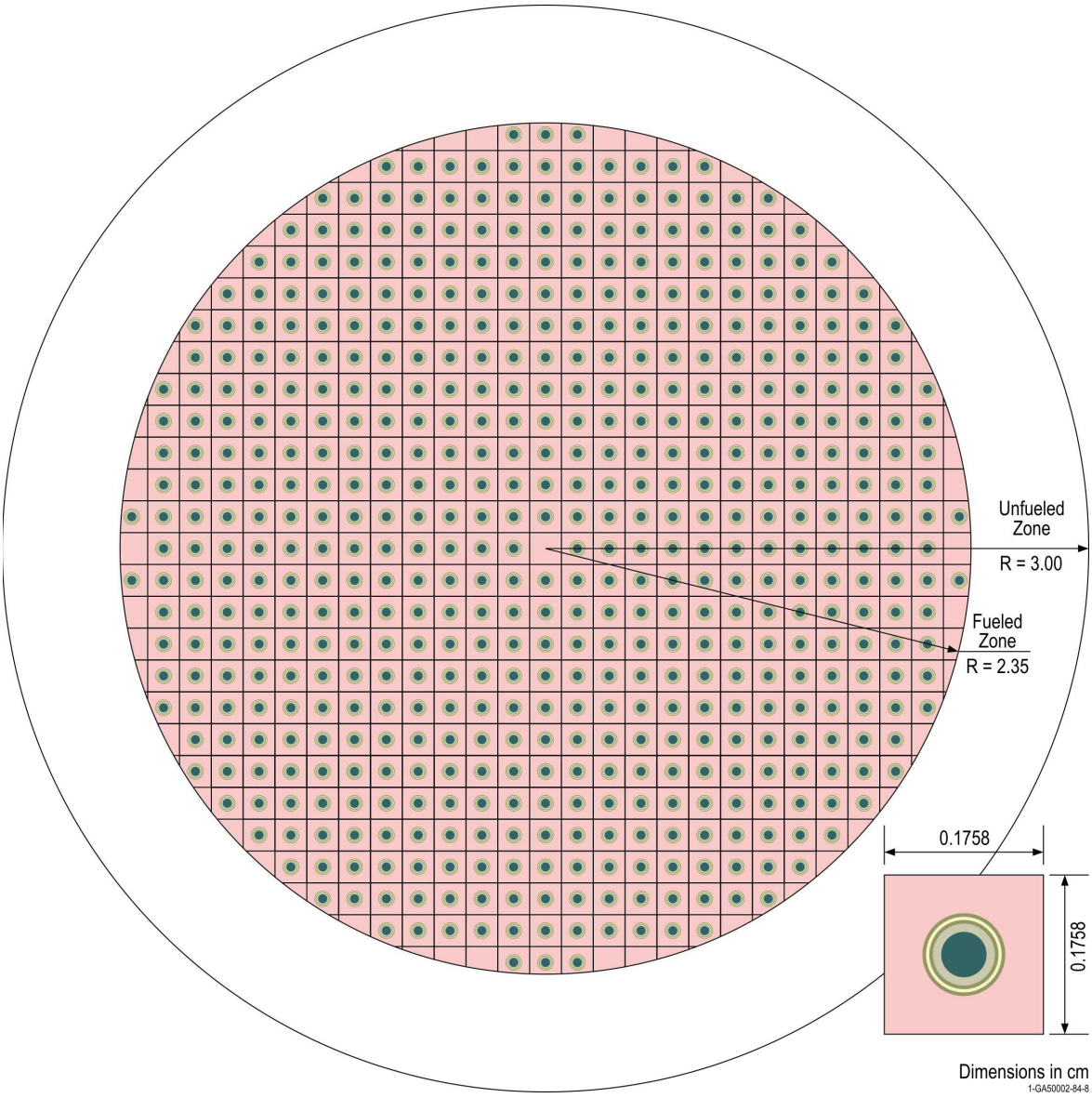

Figure 4.1-1. Regular TRISO Lattice Used in MCNP Calculations of the Benchmark Models.

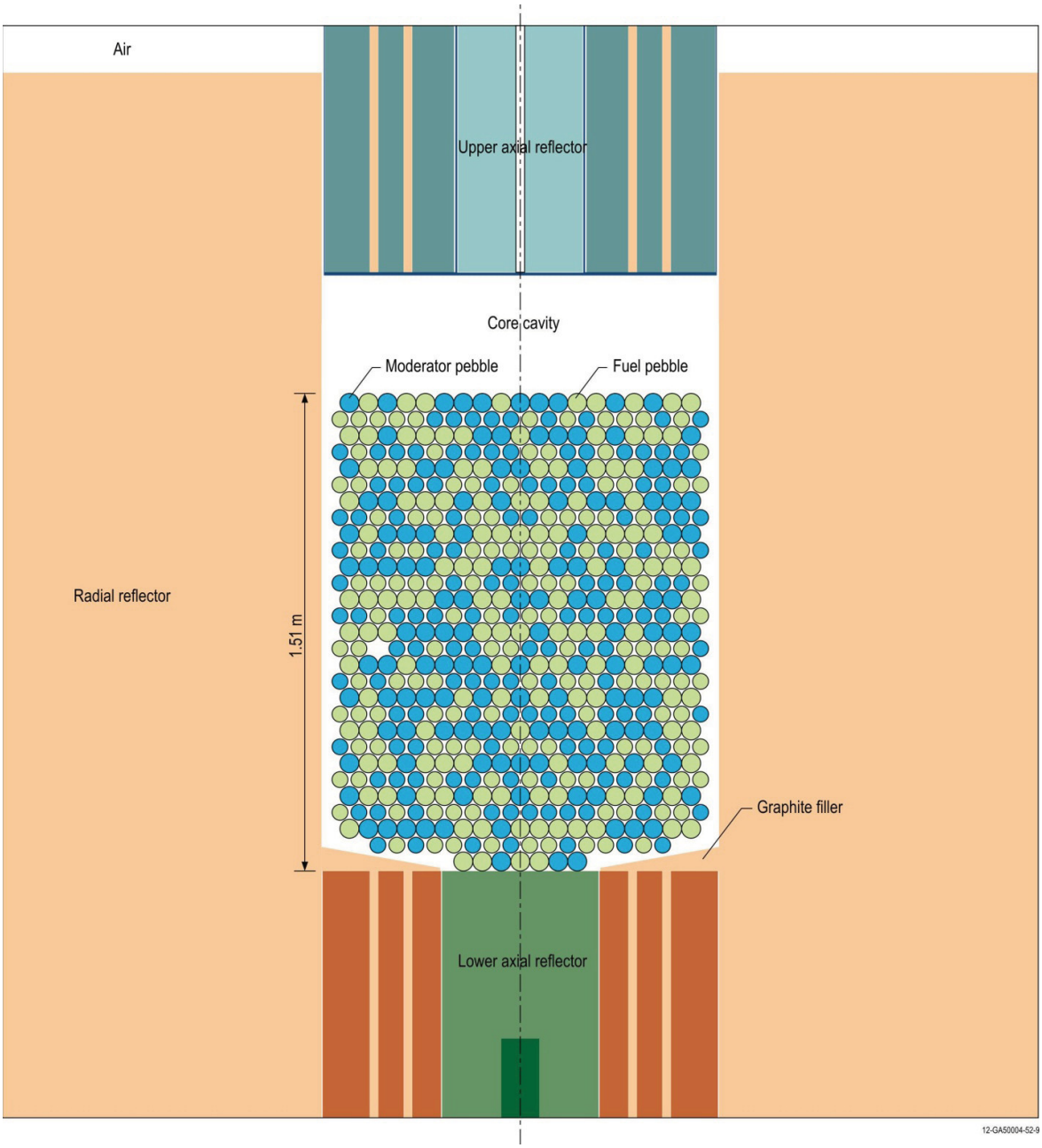

Figure 4.1-2. Vertical Cross Section View of Randomly Distributed Pebbles.

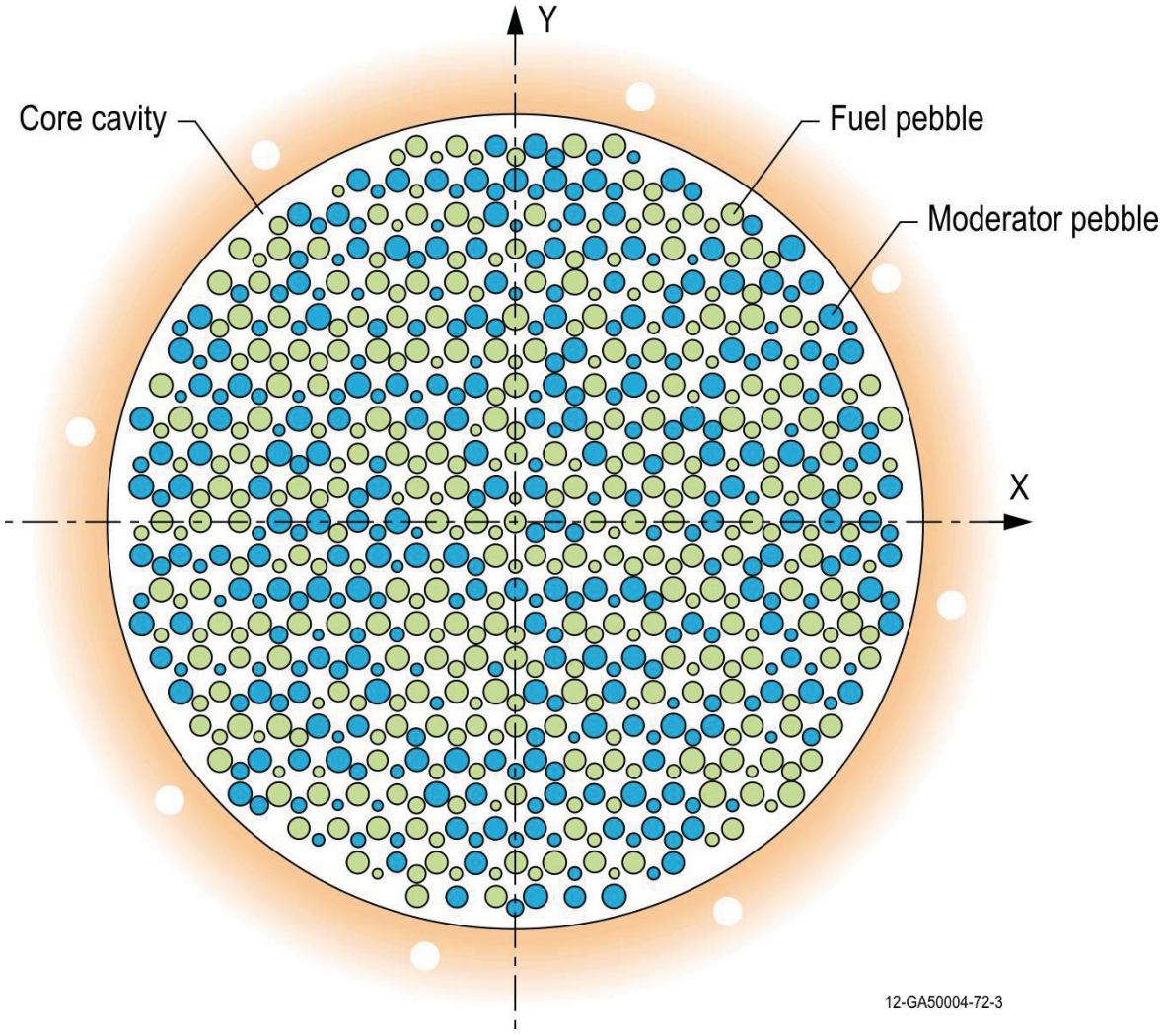

Figure 4.1-3. Horizontal Cross Section View of Randomly Distributed Pebbles.

Table 4.1-1. Comparison of Benchmark Eigenvalues using MCNP5.

Case	Core	Neutron Cross Section Library	Calculated			Benchmark			$\frac{C-E}{E}(\%)$	Difference (pcm)
			k_{eff}	±	σ	k_{eff}	±	σ		
1	4	ENDF/B-VII.0	1.01736	±	0.00007	1.0039	±	0.0036	1.34	1346

Three additional MONK calculations were performed using the explicit pebble locations utilized in the MCNP input deck (see Appendix A) for the MCNP results provided in Table 4.1-2. The only difference being that the location of the fuel and moderator pebbles were randomized while still maintaining the exact 1:1 moderator-to-fuel pebble ratio and quantity of pebbles within the core. The final result is provided in Table 4.1-2, which is within 1σ of the other MONK results, and between the MONK and MCNP results. This analysis indicates that the result is not sensitive to the actual random distribution of fuel and moderator material as long as the fuel-to-moderator ratio is maintained. However, the ~400 pcm difference between the different MONK calculations potentially indicates a high level of modeling uncertainty associated with the positioning of the spheres within the core cavity.

Table 4.1-2. Comparison of Benchmark Eigenvalues using MONK10(DEV).[(a)]

Case	Core	Neutron Cross Section Library (Model Mode)	Calculated			Benchmark			$\frac{C-E}{E}(\%)$	Difference (pcm)
			k_{eff}	±	σ	k_{eff}	±	σ		
1	4	ENDF/B-VII.0 (Mode 0)	1.0092	±	0.0052	1.0039	±	0.0036	0.53	528
		ENDF/B-VII.0 (Mode 2)	1.0090	±	0.0050				0.52	518
		ENDF/B-VII.0 (MCNP Pebble Locations)	1.0130	±	0.0003				0.91	906

(a) Results provided by David Hanlon from AMEC. Sample input decks are provided in Appendix A.

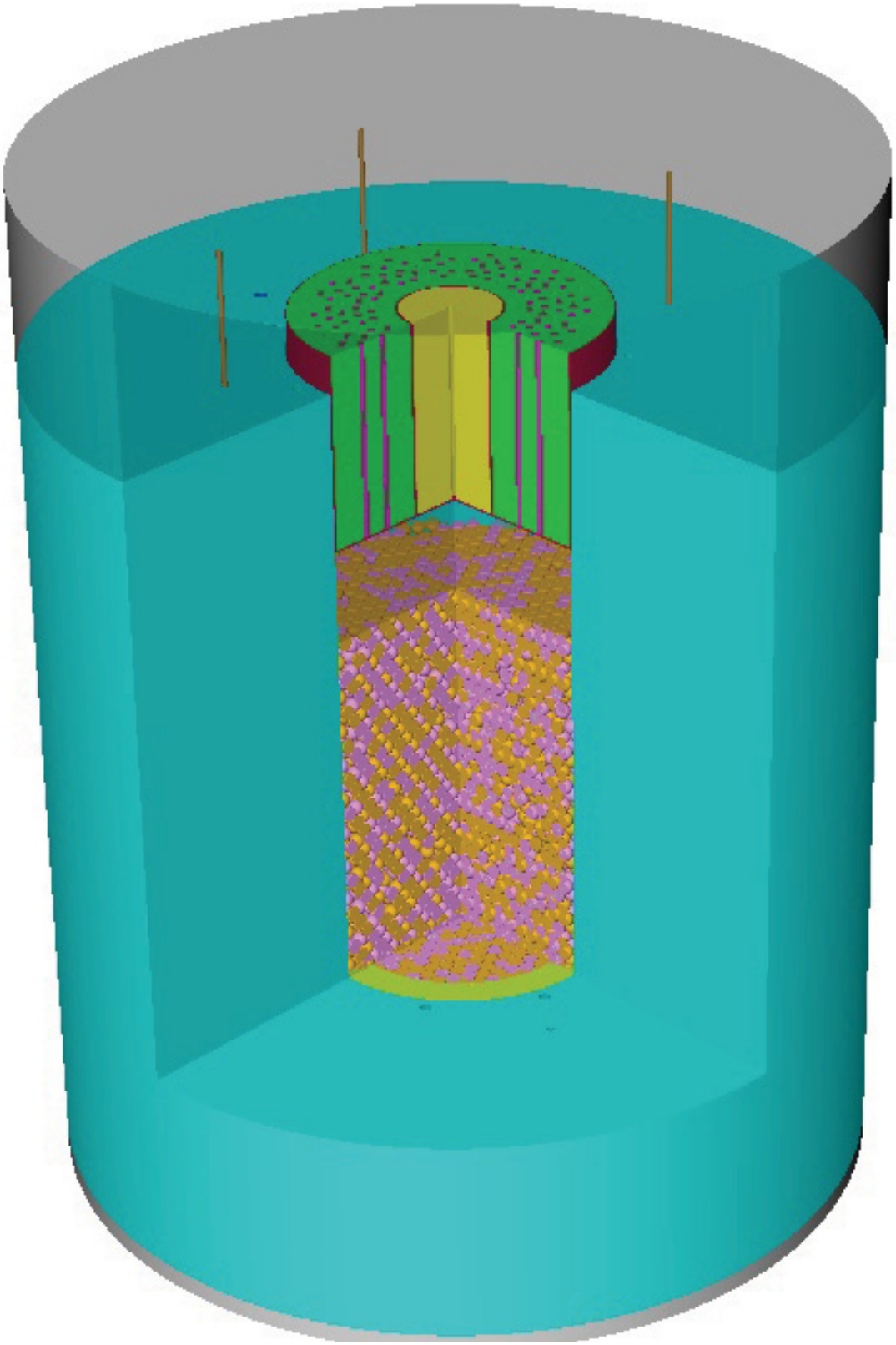

Figure 4.1-4. Visual Representation of Mode 0 Core Loading for MONK10(DEV).

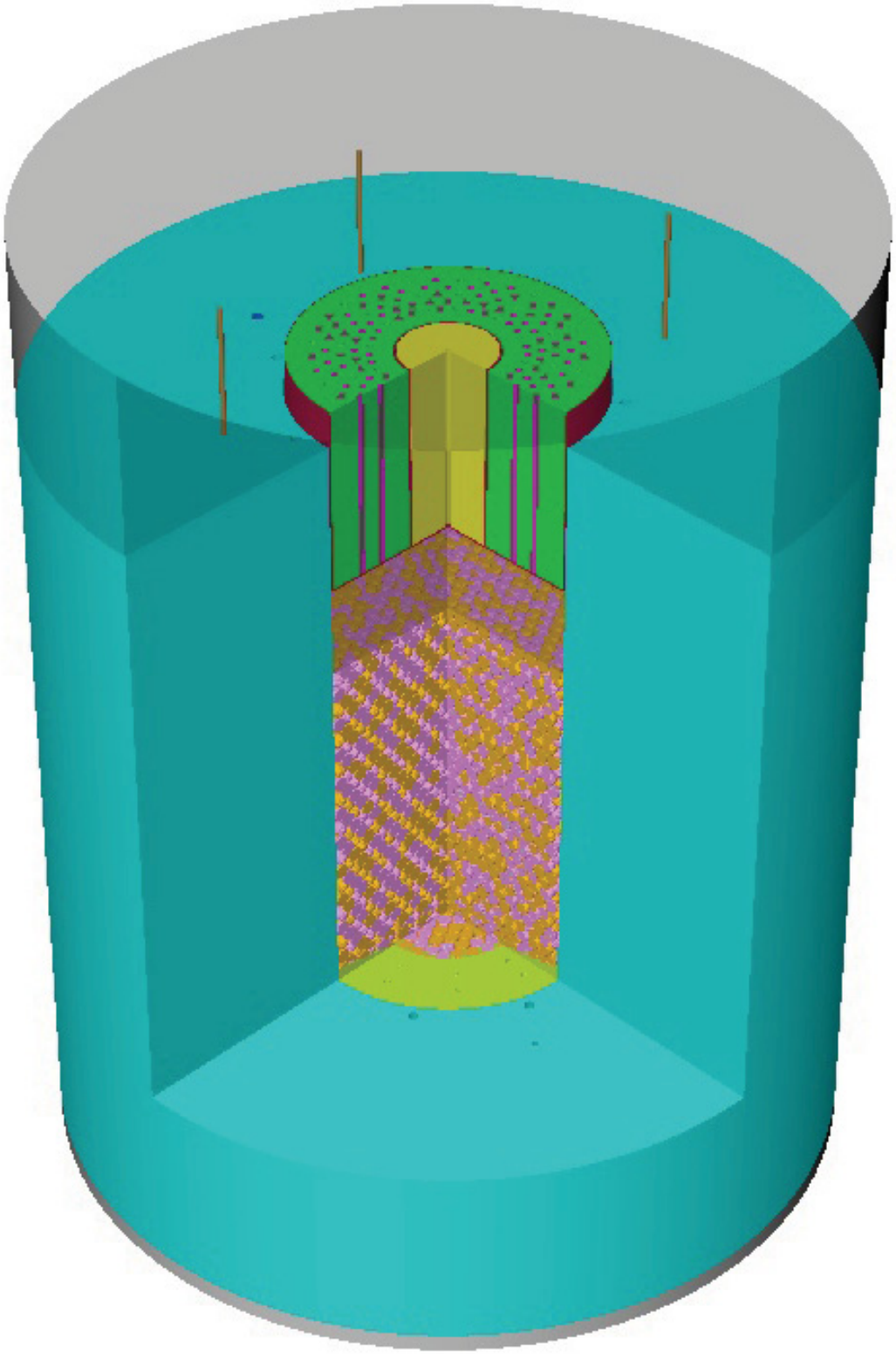

Figure 4.1-5. Visual Representation of Mode 2 Core Loading for MONK10(DEV).

4.2 Results of Buckling and Extrapolation Length Calculations

Buckling and extrapolation length measurements were made but have not yet been evaluated.

4.3 Results of Spectral-Characteristics Calculations

Spectral characteristics measurements were not made.

4.4 Results of Reactivity-Effects Calculations

Reactivity effects measurements were made but have not yet been evaluated.

4.5 Results of Reactivity Coefficient Calculations

Reactivity coefficient measurements were made but have not yet been evaluated.

4.6 Results of Kinetics Parameter Calculations

Kinetics measurements were made but have not yet been evaluated.

4.7 Results of Reaction-Rate Distribution Calculations

Reaction-rate distribution measurements were made but have not yet been evaluated.

4.8 Results of Power Distribution Calculations

Power distribution measurements were not made.

4.9 Results of Isotopic Calculations

Isotopic measurements were not made.

4.10 Results of Calculations for Other Miscellaneous Types of Measurements

Other miscellaneous types of measurements were not made.

5.0 REFERENCES

1. Williams, T., "LEU-HTR PROTEUS: Configuration Descriptions and Critical Balances for the Cores of the HTR-PROTEUS Experimental Programme," TM-41-95-18, v. 1.00, Paul Sherrer Institut, Villigen, November 25, 1996.
2. Mathews, D. and Williams, T., "LEU-HTR PROTEUS System Component Description," TM-41-93-43, v. 2.0, Paul Scherrer Institut, Villigen, November 25, 1996.
3. Williams, T., Rosselet, M., and Scherer, W. (editors), "Critical Experiments and Reactor Physics Calculations for Low-Enriched High Temperature Gas Cooled Reactors," IAEA-TECDOC-1249, International Atomic Energy Agency, Vienna (2001).

APPENDIX A: COMPUTER CODES, CROSS SECTIONS, AND TYPICAL INPUT LISTINGS

A.1 Critical/Subcritical Configurations

A.1.1 Name(s) of code system(s) used.

Monte Carlo n-Particle, version 5.1.60 (MCNP5).

A.1.2 Bibliographic references for the codes used.

X-5 Monte Carlo Team, "MCNP – a General Monte Carlo n-Particle Transport Code, version 5," LA-UR-03-1987, Los Alamos National Laboratory (2003).

A.1.3 Origin of cross-section data.

The Evaluated Neutron Data File library, ENDF/B-VII.0[a] was utilized in the benchmark model analysis.

A.1.4 Spectral calculations and data reduction methods used.

Not applicable.

A.1.5 Number of energy groups or if continuous-energy cross sections are used in the different phases of calculation.

Continuous-energy cross sections.

A.1.6 Component calculations.

- Type of cell calculation – Reactor core, reflectors, and moderator
- Geometry – TRISO particles in graphite pebbles
- Theory used – Not applicable
- Method used – Monte Carlo
- Calculation characteristics
  - MCNP5 – histories/cycles/cycles skipped = 100,000/1,650/150 continuous-energy cross sections

A.1.7 Other assumptions and characteristics.

Not applicable.

A.1.8 Typical input listings for each code system type.

The MCNP input deck for the benchmark model, core configuration 4 (Case 1), is provided in a separate file (ASCII format), htr4.benchmark.mcnp5.nf7.inp, which is located in the input folder of the directory of this evaluation.

Sample MONK10(DEV) input decks for Modes 0 and 2 are provided below:

[a] M. B. Chadwick, et al., "ENDF/B-VII.0: Next Generation Evaluated Nuclear Data Library for Nuclear Science and Technology," *Nucl. Data Sheets*, **107**: 2931-3060 (2006).

Sample Input Listing for MONK10(DEV) using Mode 0:

```
COLUMNS 1 132
* MONK10  Model of PROTEUS Core 4.
*
* Specification PROTEUS-GCR-EXP-002 CRIT Revision 0 March 31, 2013

* Fixed Run Parameters
@NUMSET=10       ! Number of Settling Stages
@NUMSTG=500      ! Maximum Number of Ordinary Stages
@NUMNEUT=5000    ! Number of SuperHistories per Stage
@NGEN=10         ! Number of Generations per SuperHistory
@FACTNU=1.0      ! Estimate of 1/k-eff for 1st stage
@LSTAGE=10       ! Suppress checking of STDV until this ordinary stage
@STDV=0.0005     ! Target Standard Deviation

BEGIN MATERIAL SPECIFICATION

TYPE BINGO

* Radial Reflector Graphite
NUMBER DENSITY
MATERIAL Radial_Refl
B10      2.3261E-08
B11      9.3627E-08
GRAPHITE 8.7886E-02

* Upper Axial Reflector Graphite - Cylinder
NUMBER DENSITY
MATERIAL UARG_Cyl
B10      2.3235E-08
B11      9.3524E-08
GRAPHITE 8.7789E-02

* Upper Axial Reflector Graphite - Annulus
NUMBER DENSITY
MATERIAL UARG_Ann
B10      2.3368E-08
B11      9.4059E-08
GRAPHITE 8.8291E-02

* Upper Axial Reflector Graphite - Plugs
NUMBER DENSITY
MATERIAL UARG_Plg
B10      2.3356E-08
B11      9.4011E-08
GRAPHITE 8.8245E-02

* Upper Axial Reflector Peraluman-300 Support Structure
NUMBER DENSITY
MATERIAL UAR_Peral
B10      1.4688E-07
B11      5.9119E-07
Mg       1.0177E-03
Al       5.7575E-02
Si       2.2729E-04
Mn       7.2621E-05
Fe       8.5730E-05
Cu       1.2557E-05
Zn       2.4398E-05
Ga       1.1444E-06
Cd       7.0983E-08

* Lower Axial Reflector Graphite - Cylinder
NUMBER DENSITY
MATERIAL LARG_Cyl
B10      2.3223E-08
B11      9.3476E-08
GRAPHITE 8.7744E-02

* Lower Axial Reflector Graphite - Annulus / Source Plug
NUMBER DENSITY
MATERIAL LARG_Ann
B10      2.3356E-08
B11      9.4011E-08
```

```
GRAPHITE 8.8245E-02

* Autorod Copper (Type C110) Wedge
NUMBER DENSITY
MATERIAL AutoRod_Cu
Cu       8.4206E-02
O        6.6923E-05
Ag       3.7224E-06
S        1.2522E-05
Ni       6.8410E-06
Fe       7.1900E-06

* Autorod Aluminum (Type 1100) Tube
NUMBER DENSITY
MATERIAL AutoRod_Tube
Si       2.8947E-04
Fe       1.4558E-04
Cu       3.1984E-05
Mn       7.6610E-06
Zn       1.2429E-05
Co       6.8975E-05
Ni       6.9257E-05
Sn       3.4242E-05
Al       5.9087E-02

* UO2 Fuel Kernel
NUMBER DENSITY
MATERIAL Kernel
O        4.8612E-02
U234     3.3079E-05
U235     4.1172E-03
U236     2.0499E-05
U238     2.0135E-02

* TRISO SiC and Graphite Layer - Buffer
NUMBER DENSITY
MATERIAL Buffer
GRAPHITE 5.2640E-02

* TRISO SiC and Graphite Layer - PyC (Inner)
NUMBER DENSITY
MATERIAL IPyC
GRAPHITE 9.5254E-02

* TRISO SiC and Graphite Layer - SiC
NUMBER DENSITY
MATERIAL SiC
GRAPHITE 4.8055E-02
Si       4.8055E-02

* TRISO SiC and Graphite Layer - PyC (Outer)
NUMBER DENSITY
MATERIAL OPyC
GRAPHITE 9.4752E-02

* Fuel Pebble Graphite
NUMBER DENSITY
MATERIAL FP_Graphite
GRAPHITE 8.6842E-02
AG       9.6706E-10
B10      1.9393E-09
B11      7.8061E-09
Ca       2.4154E-07
Cd       4.7791E-10
Cl       4.4135E-08
Co       1.1505E-09
Cr       3.6312E-08
!Dy       3.2097E-11
Eu       3.4322E-11
Fe       5.5104E-08
Gd       3.3169E-11
Li6      5.7034E-09
Li7      6.9441E-08
Mn       8.1647E-09
Ni       8.8864E-09
```

```
S         1.7893E-10
Ti        1.0831E-08
V         4.4334E-09
H         1.1581E-05
O         5.7904E-06

* Moderator Pebble Graphite
NUMBER DENSITY
MATERIAL MP_Graphite
GRAPHITE 8.4434E-02
B10       1.4193E-08
B11       5.7130E-08
Ca        3.2656E-06
Cd        2.7077E-09
Cl        5.3343E-07
!Dy        4.0583E-10
Eu        8.6793E-10
Fe        1.0719E-07
Gd        2.5808E-10
Li6       9.7630E-09
Li7       1.1887E-07
Ni        1.3483E-08
S         4.4297E-06
Si        1.2644E-06
Sm        5.8029E-10
Ti        2.1196E-07
V         2.5891E-07
H         1.1263E-05
O         5.6317E-06

* Control Rod Stainless Steel (Type St1.4301) Tube
NUMBER DENSITY
MATERIAL CR_SS_4301
C         1.3864E-04
Si        8.4696E-04
Mn        8.6597E-04
Cr        1.6927E-02
Ni        8.3083E-03
Fe        5.9391E-02

* Control Rod Stainless Steel (Type St1.4541) Tube and End Plug Composition
NUMBER DENSITY
MATERIAL CR_SS_4541
C         1.9805E-04
Si        8.4696E-04
Mn        8.6597E-04
Cr        1.6469E-02
Ni        8.3083E-03
Ti        4.9695E-05
Fe        5.9761E-02

* Graphite Cavity Floor Fillers
NUMBER DENSITY
MATERIAL Cavity_Graphite
B10       2.3214E-08
B11       9.3439E-08
GRAPHITE 8.7709E-02

* Ambient Air
NUMBER DENSITY
MATERIAL Air
H         5.7098E-07
N         3.7362E-05
O         1.0326E-05
!Ar        2.2345E-07
C         9.1319E-09


END

BEGIN MATERIAL GEOMETRY

PART PROTEUS_CORE4 ! Entire Geometry
ZROD   1   0.0    0.0   -7.5          [327.53972/2.0] [78.0+189.3+78.0+7.5+60.0]
ZSEC   2   0.0    0.0    0.0          [125.66796/2.0] [327.53972/2.0] 330.4 FULL
```

```
ZROD   3 -38.45  56.57   0.0          [4.5/2.0]       330.4 ! Safety/Shutdown Rod Hole 1
ZROD   4  32.74 -60.05   0.0          [4.5/2.0]       330.4 ! Safety/Shutdown Rod Hole 2
ZROD   5  57.17  37.55   0.0          [4.5/2.0]       330.4 ! Safety/Shutdown Rod Hole 3
ZROD   6 -53.23 -42.95   0.0          [4.5/2.0]       330.4 ! Safety/Shutdown Rod Hole 4
ZROD   7  67.19 -12.82   0.0          [4.5/2.0]       330.4 ! Safety/Shutdown Rod Hole 5
ZROD   8 -66.98  13.87   0.0          [4.5/2.0]       330.4 ! Safety/Shutdown Rod Hole 6
ZROD   9  19.31  65.62   0.0          [4.5/2.0]       330.4 ! Safety/Shutdown Rod Hole 7
ZROD  10 -13.87 -66.98   0.0          [4.5/2.0]       330.4 ! Safety/Shutdown Rod Hole 8
ZROD  11  17.36 -87.29   -7.5         [5.5/2.0]       [330.4+7.5] ! Autorod Hole
ZROD  12 -83.70  34.67   0.0          [2.743/2.0]     383.5 ! Withdrawable Control Rod Hole 1
ZROD  13  34.67  83.70   0.0          [2.743/2.0]     383.5 ! Withdrawable Control Rod Hole 2
ZROD  14  83.70 -34.67   0.0          [2.743/2.0]     383.5 ! Withdrawable Control Rod Hole 3
ZROD  15 -34.67 -83.70   0.0          [2.743/2.0]     383.5 ! Withdrawable Control Rod Hole 4
ZROD  16   0.0    0.0    0.0          [125.66796/2.0]  78.0 ! Lower Axial Reflector
ZROD  17   0.0    0.0    [78.0+189.3] [125.66796/2.0]  78.0 ! Upper Axial Reflector
ZROD  18   0.0    0.0    [78.0+188.3] 62.1              1.0 ! Aluminium Support
ZSEC  19   0.0    0.0    78.0         24.96893 [125.66796/2.0]   7.611 FULL ! Graphite Cavity
Floor Filler
ZCONE 20   0.0    0.0    [78.0+0.934366]     24.96893 [125.66796/2.0] [7.611-0.934366] ! Remove
conic shape from Floor Filler
ZROD  21   0.0    0.0    [78.0+7.611] [125.66796/2.0]  [151.0-7.611] ! Core Cavity Cylinder
ZONES
M Air         +1 -2 -11 -12 -13 -14 -15 -16 -17 -18 -19 -20 -21
M Radial_Refl +2 -3 -4 -5 -6 -7 -8 -9 -10 -11 -12 -13 -14 -15
M Air         +3
M Air         +4
M Air         +5
M Air         +6
M Air         +7
M Air         +8
M Air         +9
M Air         +10
P Autorod     +11
P Cont_Rod    +12
P Cont_Rod    +13
P Cont_Rod    +14
P Cont_Rod    +15
P Low_Ax_Ref  +16
P Upp_Ax_Ref  +17
M UAR_Peral   +18
BH Cav_Graph  +19 -20
BH Core       +20
BH Core       +21

PART Upp_Ax_Ref
NEST
ZROD  M  Air        0.0    0.0    0.0  [2.743/2.0]     78.0 ! Single Coolant Channel
ZROD  M  UARG_Cyl   0.0    0.0    0.0  19.7            78.0 ! Graphite Cylinder
ZROD  M  Air        0.0    0.0    0.0  19.8            78.0 ! Air Gap 1
ZROD  M  UAR_Peral  0.0    0.0    0.0  20.5            78.0 ! Aluminum Supprot Structure
ZROD  M  Air        0.0    0.0    0.0  20.93           78.0 ! Air Gap 2
ZROD  BH UARG_Ann   0.0    0.0    0.0  61.7            78.0 ! Graphite Annulus
ZROD  M  Air        0.0    0.0    0.0  61.8            78.0 ! Air Gap 2
ZROD  M  UAR_Peral  0.0    0.0    0.0  62.1            78.0 ! Aluminum Supprot Structure
ZROD  M  Air        0.0    0.0    0.0  [125.66796/2.0] 78.0 ! Upper Axial Reflector

PART Low_Ax_Ref
NEST
ZROD  M  LARG_Ann   0.0    0.0    0.0  6.0             25.0 ! Source Plug
ZROD  M  LARG_Cyl   0.0    0.0    0.0  24.75           78.0 ! Central Cylinder
ZROD  M  Air        0.0    0.0    0.0  25.05171        78.0 ! Air Gap
ZROD  BH LARG_Ann   0.0    0.0    0.0  62.71754        78.0 ! Annulus
ZROD  M  Air        0.0    0.0    0.0  [125.66796/2.0] 78.0 ! Lower Axial Reflector

PART Autorod
ZROD     1 0.0 0.0 -7.5 [5.5/2.0] [330.4+7.5]
ZROD     2 0.0 0.0  0.0 [4.4/2.0] 330.4
ZROD     3 0.0 0.0  0.0 [4.0/2.0] 330.4
+XZPRISM 4 [(3.9/2.0)] [-1.0*(0.3/2)]  [-7.5+230.0+48.5]
            3.9 230.0 0.3 89.514243 89.514243
YROT 180.0
ZONES
M Air          +1 -2 -4
M AutoRod_Tube +2 -3
M Air          +3 -4
```

```
M AutoRod_Cu   +4

PART Cont_Rod
ZROD     1 0.0 0.0 0.0 [2.743/2.0] 383.5
ZROD     2 0.0 0.0 [75.5+89.0] [2.2/2.0] 219.0
ZSEC     3 0.0 0.0 [75.5+89.0+1.5] [1.35/2.0] [1.4/2.0] 215.0 FULL
ZSEC     4 0.0 0.0 [75.5+89.0+1.5] [0.95/2.0] [1.35/2.0] 215.0 FULL
ZROD     5 0.0 0.0 [75.5+89.0+1.5+1.0] [0.95/2.0] [219.0-1.5-1.0-2.5-2.5]
ZROD     6 0.0 0.0 0.0 [2.65/2.0] 73.0
ZONES
M Air          +1 -2 -6
M CR_SS_4541   +2 -3 -4 -5
M Air          +3
M CR_SS_4301   +4
M Air          +5
M UARG_Plg     +6

END

BEGIN HOLE GEOMETRY

HOLE UARG_Ann
GLOBE
5
[(35.5+30.0)/2.0] SUB 32 0.0 30.0 M UARG_Plg M UARG_Plg M UARG_Plg [2.743/2.0] [2.743/2.0]
[2.743/2.0]
PINS
M UARG_Plg M UARG_Plg M Air M UARG_Plg M UARG_Plg M Air M UARG_Plg M UARG_Plg
M Air M UARG_Plg M UARG_Plg M Air M UARG_Plg M UARG_Plg M Air M UARG_Plg
M UARG_Plg  M Air M UARG_Plg M UARG_Plg M Air M UARG_Plg M Air M UARG_Plg
M UARG_Plg  M Air M UARG_Plg M UARG_Plg M Air M UARG_Plg M UARG_Plg M Air
[(41.0+35.5)/2.0] SUB 32 1.0 35.5 M UARG_Plg M UARG_Plg M UARG_Plg [2.743/2.0] [2.743/2.0]
[2.743/2.0]
[(46.25+41.0)/2.0] SUB 32 0.0 41.0 M UARG_Plg M UARG_Plg M UARG_Plg [2.743/2.0] [2.743/2.0]
[2.743/2.0]
PINS
M UARG_Plg M UARG_Plg M Air M UARG_Plg M UARG_Plg M Air M UARG_Plg M UARG_Plg
M Air M UARG_Plg M UARG_Plg M Air M UARG_Plg M UARG_Plg M Air M UARG_Plg
M UARG_Plg  M Air M UARG_Plg M UARG_Plg M Air M UARG_Plg M Air M UARG_Plg
M UARG_Plg  M Air M UARG_Plg M UARG_Plg M Air M UARG_Plg M UARG_Plg M Air
[(51.5+46.25)/2.0] SUB 32 1.0 46.25 M UARG_Plg M UARG_Plg M UARG_Plg [2.743/2.0] [2.743/2.0]
[2.743/2.0]
61.7 SUB 32 0.0 51.5 M UARG_Plg M UARG_Plg M UARG_Plg [2.743/2.0] [2.743/2.0] [2.743/2.0]
PINS
M UARG_Plg M UARG_Plg M Air M UARG_Plg M UARG_Plg M Air M UARG_Plg M UARG_Plg
M Air M UARG_Plg M UARG_Plg M Air M UARG_Plg M UARG_Plg M Air M UARG_Plg
M UARG_Plg  M Air M UARG_Plg M UARG_Plg M Air M UARG_Plg M Air M UARG_Plg
M UARG_Plg  M Air M UARG_Plg M UARG_Plg M Air M UARG_Plg M UARG_Plg M Air
M UARG_Ann

HOLE LARG_Ann
GLOBE
5
[(35.5+30.0)/2.0] SUB 32 0.0 30.0 M UARG_Plg M UARG_Plg M UARG_Plg [2.743/2.0] [2.743/2.0]
[2.743/2.0]
PINS
M UARG_Plg M UARG_Plg M Air M UARG_Plg M UARG_Plg M Air M UARG_Plg M UARG_Plg
M Air M UARG_Plg M UARG_Plg M Air M UARG_Plg M UARG_Plg M Air M UARG_Plg
M UARG_Plg  M Air M UARG_Plg M UARG_Plg M Air M UARG_Plg M Air M UARG_Plg
M UARG_Plg  M Air M UARG_Plg M UARG_Plg M Air M UARG_Plg M UARG_Plg M Air
[(41.0+35.5)/2.0] SUB 32 1.0 35.5 M UARG_Plg M UARG_Plg M UARG_Plg [2.743/2.0] [2.743/2.0]
[2.743/2.0]
[(46.25+41.0)/2.0] SUB 32 0.0 41.0 M UARG_Plg M UARG_Plg M UARG_Plg [2.743/2.0] [2.743/2.0]
[2.743/2.0]
PINS
M UARG_Plg M UARG_Plg M Air M UARG_Plg M UARG_Plg M Air M UARG_Plg M UARG_Plg
M Air M UARG_Plg M UARG_Plg M Air M UARG_Plg M UARG_Plg M Air M UARG_Plg
M UARG_Plg  M Air M UARG_Plg M UARG_Plg M Air M UARG_Plg M Air M UARG_Plg
M UARG_Plg  M Air M UARG_Plg M UARG_Plg M Air M UARG_Plg M UARG_Plg M Air
[(51.5+46.25)/2.0] SUB 32 1.0 46.25 M UARG_Plg M UARG_Plg M UARG_Plg [2.743/2.0] [2.743/2.0]
[2.743/2.0]
61.7 SUB 32 0.0 51.5 M UARG_Plg M UARG_Plg M UARG_Plg [2.743/2.0] [2.743/2.0] [2.743/2.0]
PINS
M UARG_Plg M UARG_Plg M Air M UARG_Plg M UARG_Plg M Air M UARG_Plg M UARG_Plg
M Air M UARG_Plg M UARG_Plg M Air M UARG_Plg M UARG_Plg M Air M UARG_Plg
```

```
M UARG_Plg  M Air M UARG_Plg M UARG_Plg M Air M UARG_Plg M Air M UARG_Plg
M UARG_Plg  M Air M UARG_Plg M UARG_Plg M Air M UARG_Plg M UARG_Plg M Air
M LARG_Ann

HOLE Cav_Graph
GLOBE
3
[(41.0+30.0)/2.0] SUB 11 0.0 30.0 M Air M Air M Air 1.35 1.35 1.35
[(51.5+41.0)/2.0] SUB 11 0.0 41.0 M Air M Air M Air 1.35 1.35 1.35
[125.66796/2.0]   SUB 11 0.0 51.5 M Air M Air M Air 1.35 1.35 1.35
M Cavity_Graphite

& * Hole 1 - PBMR Hole

HOLE Core PBMR

ANNULUS 0.0 [125.66796/2.0] 151.0
SPHERES
H Fuel 3.0 H Fuel 3.0
1.0
M MP_Graphite 3.0 M MP_Graphite 3.0
1.0
PACK 0.60898
! Now choose the method for packing the spheres:
@MODE=0

|IF @MODE=0
   MODE 0 ! close packed hexagonal, but with 4 pebbles replaced by 1 at their centre
|ENDIF
|IF @MODE=1
   MODE 1 ! close packed hexagonal, pitch chosen to get packing fraction
|ENDIF
|IF @MODE=2
   MODE 2 ! layers of pebbles in an hexagonal array, sits optimally on layer below, pitch to get
packing fraction
|ENDIF
|IF @MODE=3
   MODE 3 ! most complex: layers built up & dropped down to create 'bands' - most realistic
option
|ENDIF

COOLANT M Air

HOLE Fuel PEBBLE
GRAIN
M Kernel [0.05020/2.0]
M Buffer [(0.05020/2.0)+0.00915]
M IPyC   [(0.05020/2.0)+0.00915+0.00399]
M SiC    [(0.05020/2.0)+0.00915+0.00399+0.00353]
M OPyC   [(0.05020/2.0)+0.00915+0.00399+0.00353+0.00400]
PEBBLE
M FP_Graphite [4.7/2.0]
M FP_Graphite [(4.7/2.0)+0.65]
M Air
BUFFER 0.065
SEED 29012013
NUMBER 9394

END

BEGIN SOURCE GEOMETRY
ZONEMAT
ALL / MATERIAL Kernel
END

BEGIN CONTROL DATA
 STAGES [1-@NUMSET] @NUMSTG @NUMNEUT
 STDV @STDV
END
```

Sample Input Listing for MONK10(DEV) using Mode 2:

```
COLUMNS 1 132
* MONK10  Model of PROTEUS Core 4.
*
* Specification PROTEUS-GCR-EXP-002 CRIT Revision 0 March 31, 2013

* Fixed Run Parameters
@NUMSET=10       ! Number of Settling Stages
@NUMSTG=500      ! Maximum Number of Ordinary Stages
@NUMNEUT=5000    ! Number of SuperHistories per Stage
@NGEN=10         ! Number of Generations per SuperHistory
@FACTNU=1.0      ! Estimate of 1/k-eff for 1st stage
@LSTAGE=10       ! Suppress checking of STDV until this ordinary stage
@STDV=0.0005     ! Target Standard Deviation

BEGIN MATERIAL SPECIFICATION

TYPE BINGO

* Radial Reflector Graphite
NUMBER DENSITY
MATERIAL Radial_Refl
B10      2.3261E-08
B11      9.3627E-08
GRAPHITE 8.7886E-02

* Upper Axial Reflector Graphite - Cylinder
NUMBER DENSITY
MATERIAL UARG_Cyl
B10      2.3235E-08
B11      9.3524E-08
GRAPHITE 8.7789E-02

* Upper Axial Reflector Graphite - Annulus
NUMBER DENSITY
MATERIAL UARG_Ann
B10      2.3368E-08
B11      9.4059E-08
GRAPHITE 8.8291E-02

* Upper Axial Reflector Graphite - Plugs
NUMBER DENSITY
MATERIAL UARG_Plg
B10      2.3356E-08
B11      9.4011E-08
GRAPHITE 8.8245E-02

* Upper Axial Reflector Peraluman-300 Support Structure
NUMBER DENSITY
MATERIAL UAR_Peral
B10      1.4688E-07
B11      5.9119E-07
Mg       1.0177E-03
Al       5.7575E-02
Si       2.2729E-04
Mn       7.2621E-05
Fe       8.5730E-05
Cu       1.2557E-05
Zn       2.4398E-05
Ga       1.1444E-06
Cd       7.0983E-08

* Lower Axial Reflector Graphite - Cylinder
NUMBER DENSITY
MATERIAL LARG_Cyl
B10      2.3223E-08
B11      9.3476E-08
GRAPHITE 8.7744E-02

* Lower Axial Reflector Graphite - Annulus / Source Plug
NUMBER DENSITY
MATERIAL LARG_Ann
B10      2.3356E-08
B11      9.4011E-08
```

```
GRAPHITE 8.8245E-02

* Autorod Copper (Type C110) Wedge
NUMBER DENSITY
MATERIAL AutoRod_Cu
Cu       8.4206E-02
O        6.6923E-05
Ag       3.7224E-06
S        1.2522E-05
Ni       6.8410E-06
Fe       7.1900E-06

* Autorod Aluminum (Type 1100) Tube
NUMBER DENSITY
MATERIAL AutoRod_Tube
Si       2.8947E-04
Fe       1.4558E-04
Cu       3.1984E-05
Mn       7.6610E-06
Zn       1.2429E-05
Co       6.8975E-05
Ni       6.9257E-05
Sn       3.4242E-05
Al       5.9087E-02

* UO2 Fuel Kernel
NUMBER DENSITY
MATERIAL Kernel
O        4.8612E-02
U234     3.3079E-05
U235     4.1172E-03
U236     2.0499E-05
U238     2.0135E-02

* TRISO SiC and Graphite Layer - Buffer
NUMBER DENSITY
MATERIAL Buffer
GRAPHITE 5.2640E-02

* TRISO SiC and Graphite Layer - PyC (Inner)
NUMBER DENSITY
MATERIAL IPyC
GRAPHITE 9.5254E-02

* TRISO SiC and Graphite Layer - SiC
NUMBER DENSITY
MATERIAL SiC
GRAPHITE 4.8055E-02
Si       4.8055E-02

* TRISO SiC and Graphite Layer - PyC (Outer)
NUMBER DENSITY
MATERIAL OPyC
GRAPHITE 9.4752E-02

* Fuel Pebble Graphite
NUMBER DENSITY
MATERIAL FP_Graphite
GRAPHITE 8.6842E-02
AG       9.6706E-10
B10      1.9393E-09
B11      7.8061E-09
Ca       2.4154E-07
Cd       4.7791E-10
Cl       4.4135E-08
Co       1.1505E-09
Cr       3.6312E-08
!Dy       3.2097E-11
Eu       3.4322E-11
Fe       5.5104E-08
Gd       3.3169E-11
Li6      5.7034E-09
Li7      6.9441E-08
Mn       8.1647E-09
Ni       8.8864E-09
```

```
S         1.7893E-10
Ti        1.0831E-08
V         4.4334E-09
H         1.1581E-05
O         5.7904E-06

* Moderator Pebble Graphite
NUMBER DENSITY
MATERIAL MP_Graphite
GRAPHITE 8.4434E-02
B10       1.4193E-08
B11       5.7130E-08
Ca        3.2656E-06
Cd        2.7077E-09
Cl        5.3343E-07
!Dy        4.0583E-10
Eu        8.6793E-10
Fe        1.0719E-07
Gd        2.5808E-10
Li6       9.7630E-09
Li7       1.1887E-07
Ni        1.3483E-08
S         4.4297E-06
Si        1.2644E-06
Sm        5.8029E-10
Ti        2.1196E-07
V         2.5891E-07
H         1.1263E-05
O         5.6317E-06

* Control Rod Stainless Steel (Type St1.4301) Tube
NUMBER DENSITY
MATERIAL CR_SS_4301
C         1.3864E-04
Si        8.4696E-04
Mn        8.6597E-04
Cr        1.6927E-02
Ni        8.3083E-03
Fe        5.9391E-02

* Control Rod Stainless Steel (Type St1.4541) Tube and End Plug Composition
NUMBER DENSITY
MATERIAL CR_SS_4541
C         1.9805E-04
Si        8.4696E-04
Mn        8.6597E-04
Cr        1.6469E-02
Ni        8.3083E-03
Ti        4.9695E-05
Fe        5.9761E-02

* Graphite Cavity Floor Fillers
NUMBER DENSITY
MATERIAL Cavity_Graphite
B10       2.3214E-08
B11       9.3439E-08
GRAPHITE 8.7709E-02

* Ambient Air
NUMBER DENSITY
MATERIAL Air
H         5.7098E-07
N         3.7362E-05
O         1.0326E-05
!Ar        2.2345E-07
C         9.1319E-09


END

BEGIN MATERIAL GEOMETRY

PART PROTEUS_CORE4 ! Entire Geometry
ZROD   1   0.0    0.0   -7.5          [327.53972/2.0] [78.0+189.3+78.0+7.5+60.0]
ZSEC   2   0.0    0.0    0.0          [125.66796/2.0] [327.53972/2.0] 330.4 FULL
```

```
ZROD   3 -38.45  56.57   0.0          [4.5/2.0]       330.4 ! Safety/Shutdown Rod Hole 1
ZROD   4  32.74 -60.05   0.0          [4.5/2.0]       330.4 ! Safety/Shutdown Rod Hole 2
ZROD   5  57.17  37.55   0.0          [4.5/2.0]       330.4 ! Safety/Shutdown Rod Hole 3
ZROD   6 -53.23 -42.95   0.0          [4.5/2.0]       330.4 ! Safety/Shutdown Rod Hole 4
ZROD   7  67.19 -12.82   0.0          [4.5/2.0]       330.4 ! Safety/Shutdown Rod Hole 5
ZROD   8 -66.98  13.87   0.0          [4.5/2.0]       330.4 ! Safety/Shutdown Rod Hole 6
ZROD   9  19.31  65.62   0.0          [4.5/2.0]       330.4 ! Safety/Shutdown Rod Hole 7
ZROD  10 -13.87 -66.98   0.0          [4.5/2.0]       330.4 ! Safety/Shutdown Rod Hole 8
ZROD  11  17.36 -87.29   -7.5         [5.5/2.0]       [330.4+7.5] ! Autorod Hole
ZROD  12 -83.70  34.67   0.0          [2.743/2.0]     383.5 ! Withdrawable Control Rod Hole 1
ZROD  13  34.67  83.70   0.0          [2.743/2.0]     383.5 ! Withdrawable Control Rod Hole 2
ZROD  14  83.70 -34.67   0.0          [2.743/2.0]     383.5 ! Withdrawable Control Rod Hole 3
ZROD  15 -34.67 -83.70   0.0          [2.743/2.0]     383.5 ! Withdrawable Control Rod Hole 4
ZROD  16   0.0    0.0    0.0          [125.66796/2.0]  78.0 ! Lower Axial Reflector
ZROD  17   0.0    0.0    [78.0+189.3] [125.66796/2.0]  78.0 ! Upper Axial Reflector
ZROD  18   0.0    0.0    [78.0+188.3] 62.1              1.0 ! Aluminium Support
ZSEC  19   0.0    0.0    78.0         24.96893 [125.66796/2.0]   7.611 FULL ! Graphite Cavity
Floor Filler
ZCONE 20   0.0    0.0    [78.0+0.934366]     24.96893 [125.66796/2.0] [7.611-0.934366] ! Remove
conic shape from Floor Filler
ZROD  21   0.0    0.0    [78.0+7.611] [125.66796/2.0]  [151.0-7.611] ! Core Cavity Cylinder
ZONES
M Air         +1 -2 -11 -12 -13 -14 -15 -16 -17 -18 -19 -20 -21
M Radial_Refl +2 -3 -4 -5 -6 -7 -8 -9 -10 -11 -12 -13 -14 -15
M Air         +3
M Air         +4
M Air         +5
M Air         +6
M Air         +7
M Air         +8
M Air         +9
M Air         +10
P Autorod     +11
P Cont_Rod    +12
P Cont_Rod    +13
P Cont_Rod    +14
P Cont_Rod    +15
P Low_Ax_Ref  +16
P Upp_Ax_Ref  +17
M UAR_Peral   +18
BH Cav_Graph  +19 -20
BH Core       +20
BH Core       +21

PART Upp_Ax_Ref
NEST
ZROD  M  Air        0.0    0.0    0.0  [2.743/2.0]     78.0 ! Single Coolant Channel
ZROD  M  UARG_Cyl   0.0    0.0    0.0  19.7            78.0 ! Graphite Cylinder
ZROD  M  Air        0.0    0.0    0.0  19.8            78.0 ! Air Gap 1
ZROD  M  UAR_Peral  0.0    0.0    0.0  20.5            78.0 ! Aluminum Supprot Structure
ZROD  M  Air        0.0    0.0    0.0  20.93           78.0 ! Air Gap 2
ZROD  BH UARG_Ann   0.0    0.0    0.0  61.7            78.0 ! Graphite Annulus
ZROD  M  Air        0.0    0.0    0.0  61.8            78.0 ! Air Gap 2
ZROD  M  UAR_Peral  0.0    0.0    0.0  62.1            78.0 ! Aluminum Supprot Structure
ZROD  M  Air        0.0    0.0    0.0  [125.66796/2.0] 78.0 ! Upper Axial Reflector

PART Low_Ax_Ref
NEST
ZROD  M  LARG_Ann   0.0    0.0    0.0  6.0             25.0 ! Source Plug
ZROD  M  LARG_Cyl   0.0    0.0    0.0  24.75           78.0 ! Central Cylinder
ZROD  M  Air        0.0    0.0    0.0  25.05171        78.0 ! Air Gap
ZROD  BH LARG_Ann   0.0    0.0    0.0  62.71754        78.0 ! Annulus
ZROD  M  Air        0.0    0.0    0.0  [125.66796/2.0] 78.0 ! Lower Axial Reflector

PART Autorod
ZROD     1 0.0 0.0 -7.5 [5.5/2.0] [330.4+7.5]
ZROD     2 0.0 0.0  0.0 [4.4/2.0] 330.4
ZROD     3 0.0 0.0  0.0 [4.0/2.0] 330.4
+XZPRISM 4 [(3.9/2.0)] [-1.0*(0.3/2)]  [-7.5+230.0+48.5]
            3.9 230.0 0.3 89.514243 89.514243
YROT 180.0
ZONES
M Air          +1 -2 -4
M AutoRod_Tube +2 -3
M Air          +3 -4
```

```
M AutoRod_Cu   +4

PART Cont_Rod
ZROD     1 0.0 0.0 0.0 [2.743/2.0] 383.5
ZROD     2 0.0 0.0 [75.5+89.0] [2.2/2.0] 219.0
ZSEC     3 0.0 0.0 [75.5+89.0+1.5] [1.35/2.0] [1.4/2.0] 215.0 FULL
ZSEC     4 0.0 0.0 [75.5+89.0+1.5] [0.95/2.0] [1.35/2.0] 215.0 FULL
ZROD     5 0.0 0.0 [75.5+89.0+1.5+1.0] [0.95/2.0] [219.0-1.5-1.0-2.5-2.5]
ZROD     6 0.0 0.0 0.0 [2.65/2.0] 73.0
ZONES
M Air          +1 -2 -6
M CR_SS_4541   +2 -3 -4 -5
M Air          +3
M CR_SS_4301   +4
M Air          +5
M UARG_Plg     +6

END

BEGIN HOLE GEOMETRY

HOLE UARG_Ann
GLOBE
5
[(35.5+30.0)/2.0] SUB 32 0.0 30.0 M UARG_Plg M UARG_Plg M UARG_Plg [2.743/2.0] [2.743/2.0]
[2.743/2.0]
PINS
M UARG_Plg M UARG_Plg M Air M UARG_Plg M UARG_Plg M Air M UARG_Plg M UARG_Plg
M Air M UARG_Plg M UARG_Plg M Air M UARG_Plg M UARG_Plg M Air M UARG_Plg
M UARG_Plg  M Air M UARG_Plg M UARG_Plg M Air M UARG_Plg M Air M UARG_Plg
M UARG_Plg  M Air M UARG_Plg M UARG_Plg M Air M UARG_Plg M UARG_Plg M Air
[(41.0+35.5)/2.0] SUB 32 1.0 35.5 M UARG_Plg M UARG_Plg M UARG_Plg [2.743/2.0] [2.743/2.0]
[2.743/2.0]
[(46.25+41.0)/2.0] SUB 32 0.0 41.0 M UARG_Plg M UARG_Plg M UARG_Plg [2.743/2.0] [2.743/2.0]
[2.743/2.0]
PINS
M UARG_Plg M UARG_Plg M Air M UARG_Plg M UARG_Plg M Air M UARG_Plg M UARG_Plg
M Air M UARG_Plg M UARG_Plg M Air M UARG_Plg M UARG_Plg M Air M UARG_Plg
M UARG_Plg  M Air M UARG_Plg M UARG_Plg M Air M UARG_Plg M Air M UARG_Plg
M UARG_Plg  M Air M UARG_Plg M UARG_Plg M Air M UARG_Plg M UARG_Plg M Air
[(51.5+46.25)/2.0] SUB 32 1.0 46.25 M UARG_Plg M UARG_Plg M UARG_Plg [2.743/2.0] [2.743/2.0]
[2.743/2.0]
61.7 SUB 32 0.0 51.5 M UARG_Plg M UARG_Plg M UARG_Plg [2.743/2.0] [2.743/2.0] [2.743/2.0]
PINS
M UARG_Plg M UARG_Plg M Air M UARG_Plg M UARG_Plg M Air M UARG_Plg M UARG_Plg
M Air M UARG_Plg M UARG_Plg M Air M UARG_Plg M UARG_Plg M Air M UARG_Plg
M UARG_Plg  M Air M UARG_Plg M UARG_Plg M Air M UARG_Plg M Air M UARG_Plg
M UARG_Plg  M Air M UARG_Plg M UARG_Plg M Air M UARG_Plg M UARG_Plg M Air
M UARG_Ann

HOLE LARG_Ann
GLOBE
5
[(35.5+30.0)/2.0] SUB 32 0.0 30.0 M UARG_Plg M UARG_Plg M UARG_Plg [2.743/2.0] [2.743/2.0]
[2.743/2.0]
PINS
M UARG_Plg M UARG_Plg M Air M UARG_Plg M UARG_Plg M Air M UARG_Plg M UARG_Plg
M Air M UARG_Plg M UARG_Plg M Air M UARG_Plg M UARG_Plg M Air M UARG_Plg
M UARG_Plg  M Air M UARG_Plg M UARG_Plg M Air M UARG_Plg M Air M UARG_Plg
M UARG_Plg  M Air M UARG_Plg M UARG_Plg M Air M UARG_Plg M UARG_Plg M Air
[(41.0+35.5)/2.0] SUB 32 1.0 35.5 M UARG_Plg M UARG_Plg M UARG_Plg [2.743/2.0] [2.743/2.0]
[2.743/2.0]
[(46.25+41.0)/2.0] SUB 32 0.0 41.0 M UARG_Plg M UARG_Plg M UARG_Plg [2.743/2.0] [2.743/2.0]
[2.743/2.0]
PINS
M UARG_Plg M UARG_Plg M Air M UARG_Plg M UARG_Plg M Air M UARG_Plg M UARG_Plg
M Air M UARG_Plg M UARG_Plg M Air M UARG_Plg M UARG_Plg M Air M UARG_Plg
M UARG_Plg  M Air M UARG_Plg M UARG_Plg M Air M UARG_Plg M Air M UARG_Plg
M UARG_Plg  M Air M UARG_Plg M UARG_Plg M Air M UARG_Plg M UARG_Plg M Air
[(51.5+46.25)/2.0] SUB 32 1.0 46.25 M UARG_Plg M UARG_Plg M UARG_Plg [2.743/2.0] [2.743/2.0]
[2.743/2.0]
61.7 SUB 32 0.0 51.5 M UARG_Plg M UARG_Plg M UARG_Plg [2.743/2.0] [2.743/2.0] [2.743/2.0]
PINS
M UARG_Plg M UARG_Plg M Air M UARG_Plg M UARG_Plg M Air M UARG_Plg M UARG_Plg
M Air M UARG_Plg M UARG_Plg M Air M UARG_Plg M UARG_Plg M Air M UARG_Plg
```

```
M UARG_Plg  M Air M UARG_Plg M UARG_Plg M Air M UARG_Plg M Air M UARG_Plg
M UARG_Plg  M Air M UARG_Plg M UARG_Plg M Air M UARG_Plg M UARG_Plg M Air
M LARG_Ann

HOLE Cav_Graph
GLOBE
3
[(41.0+30.0)/2.0] SUB 11 0.0 30.0 M Air M Air M Air 1.35 1.35 1.35
[(51.5+41.0)/2.0] SUB 11 0.0 41.0 M Air M Air M Air 1.35 1.35 1.35
[125.66796/2.0]   SUB 11 0.0 51.5 M Air M Air M Air 1.35 1.35 1.35
M Cavity_Graphite

& * Hole 1 - PBMR Hole

HOLE Core PBMR

ANNULUS 0.0 [125.66796/2.0] 151.0
SPHERES
H Fuel 3.0 H Fuel 3.0
1.0
M MP_Graphite 3.0 M MP_Graphite 3.0
1.0
PACK 0.60898
! Now choose the method for packing the spheres:
@MODE=2

|IF @MODE=0
   MODE 0 ! close packed hexagonal, but with 4 pebbles replaced by 1 at their centre
|ENDIF
|IF @MODE=1
   MODE 1 ! close packed hexagonal, pitch chosen to get packing fraction
|ENDIF
|IF @MODE=2
   MODE 2 ! layers of pebbles in an hexagonal array, sits optimally on layer below, pitch to get
packing fraction
|ENDIF
|IF @MODE=3
   MODE 3 ! most complex: layers built up & dropped down to create 'bands' - most realistic
option
|ENDIF

COOLANT M Air

HOLE Fuel PEBBLE
GRAIN
M Kernel [0.05020/2.0]
M Buffer [(0.05020/2.0)+0.00915]
M IPyC   [(0.05020/2.0)+0.00915+0.00399]
M SiC    [(0.05020/2.0)+0.00915+0.00399+0.00353]
M OPyC   [(0.05020/2.0)+0.00915+0.00399+0.00353+0.00400]
PEBBLE
M FP_Graphite [4.7/2.0]
M FP_Graphite [(4.7/2.0)+0.65]
M Air
BUFFER 0.065
SEED 29012013
NUMBER 9394

END

BEGIN SOURCE GEOMETRY
ZONEMAT
ALL / MATERIAL Kernel
END

BEGIN CONTROL DATA
 STAGES [1-@NUMSET] @NUMSTG @NUMNEUT
 STDV @STDV
END
```

A.2 Buckling and Extrapolation Length Configurations

Buckling and extrapolation length measurements were made but have not yet been evaluated.

A.3 Spectral-Characteristics Configurations

Spectral characteristics measurements were not made.

A.4 Reactivity-Effects Configurations

Reactivity effects measurements were made but have not yet been evaluated.

A.5 Reactivity Coefficient Configurations

Reactivity coefficient measurements were made but have not yet been evaluated.

A.6 Kinetics Parameter Configurations

Kinetics measurements were made but have not yet been evaluated.

A.7 Reaction-Rate Configurations

Reaction-rate distribution measurements were made but have not yet been evaluated.

A.8 Power Distribution Configurations

Power distribution measurements were not made.

A.9 Isotopic Configurations

Isotopic measurements were not made.

A.10 Configurations of Other Miscellaneous Types of Measurements

Other miscellaneous types of measurements were not made.

APPENDIX B: CALCULATED SPECTRAL DATA

The neutron spectral calculations provided below were obtained from the output files for the input decks used to obtain the results in Section 4.1. Spectral data using the ENDF/B-VII.0 neutron cross section library is provided here for the MCNP5 analysis.

B.1 MCNP-Calculated Spectral Data

A summary of the computed neutron spectral data using MCNP5 for the benchmark model is provided in Table B.1-1. for Case 1 (Cores 4).

Table B.1-1. Neutron Spectral Data for Benchmark Model for Case 1 (Core 4).

Neutron Cross Section Library		ENDF/B-VII.0
k_{eff}		1.01736
$\pm\sigma_k$		0.00007
Neutron Leakage (%)[(a)]		15.48
Fission Fraction, by Energy (%)	**Thermal (<0.625 eV)**	94.78
	Intermediate	4.88
	Fast (>100 keV)	0.34
Average Number of Neutrons Produced per Fission		2.437
Energy of Average Neutron Lethargy Causing Fission (eV)		0.056679
Neutron Generation Time, Λ (msec)		1.92116
Rossi-α ($msec^{-1}$)		-3.61035E-03
β_{eff}		0.00694

(a) The neutron leakage is calculated using the neutron balance tables provided in the MCNP output file. The weight fraction of neutrons lost due to escaping the boundaries of the benchmark model are divided by the total weight fraction of neutron loss.

APPENDIX C: DETAILED MODELS OF HTR-PROTEUS

C.1 Detailed MCNP Models of the HTR-PROTEUS (NOT BENCHMARKED)

A detailed model of HTR-PROTEUS core configuration 4 was prepared to evaluate biases in the benchmark model. Because the effects of many of the model simplifications produced small or otherwise negligible biases (in regards to criticality) in the benchmark model, development of a detailed benchmark model was unnecessary. An example MCNP5 input deck, using ENDF/B-VII.0 neutron cross section data, is preserved in this appendix for future use. Calculations were performed with 1,650 generations with 100,000 neutrons per generation. The k_{eff} estimates (with the first 150 generations skipped) are the result of 150,000,000 neutron histories. Calculated results obtained with this input deck are provided in Table C.1-1.

Table C.1-1. Neutron Spectral Data for Detailed Model (Core 4).

Neutron Cross Section Library		ENDF/B-VII.0
k_{eff}		1.01642
$\pm\sigma_k$		0.00007
Neutron Leakage (%)[(a)]		1.71
Fission Fraction, by Energy (%)	**Thermal (<0.625 eV)**	94.78
	Intermediate	4.88
	Fast (>100 keV)	0.34
Average Number of Neutrons Produced per Fission		2.437
Energy of Average Neutron Lethargy Causing Fission (eV)		0.056715
Neutron Generation Time, Λ (msec)		1.92834
Rossi-α ($msec^{-1}$)		-3.64795E-03
β_{eff}		0.00703

(a) The neutron leakage is calculated using the neutron balance tables provided in the MCNP output file. The weight fraction of neutrons lost due to escaping the boundaries of the benchmark model are divided by the total weight fraction of neutron loss.

C.2 Input Listing for Detailed Models

The MCNP input deck for the detailed model, core configuration 4 (Case 1), is provided in a separate file (ASCII format), htr4.detailed.mcnp5.nf7.inp, which is located in the input folder of the directory of this evaluation.

APPENDIX D: HTR-PROTEUS HISTORICAL DATA

D.1 Validation of Safety Related Physics Calculations for Low Enriched HTGRs

The IARA CRP on Validation of Safety Related Physics Calculations for Low Enriched HTGRs (established in 1990) represented a collaboration between China, France, Japan, Switzerland, Germany, the Netherlands, the USA, and the Russian Federation to fill the gaps in validation data for physics methods used in the core design of gas-cooled reactors fueled with low enriched uranium. An international team of researchers assembled at the PROTEUS critical experiment facility of the Paul Scherrer Institute in Villigen, Switzerland to plan, conduct, and analyze a new series of critical experiments focused on the needs of the participating countries.

The following institutes participated in this CRP:

- Paul Scherrer Institute (PSI), Villigen, Switzerland
- Institute for Nuclear Energy Technology (INET), Tsinghua University, Beijing, China
- Forschungzentrum Jülich (FZJ), Jülich, Germany
- Japan Atomic Energy Research Institute (JAERI), Tokai-mura, Japan
- Interfaculty Reactor Institute, Delft University, Delft, the Netherlands
- Centre d'Etudes de Cadarache (CEA), St. Paul les Durance-Cedex, France
- Oak Ridge National Laboratory (ORNL), Oak Ridge, USA
- Russian Research Center Kurchatov Institute (RRC-KI), Moscow, Russia
- Energy Research Center, Petten, the Netherlands
- General Atomics (GA), San Diego, USA
- Experimental Machine Building Design Bureau (OKBM), Nizhny Novgorod, Russia

The PROTEUS graphite moderated LEU critical experiments were planned to fill gaps in the base of validation data. The constraints included room temperature and 5500 LEU fuel pebbles supplied by the KFA Research Center in Jülich, Germany. Specifically, the experiments which could be conducted at the PROTEUS facility with available AVR LEU fuel are summarized in Table D.1-1. The experimental conditions achievable at PROTEUS are summarized in Table D.1-2 (Ref. 3).

Table D.1-1. Summary of PROTEUS Critical Experiments (Ref. 3).

- Clean critical cores.
- LEU pebble-type fuel with 16.76 % ^{235}U enrichment.
- A range of C/U atom ratios from 946 to 1890 (achieved by varying the moderator-to-fuel pebble ratio from 0.5 to 2.0).
- Core (equivalent) diameter = 1.25 m.
- Core height = 0.843 m to 1.73 m (with simulated water ingress smaller core heights possible).
- Core H/D from 0.7 to 1.4.
- Flux distribution measurements and spectral distribution measurements (including measurements in side reflector).
- Kinetic parameter measurements.
- Worth of reflector control rods (partially and fully inserted).
- Worth of in-core control rod (partially and fully inserted).
- Effects of moisture ingress over range of water density up to 0.25 g H_2O/cm^3 void (corresponds to 0.065 g H_2O/cm^3 core for PROTEUS). Water is simulated with polyethylene inserts.
  - Effect on core reactivity.
  - Effect on worth of reflector control rods.
  - Effect on worth of in-core control rod.
  - Effect on burnable poison worth.
  - Effect on prompt neutron lifetime.
  - Effect on flux and power distributions.

Table D.1-2. Experimental Conditions Achievable at PROTEUS (Ref. 3).

- The PROTEUS critical provide validation data for low-enriched uranium fuel with an enrichment near to that planned for advanced GCR designs.
- PROTEUS moisture ingress experiments will investigate the effects which are important for advanced GCR designs (i.e., reactivity worth of moisture, and the effect of moisture on control rod and burnable poison worth and on reaction rate distributions) over the range of moisture densities of interest.
- The achievable range of C/U atom ratios at PROTEUS is near to, but higher than, that of advanced GCR designs (this ratio is an important factor in determining the neutron energy spectrum).
- PROTEUS provides the validation data
  - For the worth of reflector control rods.
  - For the worth of an in-core control rod.
  - For the worth of small samples of burnable poison (B_4C).
  - For fission rate distributions in core and reflector.

D.2 PROTEUS Critical Experiment Facility History and HTR Reconfiguration

The zero-power reactor facility PROTEUS is a part of the Paul Scherrer Institute (formerly EIR) and is situated near Würenlingen in the canton of Aargau in northern Switzerland. In the past it had been configured as a multi-zone (driven) system for reactor physics investigations of gas-cooled fast breeder and high conversion reactors. Various test configurations were built into a central, subcritical test zone which was driven critical by means of annular, thermal driver zones. PROTEUS was configured, for the first time, as a single zone for the HTR experiments with a pebble bed system surrounded radially and axially by a thick graphite reflector (Ref. 3).

A brief history of the facility is as follows (Ref. 3):[a]

- January 1968 – September 1970
  - Operation as a "zero-reactivity experiment" with a thermal, D_2O moderated test-lattice and a graphite driver.
- September 1970 – April 1972
  - Mixed fast-thermal system with a "buffer-zone" and reduced size test-zone.
- April 1972 – April 1979
  - Sixteen different configurations of the gas-cooled fast reactor type.
- January 1980 – August 1980
  - Preliminary HTR experiments.
- August 1980 – May 1981
  - Rebuild of the test-zone to accommodate light-water high conversion reactor experiments.
- May 1981 – October 1982
  - Phase I of the advanced light-water reactor experiments. Six configurations were investigated.
- February 1983 – May 1985
  - Re-configuration of the test-zone for Phase II of the light-water high conversion reactor experiments.

[a] PROTEUS Home Page, http://proteus.web.psi.ch/, Paul Scherrer Institut, Villigen, Switzerland (Accessed January 11, 2011).

- June 1985 – December 1990
  - Phase II of the advanced light-water experiments. Fourteen different test-zones, containing more representative fuel than in Phase I.
- January 1991 – July 1991
  - Rebuild for the LEU-HTR experiments.
- July 1992 – October 1996
  - HTR-PROTEUS critical experiments. Ten core configurations, some with multiple reference states.
- 1996 – 1997
  - Rebuild for LWR-PROTEUS experiments for validation of LWR fuel design and analysis tools.
- 1997 – 2001
  - Phase I – SVEA96+ BWR fuel: fission rates and reactivity worths.
- 2001 – 2003
  - Phase II – PWR fuel: reactivity of burnt fuel segments.
- 2003 – 2005
  - Phase III – SVEA-96 Optima2 BWR fuel: fission rates and moderator density effects.
- 2005 – 2011
  - LIFE@PROTEUS experimental program (Large-scale Irradiated Fuel Experiments): power distributions and mismatch, reaction rates, reactivity effects, and characterization of burnt fuel.

A brief summary of the work performed to rebuild the PROTEUS for the HTR-PROTEUS experiments is as follows (Ref. 3):

- All driver and buffer fuel discharged and stored.
- Fuel in test-zone discharged and stored.
- All installations inside graphite reflector removed.
- Construction of upper reflector assembly for HTR, an aluminum tank containing an annular region of old graphite and a central cylinder of new graphite.
- Filling of ~50 % of the ~300 C-Driver holes with new graphite rods. The other ~50 % were filled with existing graphite rods.
- Renewal of the safety/shutdown rods – increased length to allow for greater core height and better characterization of material properties – for improved benchmark quality of experiments.
- Increased height of radial reflector by 12 cm.
- Reconstruction of lower axial reflector, including central part of new graphite.
- Mounting of graphite panels in core cavity to modify the cavity shape to accommodate deterministic loadings.
- Fuel and moderator pebbles loaded.
- After the rest worths of the original ZEBRA control rods were found to be unacceptably high, these rods were replaced with conventional withdrawable control rods.

D.3 HTR-PROTEUS Timeline and Test Matrix

The time periods spanned by each configuration is provided in Figure D.3-1. A summary of the test matrix parameters investigated as part of each configuration is presented in Table D.3-3.

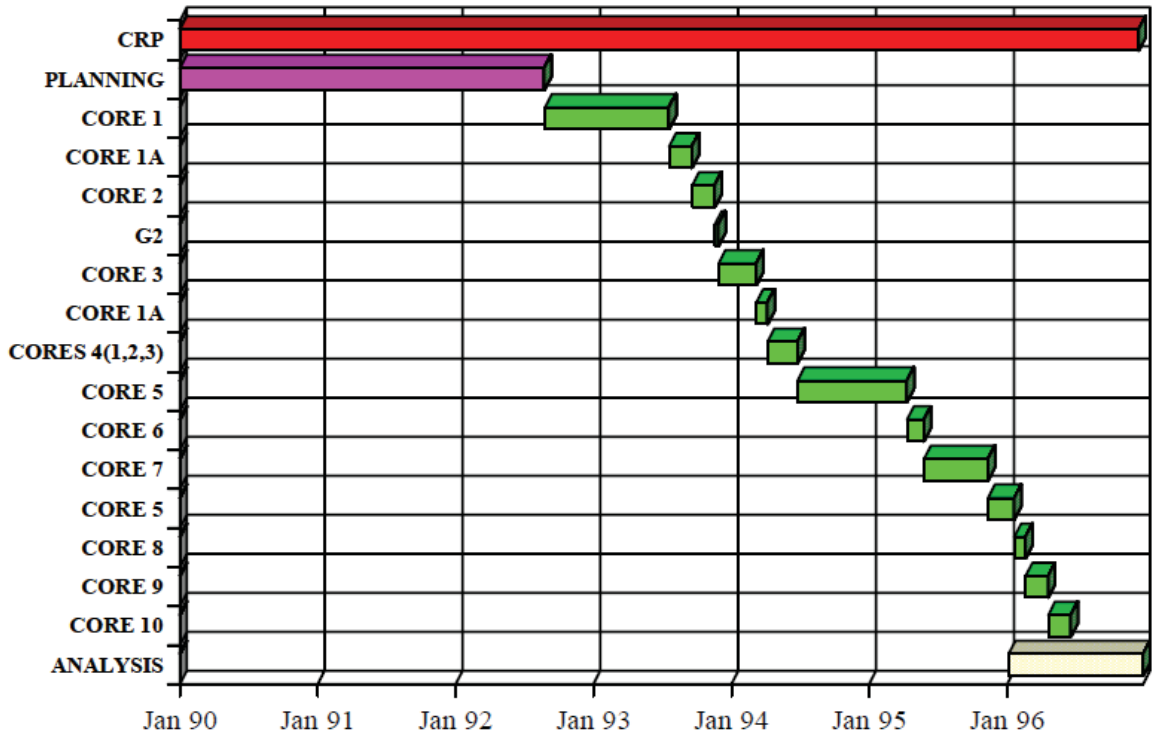

Figure D.3-1. Time Allocation for HTR-PROTEUS Experiments (Ref. 3).

Table D.3-1. Test Matrix for Cores 1 through 10 (Ref. 3).

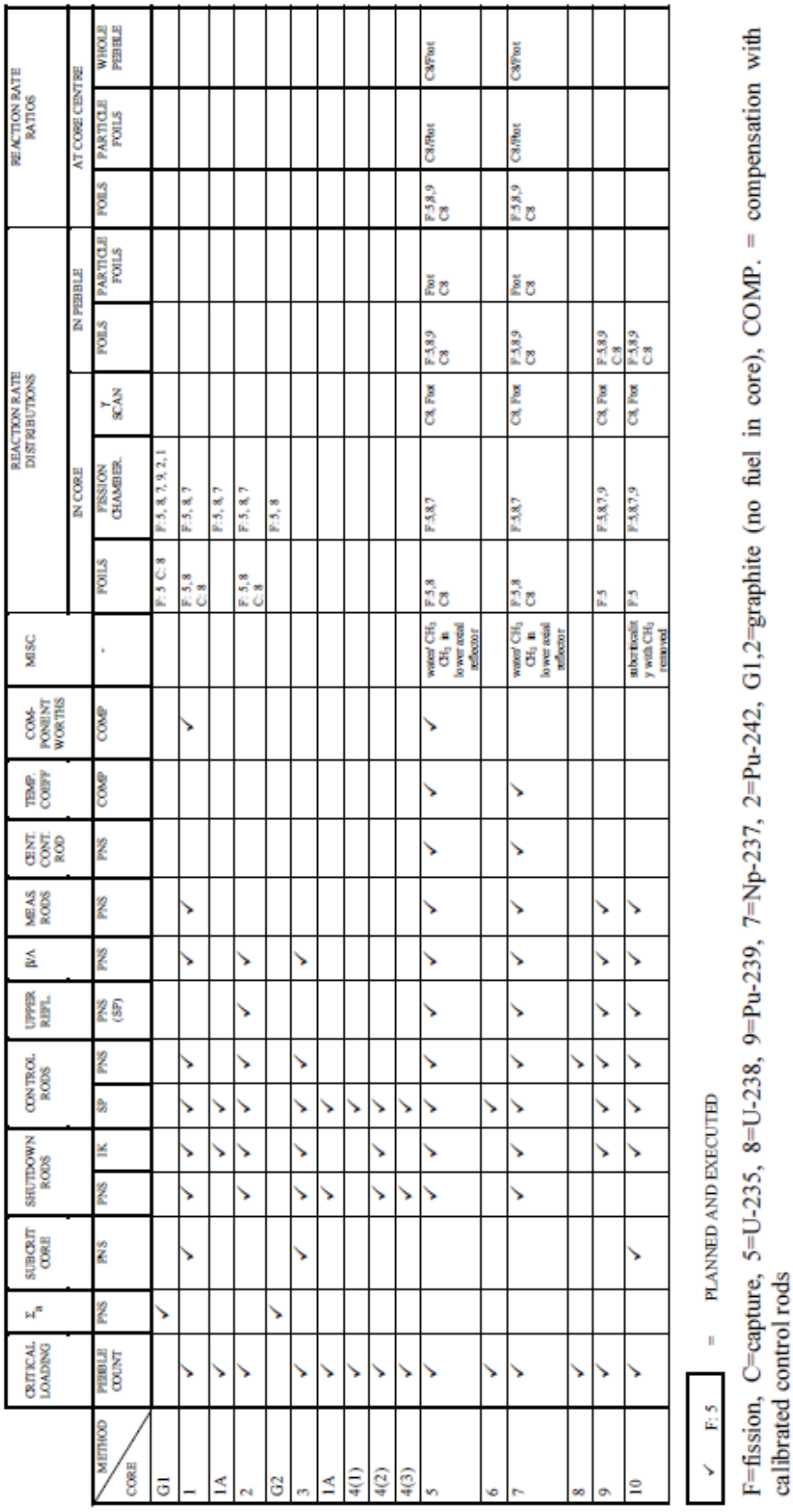

METHOD / CORE	CRITICAL LOADING: PEBBLE COUNT	CRITICAL LOADING: Σ_a PNS	SUBCRIT CORE PNS	SHUTDOWN RODS PNS	SHUTDOWN RODS 1K	CONTROL RODS SP	CONTROL RODS PNS	UPPER REFL. PNS (SP)	β/A PNS	MEAS. RODS PNS	CENT. CONT. ROD PNS	TEMP. COEFF COMP	COMPONENT WORTHS COMP	MISC. -	REACTION RATE DISTRIBUTIONS: IN CORE FOILS	REACTION RATE DISTRIBUTIONS: IN CORE FISSION CHAMBER.	REACTION RATE DISTRIBUTIONS: IN CORE γ SCAN	REACTION RATE DISTRIBUTIONS: IN PEBBLE FOILS	REACTION RATE DISTRIBUTIONS: IN PEBBLE PARTICLE FOILS	REACTION RATIOS: AT CORE CENTRE FOILS	REACTION RATIOS: AT CORE CENTRE PARTICLE FOILS	REACTION RATIOS: AT CORE CENTRE WHOLE PEBBLE
G1		✓													F: 5 C: 8	F: 5, 8, 7, 9, 2, 1						
1	✓		✓	✓	✓	✓	✓		✓	✓			✓		F: 5, 8 C: 8	F: 5, 8, 7						
1A	✓				✓	✓										F: 5, 8, 7						
2	✓			✓	✓	✓	✓	✓	✓						F: 5, 8 C: 8	F: 5, 8, 7						
G2		✓														F: 5, 8						
3	✓		✓	✓	✓	✓	✓		✓													
1A	✓			✓		✓																
4(1)	✓					✓																
4(2)	✓			✓	✓	✓																
4(3)	✓			✓		✓																
5	✓			✓	✓	✓	✓	✓	✓	✓	✓	✓	✓	wated CH_2 CH_2 in lo wer axial reflector	F:5,8 C:8	F:5,8,7	$C:8_{Pot}$	F:5,8,9 C:8	$C:8_{Pot}$	F:5,8,9 C:8	$C:8/^{Pot}$	$C:8/^{Pot}$
6	✓					✓																
7	✓			✓	✓	✓	✓	✓	✓	✓	✓	✓		wated CH_2 CH_2 in lo wer axial reflector	F:5,8 C:8	F:5,8,7	$C:8_{Pot}$	F:5,8,9 C:8	$C:8_{Pot}$	F:5,8,9 C:8	$C:8/^{Pot}$	$C:8/^{Pot}$
8	✓						✓															
9	✓				✓	✓	✓	✓	✓	✓					F:5	F:5,8,7,9	$C:8_{Pot}$	F:5,8,9 C:8				
10	✓		✓		✓	✓	✓	✓	✓	✓				aluminalli y with CH_2 removed	F:5	F:5,8,7,9	$C:8_{Pot}$	F:5,8,9 C:8				

✓ F:5 = PLANNED AND EXECUTED

F=fission, C=capture, 5=U-235, 8=U-238, 9=Pu-239, 7=Np-237, 2=Pu-242, G1,2=graphite (no fuel in core), COMP. = compensation with calibrated control rods

APPENDIX E: Data from the 16th edition chart of the Nuclides[a]

E.1 Isotopic Abundances and Atomic Weights

This evaluation incorporated atomic weights and isotopic abundances found in the 16th edition of the Chart of the Nuclides. A list of the values used in the benchmark model or in the generation of the MCNP input deck is compiled in Table E.1-1.

[a] E. M. Baum, H. D. Knox, and T. R. Miller, *Nuclides and Isotopes: 16th Edition*, Knolls Atomic Power Laboratory (2002).

Table E.1-1. Summary of Data Employed from the 16th Ed. of the Chart of the Nuclides.

Isotope or Element	Atomic Weight (g/mol)	Isotopic Abundance (at.%)	Isotope or Element	Atomic Weight (g/mol)	Isotopic Abundance (at.%)
H	1.00794	--	S	32.065	--
^{1}H	--	99.9885	^{32}S	--	94.93
^{2}H	--	0.0115	^{33}S	--	0.76
He	4.002602	--	^{34}S	--	4.29
^{3}He	--	0.000137	^{36}S	--	0.02
^{4}He	--	99.999863	Cl	35.453	--
Li	6.941	--	^{35}Cl	--	75.78
^{6}Li	--	7.59	^{37}Cl	--	24.22
^{7}Li	--	92.41	Ar	39.948	--
B	10.811	--	^{36}Ar	--	0.3365
^{10}B	10.012937	19.9	^{38}Ar	--	0.0632
^{11}B	11.0093055	80.1	^{40}Ar	--	99.6003
C[(a)]	12.0107	--	Ca	40.078	--
N	14.0067	--	^{40}Ca	--	96.941
^{14}N	--	99.632	^{42}Ca	--	0.647
^{15}N	--	0.368	^{43}Ca	--	0.135
O	15.9994	--	^{44}Ca	--	2.086
^{16}O	--	99.757	^{46}Ca	--	0.004
^{17}O	--	0.038	^{48}Ca	--	0.187
^{18}O[(a)]	--	0.205	Ti	47.867	--
Ne	20.1797	--	^{46}Ti	--	8.25
Mg	24.3050	--	^{47}Ti	--	7.44
^{24}Mg	--	78.99	^{48}Ti	--	73.72
^{25}Mg	--	10	^{49}Ti	--	5.41
^{26}Mg	--	11.01	^{50}Ti	--	5.18
Al	26.981538	--	V[(a)]	50.9415	--
Si	28.0855	--	Cr	51.9961	--
^{28}Si	--	92.2297	^{50}Cr	--	4.345
^{29}Si	--	4.6832	^{52}Cr	--	83.789
^{30}Si	--	3.0872	^{53}Cr	--	9.501
P	30.973761	--	^{54}Cr	--	2.365

Table E.1-1 (cont'd.). Summary of Data Employed from the 16th Ed. of the Chart of the Nuclides.

Isotope or Element	Atomic Weight (g/mol)	Isotopic Abundance (at.%)
Mn	54.938049	--
Fe	55.845	--
^{54}Fe	--	5.845
^{56}Fe	--	91.754
^{57}Fe	--	2.119
^{58}Fe	--	0.282
Co	58.933200	--
Ni	58.6934	--
^{58}Ni	--	68.0769
^{60}Ni	--	26.2231
^{61}Ni	--	1.1399
^{62}Ni	--	3.6345
^{64}Ni	--	0.9256
Cu	63.546	--
^{63}Cu	--	69.17
^{65}Cu	--	30.83
Zn[(a)]	65.409	--
Ga	69.723	--
^{69}Ga	--	60.108
^{71}Ga	--	39.892
Kr	83.798	--
^{78}Kr	--	0.35
^{80}Kr	--	2.28
^{82}Kr	--	11.58
^{83}Kr	--	11.49
^{84}Kr	--	57
^{86}Kr	--	17.3
Mo	95.94	--
^{92}Mo	--	14.84
^{94}Mo	--	9.25
^{95}Mo	--	15.92
^{96}Mo	--	16.68
^{97}Mo	--	9.55
^{98}Mo	--	24.13
^{100}Mo	--	9.63
Ag	107.8682	--
^{107}Ag	--	51.839
^{109}Ag	--	48.161
Cd	112.411	--
^{106}Cd	--	1.25
^{108}Cd	--	0.89
^{110}Cd	--	12.49
^{111}Cd	--	12.8
^{112}Cd	--	24.13
^{113}Cd	--	12.22
^{114}Cd	--	28.73
^{116}Cd	--	7.49
Sn	118.710	--
^{112}Sn	--	0.97
^{114}Sn	--	0.66
^{115}Sn	--	0.34
^{116}Sn	--	14.54
^{117}Sn	--	7.68
^{118}Sn	--	24.22
^{119}Sn	--	8.59
^{120}Sn	--	32.58
^{122}Sn	--	4.63
^{124}Sn	--	5.79

Table E.1-1 (cont'd.). Summary of Data Employed from the 16th Ed. of the Chart of the Nuclides.

Isotope or Element	Atomic Weight (g/mol)	Isotopic Abundance (at.%)	Isotope or Element	Atomic Weight (g/mol)	Isotopic Abundance (at.%)
Ba	137.327	--	Gd	157.25	--
^{130}Ba	--	0.106	^{152}Gd	--	0.2
^{132}Ba	--	0.101	^{154}Gd	--	2.18
^{134}Ba	--	2.417	^{155}Gd	--	14.8
^{135}Ba	--	6.592	^{156}Gd	--	20.47
^{136}Ba	--	7.854	^{157}Gd	--	15.65
^{137}Ba	--	11.232	^{158}Gd	--	24.84
^{138}Ba	--	71.698	^{160}Gd	--	21.86
Sm	150.36	--	Dy	162.500	--
^{144}Sm	--	3.07	^{156}Dy	--	0.06
^{147}Sm	--	14.99	^{158}Dy	--	0.1
^{148}Sm	--	11.24	^{160}Dy	--	2.34
^{149}Sm	--	13.82	^{161}Dy	--	18.91
^{150}Sm	--	7.38	^{162}Dy	--	25.51
^{152}Sm	--	26.75	^{163}Dy	--	24.9
^{154}Sm	--	22.75	^{164}Dy	--	28.18
Eu	151.964	--	Pb	207.2	--
^{151}Eu	--	47.81	^{204}Pb	--	1.4
^{153}Eu	--	52.19	^{206}Pb	--	24.1
			^{207}Pb	--	22.1
			^{208}Pb	--	52.4
			Bi	208.98038	--
			^{234}U	234.040946	0.0055[(b)]
			^{235}U	235.043923	0.7200[(b)]
			^{238}U	238.050783	99.2745[(b)]

(a) Natural element without isotopic breakdown.
(b) Neutronically, ^{18}O is treated as ^{16}O.
(c) Natural isotopic abundance of U.